



HP-HT Laboratory
EXPERIMENTAL VOLCANOLOGY
AND GEOPHYSICS

LNTS
NEW TECHNOLOGIES and Instruments
Laboratory

ROMA 1 Section
Istituto Nazionale di Geofisica e Vulcanologia
Via di Vigna Murata 605 | 00143 Rome Italy
Phone +39-0651860437 | Fax +39-0651860507
www.ingv.it



2022

ANNUAL REPORT

HPHT - NTS LABS

[About the cover](#) | Chondrule (Barred olivine, crossed nicols). For more info read the abstract of Vitrano A. in this report

[Credits](#) | HPHT Lab - A. Vitrano

Follow us on



HPHTlab - Science, Technology & Engineering



HPHTlab (@hphtlab) | Twitter

CONTENTS

1 ABSTRACT	5
2 PERSONNEL	9
3 INSTRUMENTS and FACILITIES	13
4 LABORATORY ACTIVITIES	17
5 RESEARCH PROJECTS	23
6 PARTNER LABORATORIES	27
7 PARTNER INSTITUTIONS	29
8 RESEARCH ACTIVITY and RESULTS	31
9 SEMINARS and TEACHING	131
10 VISITING SCIENTISTS	135
11 MEETINGS, WORKSHOP and SYMPOSIA	139
12 PUBLICATIONS	147

C H A P T E R O N E

ABSTRACT

This report summarizes the facilities, activities, collaborations, scientific and technological products of the High Pressure High Temperature Laboratory of Experimental Volcanology and Geophysics (HPHT Lab) and of the Laboratory of New Technologies (LNTS) updated to the year 2022. The two laboratories are an active part of all the three main Departments of INGV: Earthquake, Volcano and Environment. Research activities were framed within 15 nationally - and internationally - funded research projects and involved 21 proposals. In collaboration with Italian and foreigner universities, the laboratories hosted 6 Master students and 9 PhD students. Scientific production for 2022 amounts to 33 publications.

Beside the three EU-funded projects that are continuing, (IMPROVE - Innovative Multi-disciplinary European Research training network on VolcanoEs; SYN FEAR - Fault activation and Earthquake Rupture; and EXCITE-Electron and X-ray microscopy Community for structural and chemical Imaging Techniques for Earth materials), a new EU-funded has begun: ENDGAME - Experiments, Numerical moDelling and field observations of basaltic maGma fragmentation. At national level, several new INGV-funded projects have been awarded to researchers of the laboratories and are just started, in both rock physics, petrology, and vulcanology.

The implementation of the two newest experimental apparata is still in progress, both for MEERA, a novel biaxial cell designed to investigate earthquake mechanics by simulating a the stress field in a prescribed tectonic regime, and for DANTE, a new high temperature furnace to study the crystallization dynamics in magmas. In the analog volcanology Lab experiments continued to investigate different aspects of the interaction between magmatic flow, conduit morphology, and magma fragmentation.

Finally, 2022 marks the twentieth anniversary of the HPHT Lab, an important milestone for all of us. In these 20 years the Lab underwent an impressive growth in terms of both infrastructures and covered scientific topics, and it now stands at the forefront of the experimental geosciences in the national and international community. To all the researchers, students, technicians, and administrators whose enthusiasm and energy made this happen goes the credit for the amazing achievements of the past and for those yet to come in the future.



C H A P T E R T W O
PERSONNEL

HPHT LABORATORY

Piergiorgio Scarlato | Senior Researcher,
Responsible of the HP-HT Laboratory

Stefano Aretusini | Contract Researcher
Emanuela Bagnato | Researcher
Clotilde Biensan | Contract Researcher
Riccardo Civico | Researcher
Chiara Cornelio | Contract Researcher
Gianfilippo De Astis | Senior Researcher
Elisabetta Del Bello | Researcher
Giuseppe La Spina | Researcher
Valeria Misiti | Technologist
Manuela Nazzari | Researcher
Francesco Pennacchia | Contract Technician
Alessio Pontesilli | Contract Researcher
Giacomo Pozzi | Contract Researcher
Tullio Ricci | Researcher
Roberta Ruggeri | Contract Researcher
Elena Spagnuolo | Researcher
Laura Spina | Researcher
Jacopo Taddeucci | Senior Researcher
Giancarlo Tamburello | Researcher

LABORATORY OF NEW TECHNOLOGIES

Giuseppe Di Stefano | Senior Technologist
Responsible of the Laboratory of New Technologies

Alessandro Iarocci | Engineer Technologist
Massimo Mari | Technician
Francesco Pongetti | Engineer Technician
Marcello Silvestri | Technician
Giuseppe Spinelli | Engineer Technologist
Massimiliano Vallocchia | Engineer Technician

ASSOCIATED RESEARCHERS

Cristiano Collettini | Sapienza Università di Roma, Italy | **Full Professor in Structural Geology**

Frances M. Deegan | Uppsala University, Sweden | **Researcher**

Giancarlo Della Ventura | Università di Roma Tre | **Full Professor in Mineralogy**

Giulio Di Toro | Università degli Studi di Padova | **Full Professor in Structural Geology**

Gianluca Iezzi | Università di Chieti | **Associate Professor of Petrology**

Silvio Mollo | Sapienza Università di Roma, Italy | **Associate Professor of Petrology**

Giovanni Romeo | INGV Retired

Marco M. Scuderi | Sapienza Università di Roma, Italy | **Associate Professor**

Vincenzo Stagno | Sapienza Università di Roma, Italy | **Associate Professor of Petrology**

COLLABORATORS

Carolina Giorgetti | Sapienza Università di Roma, Italy | **Researcher**

Matteo Masotta | Università di Pisa, Italy | **Researcher**

C H A P T E R T H R E E

INSTRUMENTS and FACILITIES

HPHT LABORATORY

- Multiple press 840 ton | [Voggenreiter](#)
- Piston cylinder - 3/4" and 1" pressure plates | [Voggenreiter](#)
- Multianvil - Walker type 6/8 | [Voggenreiter](#)
- Quick Press - Piston Cylinder 3/4" and 1" pressure plates | [Depth of the Earth](#)
- Bi-Tri-Axial Press (BRAVA) | [RMP - INGV](#)
- Low to High Velocity Apparatus (SHIVA) | [RMP - INGV](#)
- Electron microprobe equipped with 5 WDS and 1 EDS | [JEOL JXA-8200](#)
- Field Emission Scanning Electron Microscope equipped with EDS and BSE detectors | [JEOL JSM-6500F](#)
- Auto Carbon coater | [JEOL JEC-530](#)
- Fine coater | [JEOL JFC-2300HR](#)
- High and low temperature furnaces | [Lenton](#)
- Impedance analyser | [Solartron SI1260](#)
- Digital oscilloscope | [Tektronix DPO4032](#)
- Wave generator | [Agilent 33250A](#)
- H-Frame presses 10 ton | [Enerpac](#)
- Uniaxial testing machine with double load cell (15 and 250 kN) and LVDT controller | [Tecnostest](#)
- Precision balance | [Sartorius](#)
- Optical and stereo microscopes | [Leica DMRXP and Euromex](#)
- Ultra-high velocity, intensified, gated digital camera | [Cordin 204-2](#)
- Stereomicroscopes | [Leica MZ 9.5](#)
- Semiautomatic polisher | [Buehler Minimet 1000](#)
- Power Supply | [Agilent 6575A](#)
- Helium Picnometer | [AccuPyc II 1340](#)
- Permeameter with double intensifier | [Rock Physics](#)
- Rheometer MCR 301 Physica | [Anton Paar](#)
- Vertical Furnace RHTV 120-300/18 | [Nabertherm](#)
- High Temperature Furnace LHT 04/18 | [Nabertherm](#)
- Cecchi data acquisition system | [Applied Seismology](#)
- Rock drilling, cutting, and grinding equipment for samples preparation
- Thermal High speed camera | [FLIR SC 645](#)
- Welder PUK U3 | [Lampert](#)
- Laser line generator | [Edmund optics](#)
- Precision test sieves | [Endecotts](#)
- Laser MGL-III, 532nm 200mW, PSU-III-LED/Unit | [Changchun New Industries](#)
- Multi-Wavelength Analyser LUMiReader® PSA with Particle sizing according to ISO 13317
- 2 Polarized Free-field Microphones 40AN 1/2", Low Frequency (0.5Hz - 20kHz) | [G.R.A.S.](#)
- Ext. Polarized Pressure Microphone 46DP-1 1/8", High Frequency (6.5Hz -140kHz) | [G.R.A.S.](#)
- Vacuometro Pirani PVG-500

- Petrographic microscope ECLIPSE E-50i POL | [Nikon](#)
- Drying oven UF 75 | [Mettler](#)
- 4K digital camcorders | [Sony](#)
- High Speed digital camcorder | [NAC Memrecam - HX6](#)
- Shock-tube apparatus (Jet-Buster) | [INGV](#)
- High speed digital camcorders | [NAC 512 SC](#), [Optronis CR600x2](#), [NAC HX6](#), [NAC HX3](#)
- Laser range finder | [Vectronix VECTOR 21](#)
- Time Lapse Camera with 24-70 lens | [Brinno TLC200 Pro](#)
- Precision Syringe Pumps | [ISCO](#)
- Ash dispersal/settling apparatus (Ash-Buster) | [INGV](#)
- Drone Matrice 300 RTK | [DJI](#)
- Drone Mavic 2 Pro | [DJI](#)
- Drone Phantom 4 RTK | [DJI](#)
- Drone Mini 2 | [DJI](#)
- Dual UV cameras 340 UVGE | [Thorlabs](#)
- Laboratory sieve shaker Octagon 200 | [Endecotts](#)
- Optical Profilometer Modus6ZS-3D | [DeltaPIX](#)
- Triaxial ICP accelerometer | [PCB Piezotronics](#)
- Two high frequency ICP pressure sensors | [PCB Piezotronics](#)
- Three ceramic shear ICP accelerometers | [PCB Piezotronics](#)
- Two 4-channel ICP sensor signal conditioners | [PCB Piezotronics](#)
- MEERA biaxial direct shear apparatus
- High-temperature, vacuum, inert, and reactive gas furnace
- Microdriller for experimental glasses | [ARNOLD 561/01](#)
- Mortar grinder for experimental glasses | [PULVERISETTE 23 FRITSCH](#)
- SKO-D XL Orbital Shaker | [SKO](#)
- Centrifuge Neya 8 Basic | [NEYA](#)
- DANTE | [Carbolite Gero - Verder Scientific](#)
- SKATE (Setup for the Kinematic Acquisition of Explosive Eruptions) | [INGV/T.E.E.S.](#)
- Drone DJI Matrice 300 RTK with thermal, visible and lidar sensors

LABORATORY OF NEW TECHNOLOGIES

- Analog Oscilloscope | [HP](#)
- Analog Oscilloscope | [Iwatsu SS5710](#)
- Analog Oscilloscope | [Tektronix TDS220](#)
- Analog Oscilloscope | [Tektronix](#)
- Oscilloscope | [HP54201](#)
- Oscilloscope | [HP54602b](#)

- Power supply | [Elind HL series](#)
- Power supply | [Elind 6TD20](#)
- Power supply | [DC DF1731SB](#)
- Signal generator | [HP8656A](#)
- Function generator | [HP3325A](#)
- Multimeter | [HP3478A](#)
- Milling machine for printed circuit boards | [T-Tech](#)
- Logic state analyzer | [HP16500A](#)
- Superheterodyne spectrum analyzer | [Tektronix](#)
- Soldering-reworking station | [JBC advanced AM6500](#)
- Oscilloscope | [FLUKE 199C](#)
- Oscilloscope | [Tektronix DPO4000](#)
- Oscilloscope | [Tektronix MSO4034](#)
- Calibrator | [FLUKE 5700 \(series II\)](#)
- Function generator | [HP33120](#)
- Function generator | [AGILENT 33250 A](#)
- PXI Industrial computer with I/O boards | [National Instruments](#)
- Universal counter | [HP53131A](#)
- Waveform generator | [Agilent 33210 A](#)
- Oscilloscope W wave surfer | [LeCroy 44MXs-A](#)
- Drone Phantom 3 pro with termination system
- Power supply (4 items) | [-3005D](#)

MACHINE SHOP

- Lathe | [Grazioli Fortuna](#)
- Small lathe | [Ceriani](#)
- Small milling machine | [Schaublin](#)
- Cutting machine | [Ercoletta](#)
- Bending machine | [Ercoletta](#)
- Drill press | [Serrmac](#)
- Small drill press | [Webo](#)
- Bandsaw | [Femi](#)

C H A P T E R F O U R

LABORATORY ACTIVITIES

EXPERIMENTAL LABORATORY

Quick press | Piston cylinder

Experiments were conducted to study phase relations and volatile diffusion in magmas from Stromboli Volcano.

BRAVA

BRAVA performed 170 experiments during 2022 including: room pressure friction experiments (double-direct and double-direct configuration) and in-vessel experiments up to 35 MPa of confining pressure.

Slow to High Velocity Apparatus (SHIVA)

SHIVA performed 89 experiments (s1900-s1988) during 2022 including a challenging novel experiment: gouges under fluid pressure confinement and stress stepping.

Analog modeling laboratory

Fractal burster performed over 200 experiments during 2022 exploring different roughness of the analogue conduit and various starting pressure of the high-pressure reservoir. Collected data include high-speed video and acoustic and accelerometric signals from subsonic to supersonic analogue jets.

Preliminary tests have been performed to improve the construction of a novel large 2D apparatus in combination with the Schlieren shadow-photography, that will be devoted to the shock-tube experiments in bubble and particle-bearing analogue fluids.

FaMoUS (Fast Multiparametric Setup) & SKATE (Setup for the Kinematic Acquisition of Explosive Eruptions) Within the framework of the Departmental project UNO, to improve our capabilities to investigate active volcanic phenomena, we developed a new field system for sensing of explosive eruptions (SKATE) capable of imaging volcanic explosions at high frequency/resolution and measuring the related seismic and acoustic radiation. The system was tested at Stromboli (May-October).

Visible High Speed cameras/acoustic data (SKATE): i) about 10-20 hours per day of almost continuous recordings at Stromboli were filmed at 250 (120) fps and at 1280x720 pixel resolution during the period 17-24 May and 11-17 October.

Infrared Camera (FLIR Sc655): about 4 to 7 hours of continuous recording per day of the volcanic activity from the 270 m. elevation Sciara observation point of Stromboli were acquired at 25 Hz and at 640x480 pixel resolution during the periods 17-24 May and 11-17 October.

UV Camera: about 1 to 3 hours of continuous recording of the volcanic activity from the 270 m. elevation Sciara observation point of Stromboli were acquired at a 30 Hz and at 640x480 pixel resolution during the period 19, 20 and 21 May and 16 October.

Unmanned Aircraft System (UAS)

We performed UASs surveys at Stromboli (May, July, October, December), Vulcano (July and December), and Cumbre Vieja (January) volcanoes and Santa Maria Nuova - Emilia Romagna (September).

At Stromboli, Vulcano, Santa Maria Nuova and Cumbre Vieja we characterized the surface topography using Structure from Motion (SfM) photogrammetry and lidar surveys, that allowed us to produce very high resolution (10-50 cm/pixel) Digital Surface Models (DSMs), Digital Terrain Models (DSMs), and orthophotomosaics and detect elevation, volumetric, and areal variations. In addition, we performed infrared night and day-time thermal surveys at Stromboli, Vulcano, and Santa Maria Nuova and multigas flights for the measurements of CO₂, H₂S, and SO₂ concentrations in the plume.

At Stromboli and Vulcano, UASs were used to observe and characterise the volcanic and/or eruptive activity.

MICROANALYTICAL LABORATORY

FE-SEM and EMP performed 180 days of analysis in the frame of the following 20 research proposals. Analysed samples included natural rocks, minerals, experimental products.

PROPOSALS

- 1. Timescales of crystallization in basaltic magmas: effects of strain rate and undercooling**
F. Di Fiore – P. Scarlato | University of Roma Tre - INGV Roma1
- 2. UNderstanding the Ordinary to forecast the extraordinary: An integrated approach for studying and interpreting the explosive activity at Stromboli volcano**
P. Scarlato – M. Nazzari | INGV Roma 1
- 3. Tephrochronological study of the lacustrine succession of the maar of Castiglione (Central Italy) and evaluation of the possible impact on the climate of the explosive eruptions of the perithyrrenic volcanoes**
A. Di Roberto | INGV PI
- 4. Petrology and Geochemistry from Bransfield Strait (Antarctica) submarine volcanism. Evidences from volatiles (He, Ne, Ar, O, H), major and trace elements**
A. Caracausi – M. Nazzari | INGV Palermo - INGV Roma1
- 5. Probing the micromechanics of small magnitude earthquake slip in Groningen area**
S. Aretusini – E. Spagnuolo | INGV Roma 1

6. **Volcanic hazard assessment at Mt. Etna: a time-integrated, polybaric and polythermal perspective**
P. Moschini – P. Scarlato | Sapienza University of Rome - INGV Roma1
7. **Fractured microlites**
J. Taddeucci | INGV Roma 1
8. **Characterisation of the mud emissions occurred after M 6.5 earthquake in Central Italy**
V. Misiti | INGV Roma1
9. **Petrography of mortars with recycled aggregates (CDW) from post-earthquake rubble**
G. Iezzi – M. Nazzari | University of Chieti - INGV Roma1
10. **COupling of Rheology and Textures in Experimental Seismic faults (CORTES)**
G. Pozzi | INGV Roma 1
11. **Carbonatitic magmatism: the Mt Vulture volcano case**
A. Caracausi – M. Nazzari | INGV Palermo - INGV Roma1
12. **Chemical composition of olivine host and spinel inclusion combined to in situ Mössbauer spectroscopy measurements: implications for the mantle redox state, melt composition and rheology**
V. Stagno – P. Scarlato | Sapienza University of Rome - INGV Roma1
13. **Trachytic Ignimbrites magma-chambers Formation and Evolution in the pre-HOlocene history of the Campania volcanic area. Implications on magmatic processes, eruption dynamics, caldera collapse and resurgence**
S. De Vita – M. Nazzari | INGV OV - INGV Roma1
14. **MAGIC-Research project PNRA**
A. Di Roberto | INGV PI
15. **Magma-carbonate interaction under dynamic conditions: experimental insights on crystallization kinetics, element partitioning and multiphase rheology**
G. Giuliani – P. Scarlato | Sapienza University of Rome - INGV Roma1
16. **Mineralogy and Petrology of the carbonaceous chondrite NWA12800**
G. Della Ventura – M. Nazzari | Sapienza University of Rome - INGV Roma1

17. Characterising the proximal pyroclastic deposits in Central Anatolia to complet the recent explosive volcanic history, synchronise sedimentary records, and better assess volcanic hazards in Turkey

I. Sunyè Puchol – M. Nazzari | Sapienza University of Rome - INGV Roma1

18. Crystal-chemical and textural study of cicirara lava flows of Etna volcano: insights on solidification and emplacement processes

G. Iezzi – M. Nazzari | University of Chieti - INGV Roma1

19. Assessing the surface reactivity of amorphous materials: relations with iron oxidation state

V. Stagno – M. Nazzari | Sapienza University of Rome - INGV Roma1

20. Unravelling the geodynamic scenario of the Makran peridotites and chromitites (SE Iran) through the chemistry of their primary assemblages

F. Lucci – M. Nazzari | University of Bari - INGV Roma1

C H A P T E R F I V E

RESEARCH PROJECTS

1. **MIUR Progetto PRIN 2017** | Scales of solidification in magmas: applications to volcanic eruptions, silicate melts, glasses, glass- ceramics | **P.I. M. Carroll**
2. **MIUR PON** | GRINT
P.I. G. Puglisi
3. **European research project** | EXCITE 'Electron and X-ray microscopy Community for structural and chemical Imaging Techniques for Earth materials' | **P.I. V. Cnudde**
4. **European research project** | EPOS 'European Plate Observing System' Sustainability Phase, WP 16 Multi-scale Laboratories | **P.I. M. Cocco**
5. **European research project** | Marie Skłodowska-Curie European Training Network IMPROVE, Innovative Multi-disciplinary European Research training network on VolcanoEs | **P.I. P. Papale**
6. **European research project** | EUROPLANET 2024 RI-TA (coordinator University of Kent), Trans-national access project TNA20-EPN2-050, 'Turbulent suspensions of volcanic ash: an experimental simulation for eruptive and resuspension ash plumes', granted to **J. Taddeucci, E. Del Bello**.
7. **Petrobras3 - Petroleo Brasileiro S.A.** | Igneous rocks as source and sink of abiotic hydrocarbons and CO₂ | **P.I. G. Etiope**
8. **INGV "Ricerca libera" Project** | Magma dynamics triggering the 3 July and 28 August 2019 paroxysms at Stromboli volcano: A comparative approach based on the ascent rates, timescales and P-T-H₂O paths of magma | **P.I. P. Scarlato**
9. **INGV "Ricerca libera" Project, PoWAR** | a Portable Wind-tunnel for volcanic Ash Resuspension
P.I. J. Taddeucci - E. Del Bello
10. **INGV "Ricerca libera" Project, FRAMMENTI** | FRAGmentation of Mafic Magmas: Extent and Timing | **P.I. J. Taddeucci**
11. **INGV "Ricerca libera" Project, ROUGHER** | experimental Observations about irregular channel geometries | **P.I. L. Spina**
12. **INGV Departmental Strategic Projects, UNO** | UNderstanding the Ordinary to forecast the extraordinary: An integrated approach for studying and interpreting the explosive activity at Stromboli volcano | **P.I. P. Scarlato**

13. INGV "Pianeta Dinamico" Project, Task V1: Studio 3D-4D della struttura dei vulcani tramite tecniche di geofisica di esplorazione e confronto, integrazione e modellazione di dati geofisici, geochimici e geodetici.
14. INGV "Pianeta Dinamico" Project, Task S1: Studio teorico e sperimentale del processo di nucleazione e arresto dei terremoti, complessità della sorgente sismica.
15. INGV "Pianeta Dinamico" Project, Task S2: Struttura 3D dell'Italia da analisi multidata. Sismica passiva/attiva, Prospezioni magnetiche, magnetotelluriche, elettriche, gravimetriche
16. "Esopianeti" ASI-INAF Project | **G. De Astis**
17. ERC Syn Fear - Fault activation and Earthquake Rupture
P.I. Giardini D., Amman F., Cocco M., Wiemer S.
18. Marie Skłodowska-Curie Individual Fellowship "Experiments, Numerical modelling and field observations of basaltic magma fragmentation (ENDGAME)"
J. Taddeucci, G. La Spina
19. European research project | LIFE "RESPIRE" - Radon real time monitoring System and Proactive Indoor Remediation | **P.I. S. Bigi.**
20. PNRR: MEET Project: WP 3 ILGE Laboratories for Geosciences and Environment
Responsible P. Scarlato

C H A P T E R S I X

PARTNER
LABORATORIES

1. [Planetary Environmental Facilities](#) | Aarhus University | Denmark
2. [Experimental & Physical Volcanology](#) | Ludwig Maximilians Universitat | Germany
3. [Dipartimento di Scienze](#) | Università di Roma Tre | Italy
4. [Geoscience Department](#) | Utrecht University | Netherlands
5. [Institute of Geochemistry and Petrology](#) | ETH Zurich | Switzerland
6. [Dipartimento di Scienze Biologiche, Geologiche e Ambientali](#) | Università di Catania | Italy
7. [Dipartimento di Fisica e Scienze della Terra](#) | Università di Ferrara | Italy
8. [Petro-Volcanology Research Group \(PVRG\)](#) | Department of Physics and Geology
Università di Perugia | Italy
9. [School of Earth and Environmental Sciences](#) | University of Queensland | Australia
10. [Department of Geology](#) | University of Otago | New Zealand.
11. [Dipartimento di Geoscienze](#) | Università di Padova | Italy
12. [LEMR](#) | EPFL | Lausanne | Switzerland
13. [Rock Mechanics Laboratory](#) | Durham University | UK
14. [Jackson School of Geosciences](#) | Texas University of Austin | USA
15. [The Rocks Physics and Mechanics Laboratory \(RPML\)](#) | ETH | Switzerland
16. [Rock Mechanics Laboratory](#) | UCL Earth Sciences | UK
17. [Laboratoire Aleas géologiques et Dynamique sédimentaire](#) | IFREMER | France
18. [RMP LAB](#) | ETH | Switzerland
19. [Geotechnical lab](#) | RWTH Aachen University | Germany

C H A P T E R S E V E N

PARTNER INSTITUTIONS

1. Ludwig Maximilians Universitat Munchen | Munich | Germany
2. Department of Geology and Geophysics, SOEST | University of Hawaii | USA
3. Department of Physics and Astronomy | Aarhus University | Denmark
4. HVO Hawaiian volcano observatory | USGS | USA
5. School of Earth and Environmental Sciences | University of Queensland | Australia
6. Department of Geology | University of Otago | New Zealand.
7. Department of Earth Science | University of Durham | UK
8. Instituto Volcanologico de Canarias INVOLCAN | Spain
9. Dipartimento di Geoscienze | Università degli Studi di Padova | Italy
10. Departamento Tecnología Electrónica | Universidad Carlos III Madrid | Spain
11. Natural History Museum - Volcano Petrology Group | UK

C H A P T E R E I G H T

RESEARCH
ACTIVITY
and RESULTS

8.1 PETROLOGY, MINERALOGY, VOLCANOLOGY

MAGMA RECHARGE AND MUSH REJUVENATION DRIVE PAROXYSMAL ACTIVITY AT STROMBOLI VOLCANO

Petrone C.M., Mollo S., Gertisser R., Buret Y., Scarlato P., Del Bello E., Andronico D., Ellis B., Pontesilli A., De Astis G., Giacomoni P., Coltorti M., Reagan M.

Open-conduit basaltic volcanoes can be characterised by sudden large explosive events (paroxysms) that interrupt normal effusive and mild explosive activity. In June-August 2019, one major explosion and two paroxysms occurred at Stromboli volcano (Italy) within only 64 days. Here, via a multifaceted approach using clinopyroxene (Fig. 1), we show arrival of mafic recharges up to a few days before the onset of these events and their effects on the eruption pattern at Stromboli, as a prime example of a persistently active, open-conduit basaltic volcano. Our data indicate a rejuvenated Stromboli plumbing system where the extant crystal mush is efficiently permeated by recharge magmas with minimum remobilisation promoting a direct linkage between the deeper and the shallow reservoirs that sustains the currently observed larger variability of eruptive behaviour. Our approach provides vital insights into magma dynamics and their effects on monitoring signals demonstrating the power of petrological studies in interpreting patterns of surficial activity.

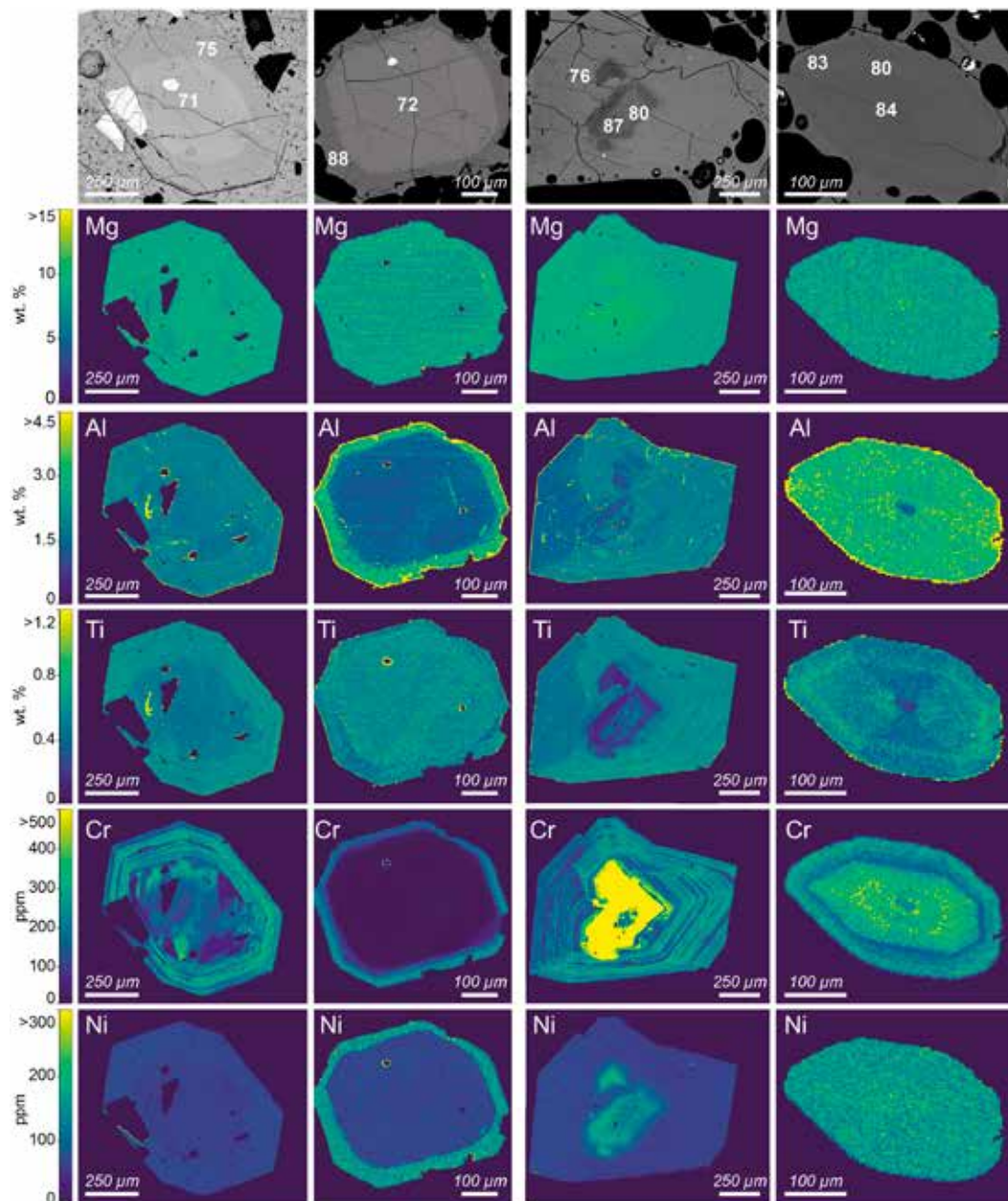


Figure 1

Major and trace elements chemical mapping for 2019 clinopyroxenes. BSE images (top) and quantitative chemical mapping of Mg, Al, Ti (wt%), Cr and Ni (ppm) for the main four subgroups of clinopyroxenes.

TRACE ELEMENT PARTITIONING IN ZONED CLINOPYROXENE AS A PROXY FOR UNDERCOOLING: EXPERIMENTAL CONSTRAINTS FROM TRACHYBASALTIC

MacDonald A., Ubide T., Mollo S., Masotta M., Pontesilli A.

Sector-zoned clinopyroxene records kinetic effects imposed by variable degrees of magma undercooling and can be utilised to track the dynamics of magmatic systems. The partitioning of trace elements into sectors grown in different crystallographic orientations can be used as a proxy for undercooling. However, an experimental assessment of the relationship between trace element zoning and undercooling has been lacking to date. Here we present trace element data from a series of undercooling crystallisation experiments on a primitive trachybasalt from Mt. Etna (Italy), at conditions of crustal storage (400 MPa, NNO^{+2}), and slow to intermediate to fast undercoolings. High-resolution elemental mapping reveals the distribution of trace elements in individual clinopyroxene zones (Fig. 1). Increasing undercooling drives a shift from polyhedral morphologies with Al-rich prism and Al-poor hourglass sectors (slow undercooling), to skeletal (intermediate undercooling) and dendritic (fast undercooling) crystals with Al-rich skeletons and Al-poor overgrowths. Aluminum-rich zones have higher concentrations of rare earth elements (REE) and high field strength elements (HFSE) than Al-poor zones across all investigated undercooling conditions, and overall, Al, REE and HFSE contents increase with undercooling. This indicates that tetrahedral aluminum and associated charge-balancing mechanisms govern the incorporation of REE and HFSE within clinopyroxene. Used to model fractional crystallisation, our data demonstrate that fractionation of clinopyroxene at low undercooling controls pre-eruptive melt evolution. Importantly, this indicates crystallisation of clinopyroxene in the deep portions of Mt. Etna's plumbing system is not rapid and is unlikely to result in the early formation of dendrites.

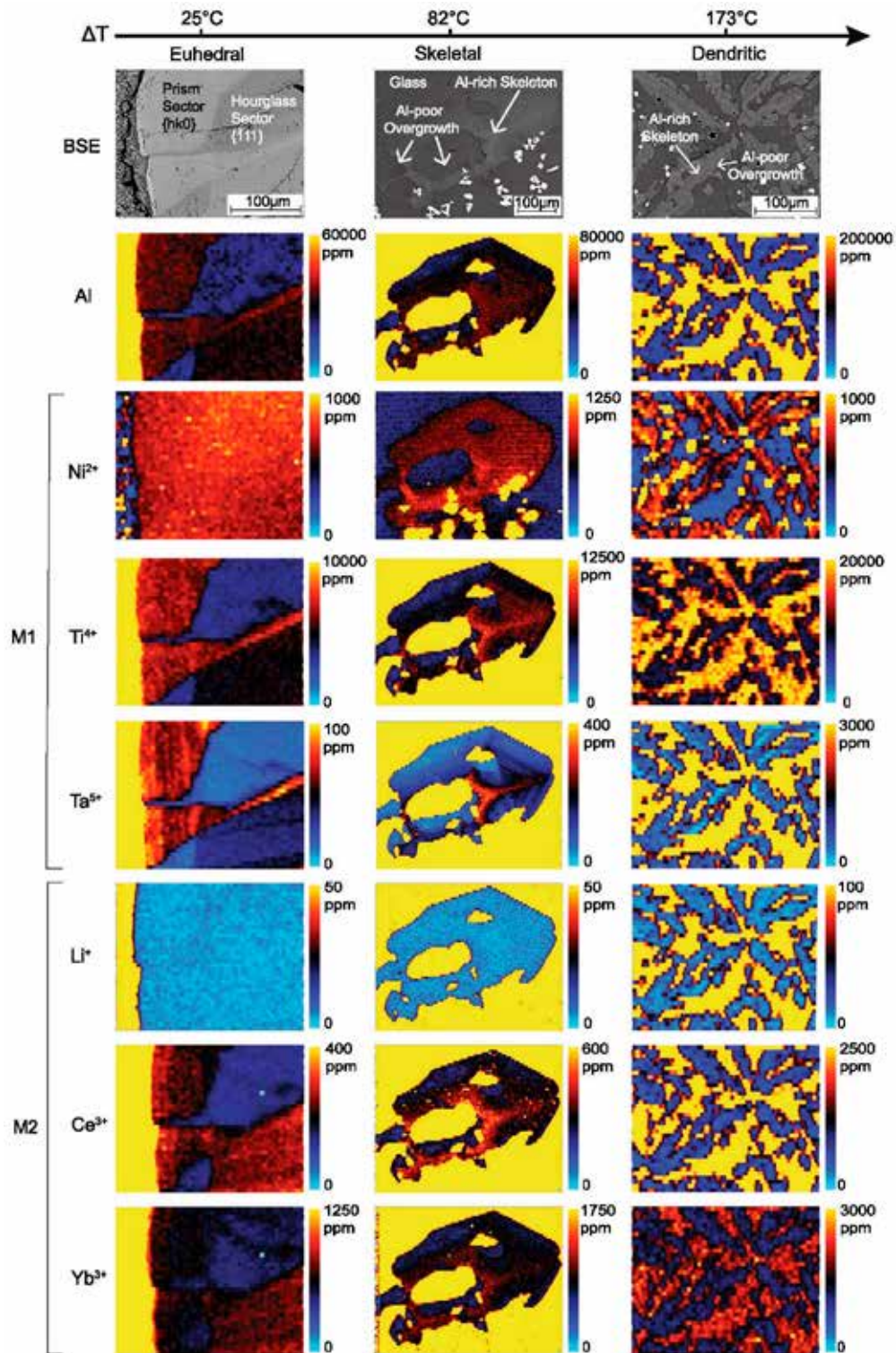


Figure 1
 Back scattered electron (BSE) images and trace element LA ICP-MS maps of selected clinopyroxene crystals formed at a range of undercooling conditions.

PARTITIONING OF TI, AL, P, AND CR BETWEEN OLIVINE AND A THOLEIITIC BASALTIC MELT: INSIGHTS ON OLIVINE ZONING PATTERNS AND CATION SUBSTITUTION REACTIONS UNDER VARIABLE COOLING RATE CONDITIONS

Lang S., Mollo S., Lyderic F., Misiti V., Nazzari M.

The mechanism governing the kinetic growth of olivine in dynamic volcanic settings has been the subject of considerable attention in recent years. Under variable cooling rate and undercooling regimes, the textural maturation of olivine proceeds from skeletal/dendritic crystals to polyhedral morphologies by infilling of the crystal framework. Owing to the establishment of a diffusion-controlled growth regime, a sharp diffusive boundary layer develops in the melt next to the advancing olivine surface. In this context, we have quantified the apparent partitioning of Ti, Al, P, and Cr between olivine and a Hawaiian tholeiitic basaltic melt under variable cooling and undercooling conditions. Differences in charge and/or size between the substituent minor cations and the major species in the olivine crystallographic site dominate the energetics of homovalent and heterovalent cation substitutions. In order to maintain charge balance, the disequilibrium uptake of minor cations in rapidly growing crystals is controlled by the same substitution mechanisms observed under equilibrium crystallization. This finding is consistent with the achievement of a local interface equilibrium at the olivine-melt interface independently of the diffusive boundary in the melt. A statistical approach based on multivariate analysis of olivine/melt compositional parameters confirms that the control of melt structure on the partitioning of Ti, Al, P, and Cr is almost entirely embodied in the olivine structure and chemistry via charge compensation reactions. Therefore, the magnitude of minor element partition coefficients is weakly dependent on diffusion kinetics in the melt but rather strongly governed by olivine zoning patterns resulting from fast crystal growth rates.

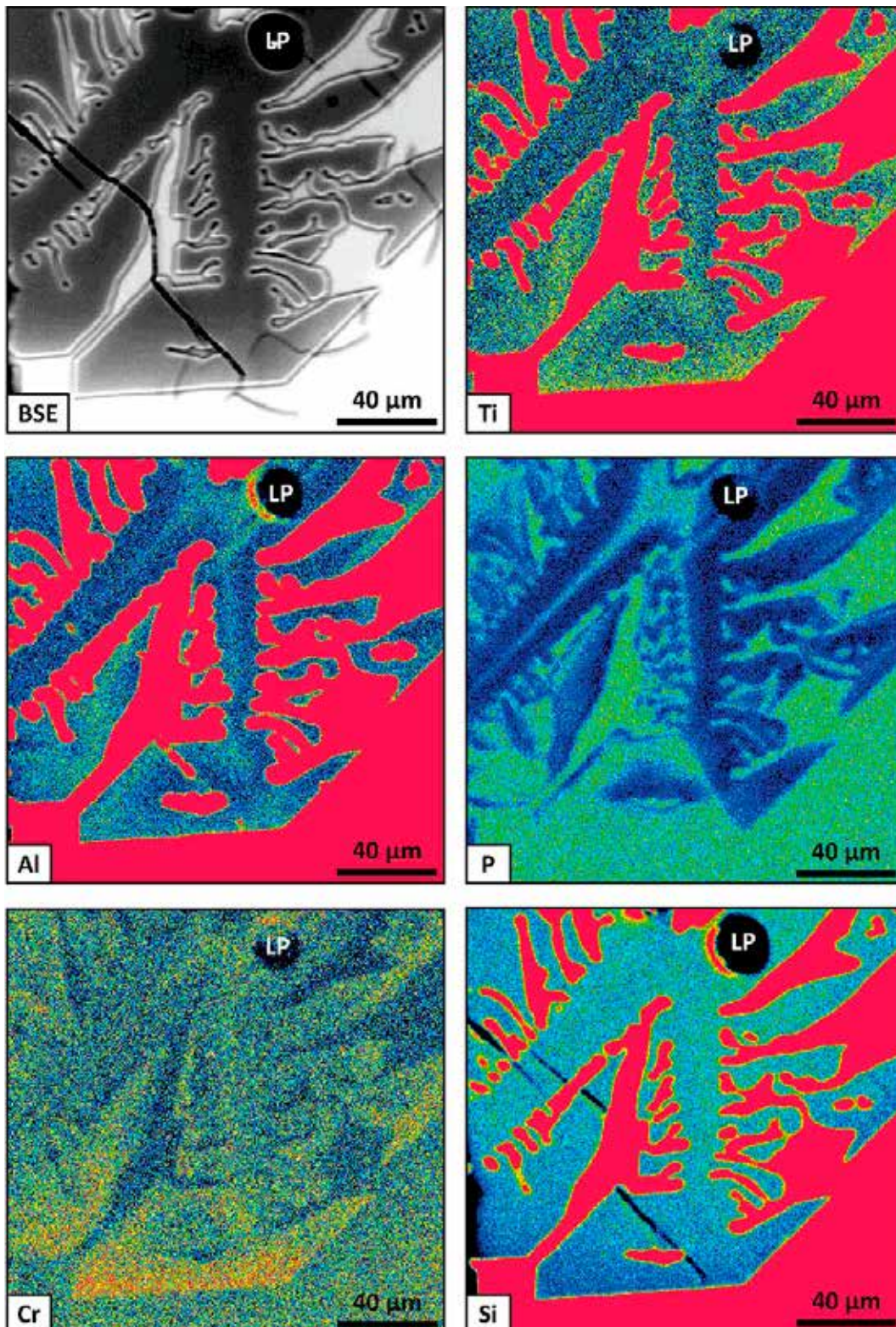


Figure 1
 Olivine zonation. The panels show a BSE photomicrograph and X-ray maps of Ti, Al, P, Cr, and Si with colour intensities adapted for crystal concentrations. Fine-scale enrichments are displayed for P, Ti, Al, and Cr, as minor cations in olivine. Conversely, subtle depletions are observable for Si, as major cation hosted in the lattice site.

MODELING THE CRYSTALLIZATION CONDITIONS OF CLINOPYROXENE CRYSTALS ERUPTED DURING FEBRUARY–APRIL 2021 LAVA FOUNTAINS AT MT. ETNA: IMPLICATIONS FOR THE DYNAMIC TRANSFER OF MAGMAS

Mollo S., Pontesilli A., Moschini P., Palummo F., Taddeucci J., Andronico D., Del Bello E., Scarlato P.

In the period February–April 2021, seventeen energetic hours-long episodes of intense lava fountaining occurred at Mt. Etna, producing lava flows and ash plumes followed by heavy fallout. Clinopyroxene mesocrysts from these paroxysms show complex sector and concentric zoning patterns, with juxtaposition of Si-Mg-rich (Al-Ti-poor) and Si-Mg-poor (Al-Ti-rich) crystal layers (Fig. 1). Clinopyroxene-based equilibrium thermobarometry and hygrometry define an overall crystallization path in the range of ~170–480 MPa, ~1060–1110 °C, and ~1.2–2.7 wt.% H₂O, with a main magma storage region estimated at depths of ~11–15 km. From this perspective, we observe that 2021 lava fountains were fed by hotter magmas of deeper origin with respect to those feeding 2011–2012 paroxysms. Zoning patterns of 2021 clinopyroxene mesocrysts formed in a vertically-extended plumbing system upon the effect of mixing phenomena and crystal recycling caused by recurrent inputs of fresh magmas into interconnected mushy reservoirs. Kinetic growth modeling constrains the formation of 2021 clinopyroxene mesocrysts over timescales of ~30–90 h and small degrees of undercooling ≤28 °C. Fe–Mg diffusion chronometry confirms that the time elapsed between the formation of clinopyroxene im and magma eruption is utterly related to growth kinetics caused by pre-eruptive dynamic transfer of magma at crustal depths. Kinetic effects are exacerbated for clinopyroxene microlites/microcrysts forming at the syn-eruptive stage, when magma decompression, degassing, and cooling become more effective in the last 1.5 km below the vent of Mt. Etna. Kinetic growth modeling reveals that eruption dynamics within the conduit promote an exceptionally rapid disequilibrium growth of clinopyroxene microlites/microcrysts in only ~0.4–3.3 min upon large degrees of undercooling >60 °C. The resulting ascent velocity of 2021 magmas within the conduit is ~8–63 m/s, a factor of ~3 higher than the less energetic 2011–2012 paroxysms.

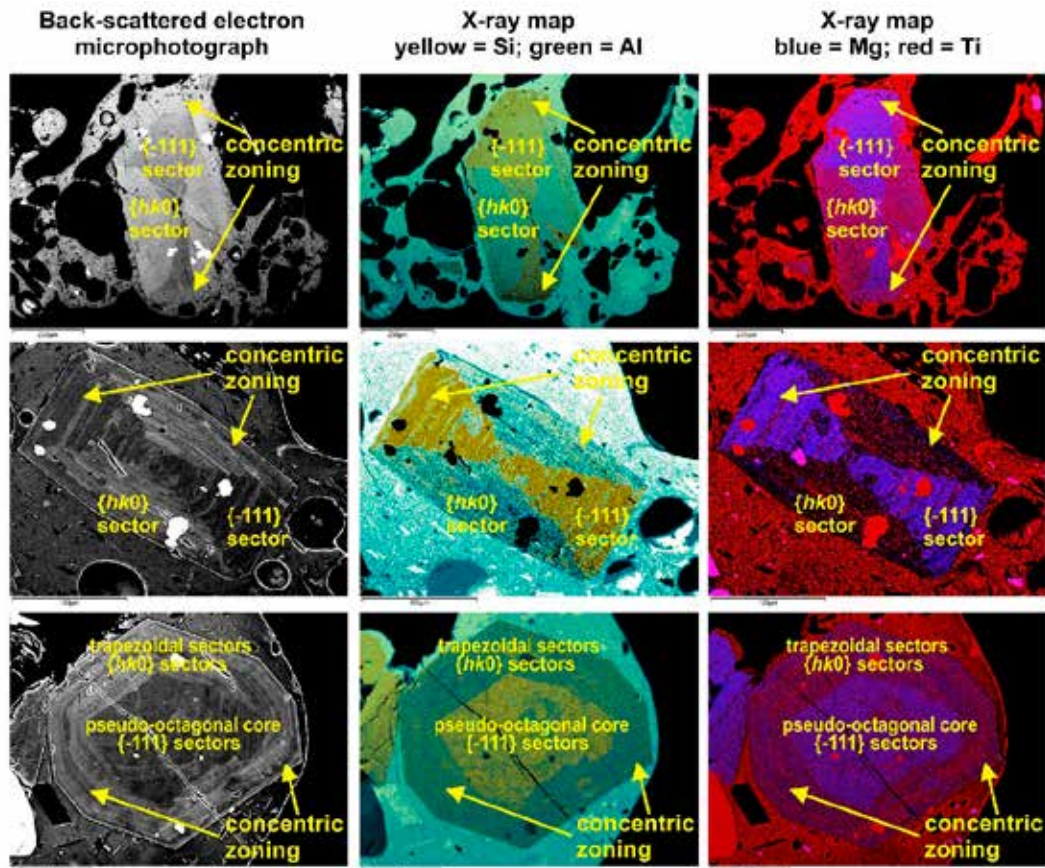


Figure 1
 BSE (backsattered electron) microphotographs and X-ray maps of colored two-band (Si + Al or Mg + Ti) images for clinopyroxene mesocrysts from 2021 lava fountains.

A REVIEW OF PLAGIOCLASE GROWTH RATE AND COMPOSITIONAL EVOLUTION IN MAFIC ALKALINE MAGMAS: GUIDELINES FOR MODELING PLUMBING SYSTEM DYNAMICS AT STROMBOLI AND MT. ETNA

Moschini P., Mollo S., Pontesilli A., Nazzari M., Petrone C. M., Fanara S., Vona A., Gaeta M., Romano C., Scarlato P.

Mafic alkaline magmas, such as those feeding the persistent eruptive activity of Stromboli and Mt. Etna volcanoes in Italy, are dominated by the crystallization of plagioclase via cooling and degassing phenomena related to the dynamics of shallow crustal reservoirs and eruptive conduits. Because plagioclase textures and compositions are extremely sensitive to the changes of intensive variables in subvolcanic plumbing systems, the phenomenological variability of erupted crystals preserves detailed evidence of complex growth histories. From this point of view, we reappraise the textural maturation and compositional complexity of plagioclase by allying thermodynamic and kinetic principles to natural and experimental observations. A multifaceted statistical method is adopted to parameterize the decay of crystal growth rate with increasing crystallization time, as relaxation kinetics prevails over melt supersaturation effects. This model parameterization is combined with the textural analysis of natural plagioclase crystals to quantify the residence time of phenocrysts in equilibrium with magmas at Stromboli and Mt. Etna and/or the timescale of rapid microlite growth during disequilibrium ascent of magmas within the conduit. The role played by temperature and melt-water content on plagioclase components and major cation substitution mechanisms is also evaluated under both isobaric-isothermal and decompression conditions. The emerging paradigm is that the influence of dissolved water on anorthite-albite exchange between plagioclase and melt is overwhelmingly mitigated by changes in temperature. As a corollary, anorthite and albite melt activities are almost fully encapsulated in the variation of anhydrous melt components as the crystallization of plagioclase proceeds during magma cooling. Key findings from our re-assessment of equilibrium, thermometric, and hygrometric models indicate that temperature and dissolved water can be iteratively estimated for different plagioclase textural patterns (Fig. 1) if crystals are sufficiently strongly zoned and probability-based criteria are applied to determine the maximum probability distribution from kernel density analysis.

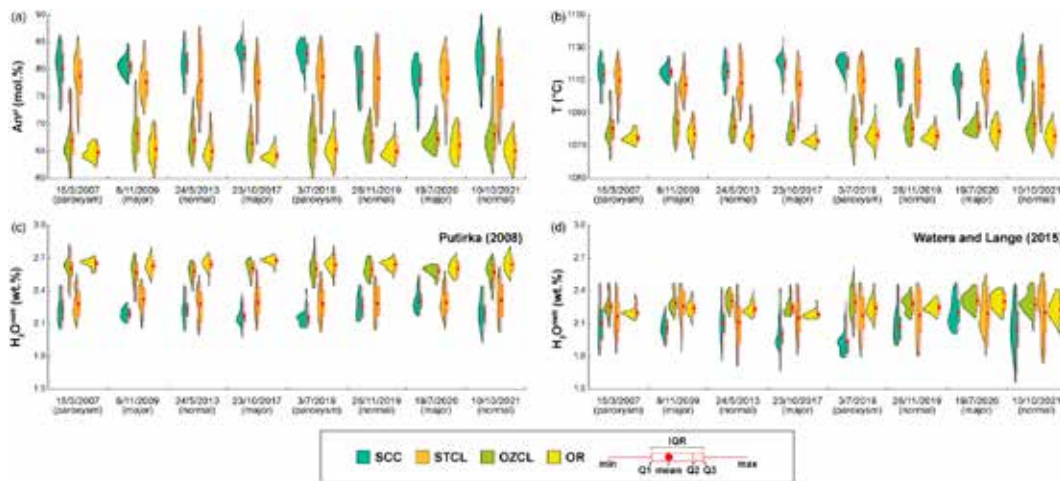


Figure 1

Violin plots and box plots for anorthite in plagioclase phenocrysts from 2007-2021 eruptions at Stromboli (a), temperature predictions (b), and melt-water content predictions (c and d). A kernel density estimation is used to visualize the underlying probability density function of each set of data in violin plots, whereas the statistical dispersion of data is illustrated by the box plot. The width of the box represents the interquartile range (IQR) extending from the first quartile (25th percentile Q1) to the third quartile (75th percentile Q3) and whiskers go from each quartile to the minimum or maximum. SCC, subrounded corroded cores. STCL, sieve-textured concentric layers. OZCL, oscillatory-zoned concentric layers. OR, overgrowth rims.

THE EFFECT OF CaO AND CaO+MgO ON THE VISCOSITY OF A PHONOTEPHRITIC MELT

Giuliani G., Di Fiore F., Valdivia P., Mollo S., Romano C., Di Genova D., Vona A.

The assimilation of carbonate rocks by magmas can dramatically change their chemistry and differentiation path, thereby affecting the rheological properties of the derived products. Here we present a set of viscosity measurements exploring the effect of variable degrees of carbonate assimilation on the melt viscosity (η) of a phonotephrite from Vesuvius (Italy). We doped the starting material with different amounts (0, 10, and 20 wt.%) of CaO and CaO+MgO, mimicking the effects of limestone and dolomite assimilation, respectively. Through this approach, we focused on the compositional change of the liquid phase, regardless of the effect of CO₂ bubbles produced by the decarbonation on the rheological properties. The high and low temperature liquid viscosity of the decarbonated melts were measured by concentric cylinder viscometry (CC) and differential scanning calorimetry (DSC), respectively (Fig. 1). Viscosity data show non-Arrhenian trends, well described by both Vogel-Fulcher-Tammann (VFT) and Mauro-Yue-Ellison-Gupta-Allan (MYEGA) equations. Trends obtained at high-T, low- η differ from those at low-T, high- η conditions. In the high-T regime, all decarbonated melts show lower viscosity than the pristine melt, the effect being more pronounced when only CaO is added. The opposite trend is observed in the low-T-regime, due to different fragility of the investigated melt. The most recent predictive viscosity models well reproduce the high-T, low- η regime, whereas modeled data are less accurate in the low-T, high- η regime. This discrepancy is apparently caused by the lack of decarbonated melt (i.e., Si poor, Ca-Mg-rich compositions) in the calibration dataset of viscosity models.

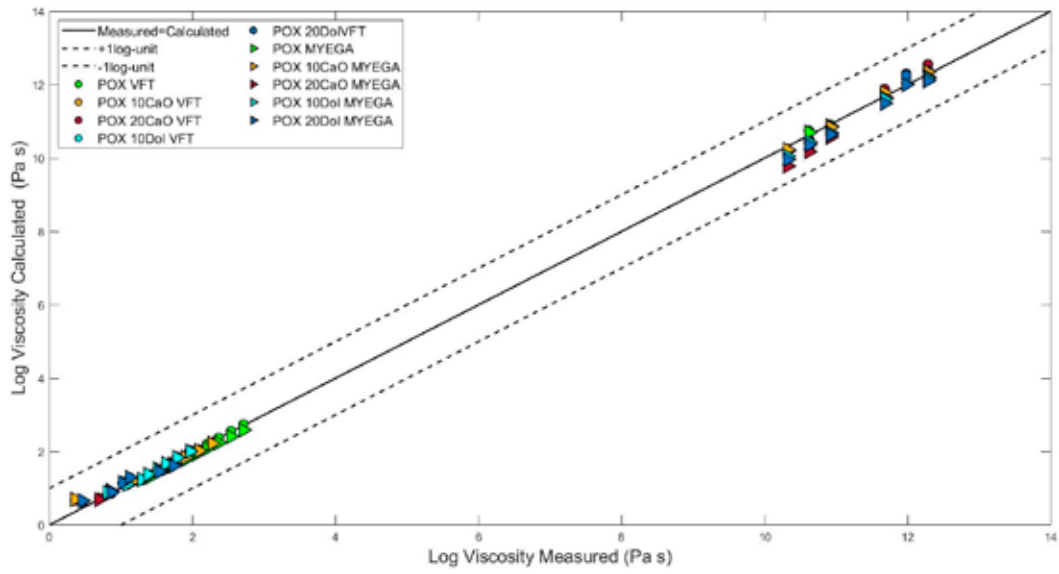


Figure 1
 Comparison of data obtained at high-T and low-T against the viscosity predicted by models. The prediction of viscosity is not as accurate, overestimating and underestimating it by ± 1 log (Pa s).

REASSESSING THE VOLCANIC HAZARDS IN THE CENTRAL ANATOLIAN VOLCANIC PROVINCE (TURKEY): CAN A MONOGENETIC TUFF CONE ERUPTION TRIGGER A CALDERA COLLAPSE IN ACIGÖL VOLCANIC COMPLEX?

Sunyé-Puchol I., Özsoy R., Aydar E., Miggins D., Akkas E., Bolós X., Nazzari M., Mollo S.

The Central Anatolian Volcanic Province (CAVP) is a 300-km-long volcanic field related to the subduction of the Neotethyan oceanic crust beneath the Anatolian block. This on-going subduction is the consequence of the convergence between the African-Arabian and Eurasian plates. Post-collisional magmatism in CAVP has produced numerous monogenetic centers, stratovolcanoes, calderas and widespread ignimbrites since late-Miocene (Fig. 1).

The most prominent are the extensively distributed Cappadocian ignimbrites, formed between ca. 10 - 2.5 Ma ago (9 different units that cover 20,000 km² with ~300 km³ of DRE). However, sources of these Neogene ignimbrites are still highly debated, as the area is generally covered by thick Quaternary tuffs that can hide the Cappadocian Ignimbrites former paleo-calderas. Two of these younger tuffs are the Lower and Upper Acigöl Tuffs (LAT and UAT; spread over 1000 km²), corresponding to late Pleistocene caldera forming ignimbrites erupted by Acigöl volcanic complex (VEI 6 eruptions produced at 190 ± 11 ka and 164 ± 4 ka, respectively).

It consists of a 150 km² rhyolitic field with a caldera of ~12 x 8 km, surrounded by mafic scoria cones and associated lava flows. The Acigöl tuffs are partially covered by monogenetic post-caldera volcanism (~26 to ~20 ka old): basaltic-andesitic maars and rhyolitic tuff cones filled by syn- to post-obsidian domes. Here we present field observations and tephrostratigraphic relationships documenting that Acigöl caldera collapses could be triggered by monogenetic tuff cone eruptions, also in agreement with glass chemistry and Ar⁴⁰/Ar³⁹ geochronological data. Therefore, for a better volcanic hazard assessment at Acigöl, we cannot exclude that a local monogenetic explosive eruption could prelude a caldera collapse and the following emplacement of large ignimbrites and/or fallout deposits in a much larger area.

Considering the slab window and the influx of asthenosphere below the CAVP, the low-velocity anomalies, the shallow Curie depths (8–12 km), the widespread geothermal activity in and around the Acigöl volcanic complex, and its long-lived magmatic activity, further geophysical and volcanological studies should be planned to investigate the state of the underground volcanic system and the likelihood of a potential future volcanic eruption.

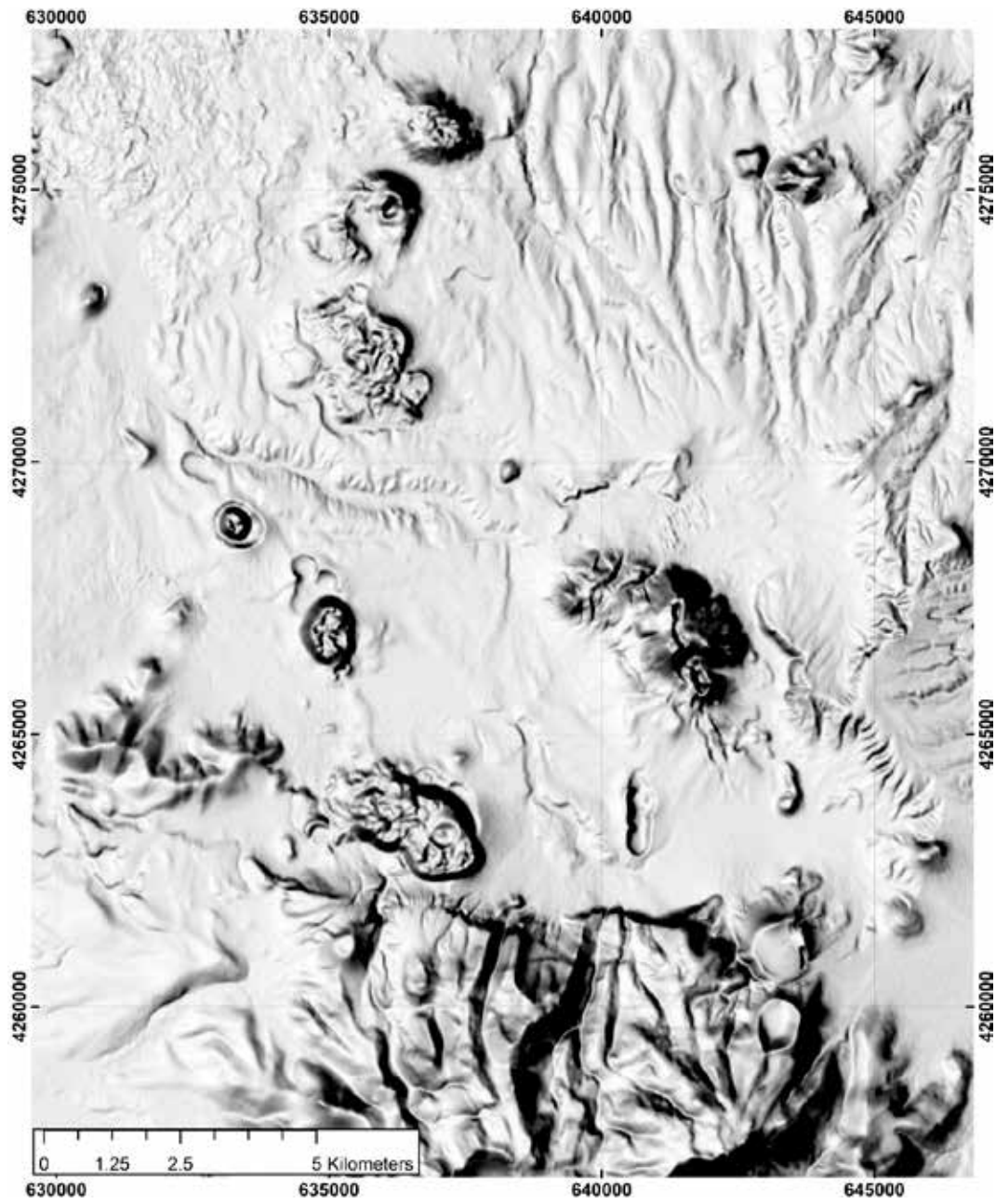


Figure 1
Central Anatolian Volcanic Province (CAVP) - Acigöl.

VOLCANIC RECONSTRUCTION OF THE BELBAŞHANI VALLEY IN THE CENTRAL ANATOLIAN VOLCANIC PROVINCE (CAVP), TURKEY

Özsoy R., Sunye-Puchol I., Aydar E., Pedrazzi D., Akkaş E., Nazzari M., Mollo S.

Central Anatolian Volcanic Province (CAVP) hosted numerous monogenetic vents, plateau lavas, wide and mostly buried calderas and extended depression fields with active Quaternary stratovolcanoes which have carried out explosive eruptions until the present days.

The complex eruptive history of Hasandağ stratovolcano from the 2.5 Ma year to the present has been represented by several ignimbrites, and block-and-ash flows, with thick pumice and ash-fall deposits. In this work, we present a detailed stratigraphy of Belbaşhani valley, glass geochemistry, which consists of three different pyroclastic deposits or tuffs.

Each tuff is separated by paleosol, which indicates hiatus. The oldest tuff deposit shows a parallel-stratified that consists, in the lower part, of poorly consolidated massive lapilli tuff, with the presence, in some part, of a lithic breccia level with diffuse parallel stratification. The middle part of this deposit consists of gray pumice fall-out displaying fine to medium lapilli with two thin levels of fine-ash-rich deposits intercalated.

At the top, there is a sequence of cross-stratified fine-ash intercalated with pumice-rich lapilli tuff. The base of the second tuff deposit consists of a well-classified, clast-supported, pumice layer, deposited over an eroded surface at the top of the first paleosol.

At the top, this member changes to a poorly consolidated massive lapilli tuff. The last eruption is the Belbaşhani Pumice dated 339 ± 50 k.a which has been recently identified as a large pumice fallout deposit. At the bottom, this pyroclastic unit has a 3-m thick massive and well-classified medium to coarse pumice fall-out deposit with larger clasts up to 50 cm in diameter, which moves to a 3.5-m thick parallel-stratified coarse to medium lapilli pumice at the upper part. The glass composition of the Belbaşhani Pumice is rhyolitic, but less than Hasandağ pyroclastic deposits, whose compositions in major elements follow different trends. The preliminary physico-chemical study, the Belbaşhani Pumice could be associated with the Ulukışla magmatic system instead of the Hasandağ volcano. In this perspective, glass chemistry is important to contribute tephrostratigraphic framework, which could be used to synchronize sedimentary sequences and to perform paleoenvironmental/paleoclimatic reconstruction and/or archaeological studies.

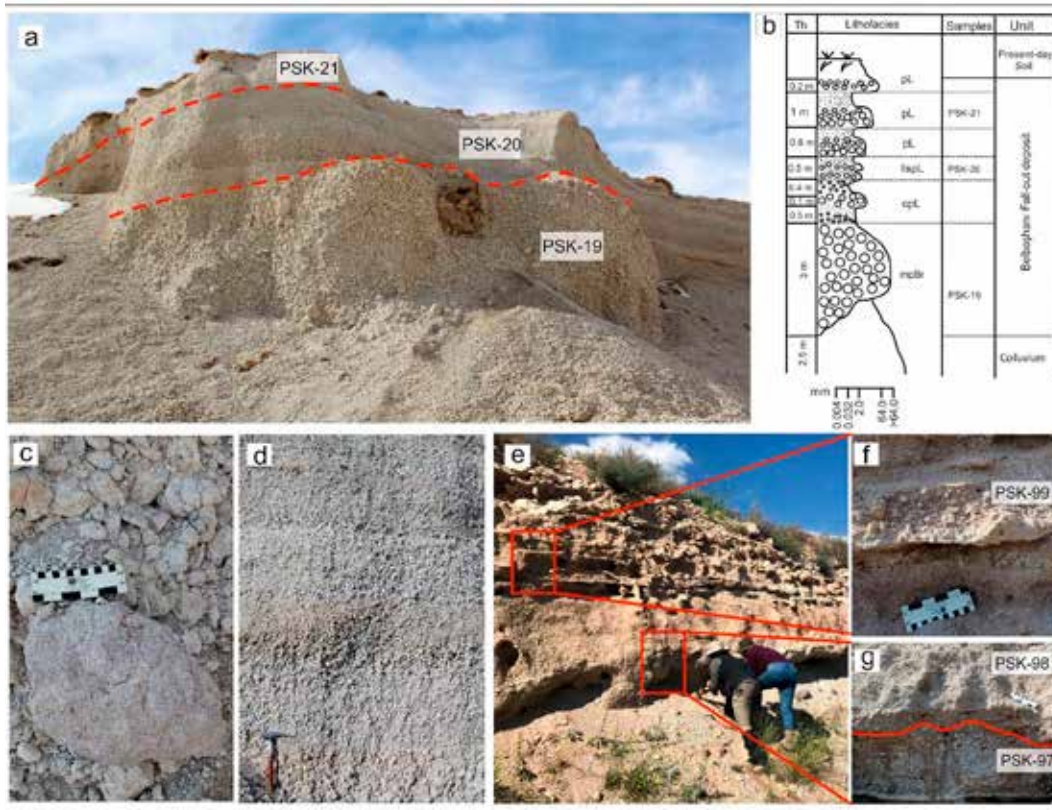


Figure 1

Belbaşanı Pumice deposit (a), stratigraphic column logged in the Belbaşanı quarry (b), and detail of a >50 cm pumice block at the bottom of the unit (c), stratified pumice lapilli at the top of the sequence (d), Altınhisar-Çiftlik road outcrop (e), and detailed photos showing textural characteristics of Altınhisar-Çiftlik road deposit (e and f).
 Th= Thickness; llspl= Parallel-stratified pumice lapilli; cpL=Coarse pumice lapilli; pL= Pumice lapilli; mpBr= Massive pumice breccia.

CARBONATITIC MAGMATISM: THE MT. VULTURE VOLCANO CASE

Carnevale G., Caracausi A., Rotolo S.G., Paternoster M., Zanon V.

A large set of chemical analyses of the mantle xenoliths-forming minerals (olivine, orthopyroxene, clinopyroxene) from products erupted during the last volcanic activity of Mt. Vulture volcano (140 ka) fed by a melilitite-carbonatite magma was performed, with the aim to improve the knowledge of the volcano plumbing system, and with considerations about carbonatitic magmatism and its mantle source.

We analysed lherzolite, dunite, clinopyroxenite, and wehrlite samples, these latter particularly important to discuss the process of “wehrlitization” of the mantle peridotite, as a consequence of the interaction with the carbonatite melt, the main metasomatic agent of the mantle metasomatism. Results show the presence of Mg-rich olivine (Fo_{88-91}), high values of MgO in orthopyroxene ($Mg\# = 0.89-0.90$) and clinopyroxene (Cr-diopside) ($Mg\# = 0.88-0.91$), and this latter, if plotted onto a $Mg\#$ vs. Ca/Al diagram, falls into the mantle-related carbonate metasomatism field. Moreover, the application of geothermobarometers based on the coexistence of two pyroxene pairs, and on Cr content in olivine and clinopyroxene, permitted to estimate a range of temperature ($T = 992-1155$ °C) and pressure (15-22 kbar), resulting in the same range of previous studies. Thus, the minero-chemistry of every single mantle xenolith, allows us to better describe the mantle source beneath the Mt. Vulture volcano in the context of the geodynamical evolution of the central Mediterranean (Fig. 1), integrating our previous detailed petrographic and micro-thermometric study on armoured mantle ultramafic cores (erupted as pelletal lapilli).

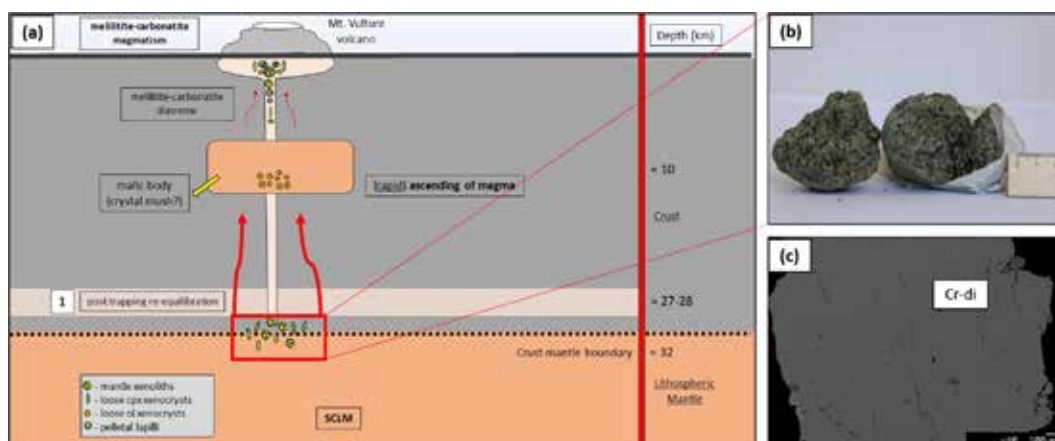


Figure 1

Simplified cross section of Mt. Vulture volcano with a particular ponding stage at the local crust-mantle boundary and the involvement of a carbon-rich subcontinental lithospheric mantle (a). Detail of a well-preserved spinel lherzolite from Mt. Vulture (b), and a SEM image of a Cr-diopside (c).

PETROLOGY AND GEOCHEMISTRY FROM BRANSFIELD STRAIT (ANTARCTICA) SUBMARINE VOLCANISM. EVIDENCES FROM VOLATILES (HE, NE, AR, O, H), MAJOR AND TRACE ELEMENTS

Polo Sánchez A., Caracausi A., Álvarez-Valero A M., Geyer A., Insinga L., Nazzari M.

Bransfield Strait, located NW Antarctica, is a back-arc basin that resulted from the subduction between the Phoenix and the Antarctica plates. Its interest is due to the fact that it is one of the scarce places accessible to study Antarctic volcanism. It hosts several submarine volcanoes (Edifice A, Edifice C, Three Sisters, Orca, Hook Ridge) and two subaerial islands (Deception Island, Bridgeman Island) along its main spreading axis. Deception Island is one of the most active volcanoes in Antarctica and is very well characterized, but also the submarine edifices seem to be active and are less studied. Orca volcano suffered a seismic unrest in 2020 associated with magma intrusion; and Three Sisters and Hook Ridge show hydrothermal episodes linked to recent activity in the 2000 decade.

The aim of this project is to explore and characterize the magmatic source conditions of the submarine volcanoes of Edifice C, Three Sisters, Orca and an unnamed seamount by analysing Noble Gas (He, Ne, Ar) and Stable Isotopes (H, O) from the inclusions hosted within olivine phenocrysts and glass shards. And major and trace elements within the hosting materials. Noble Gas analysis have been performed at INGV-Palermo and Stable Isotopes analysis at the University of Salamanca (Spain). Major elements were performed at the HP-HT laboratory employing a JEOL-JXA 8200 electron microprobe. This analysis also served as internal standard to perform the trace element analysis at the University of Perugia.

Glass shards have a basaltic andesitic / trachybasaltic andesitic composition and a subalkaline character (Fig. 1), while olivine phenocrysts show Mg-rich restricted compositions (Fo_{87-91} , Fig. 1). Glass shards agree with previous petrological results. Nevertheless, no previous study on the olivine phenocrysts was made before. Compared with Deception Island, the glass shards are less evolved and more depleted in alkaline elements; and the olivine phenocrysts are much richer in Mg in the submarine volcanoes than in Deception Island. The differences between the submarine volcanoes and Deception Island may be due to higher mantle melting degree or to deeper mantle sources at the submarine volcanoes. On the other hand, the restricted range of compositions in the submarine volcanoes point to a common source or process along Bransfield Strait.

This project falls within the frame of the PhD project of Antonio Polo Sánchez funded by Programa Propio III Universidad de Salamanca and Banco de Santander (Spain); and by a Joint COMNAP-IAATO Antarctic Fellowship 2022. It is also supported by the research projects: ERUPTING (PID2021-127189OB-I00) MCIN/AEI/10.13039/501100011033, HYDROCAL (PID2020-114876GB-I00) MCIN/AEI/10.13039/501100011033 and VOLGASDEC (PGC2018-095693-B-I00) (AEI/FEDER, UE).

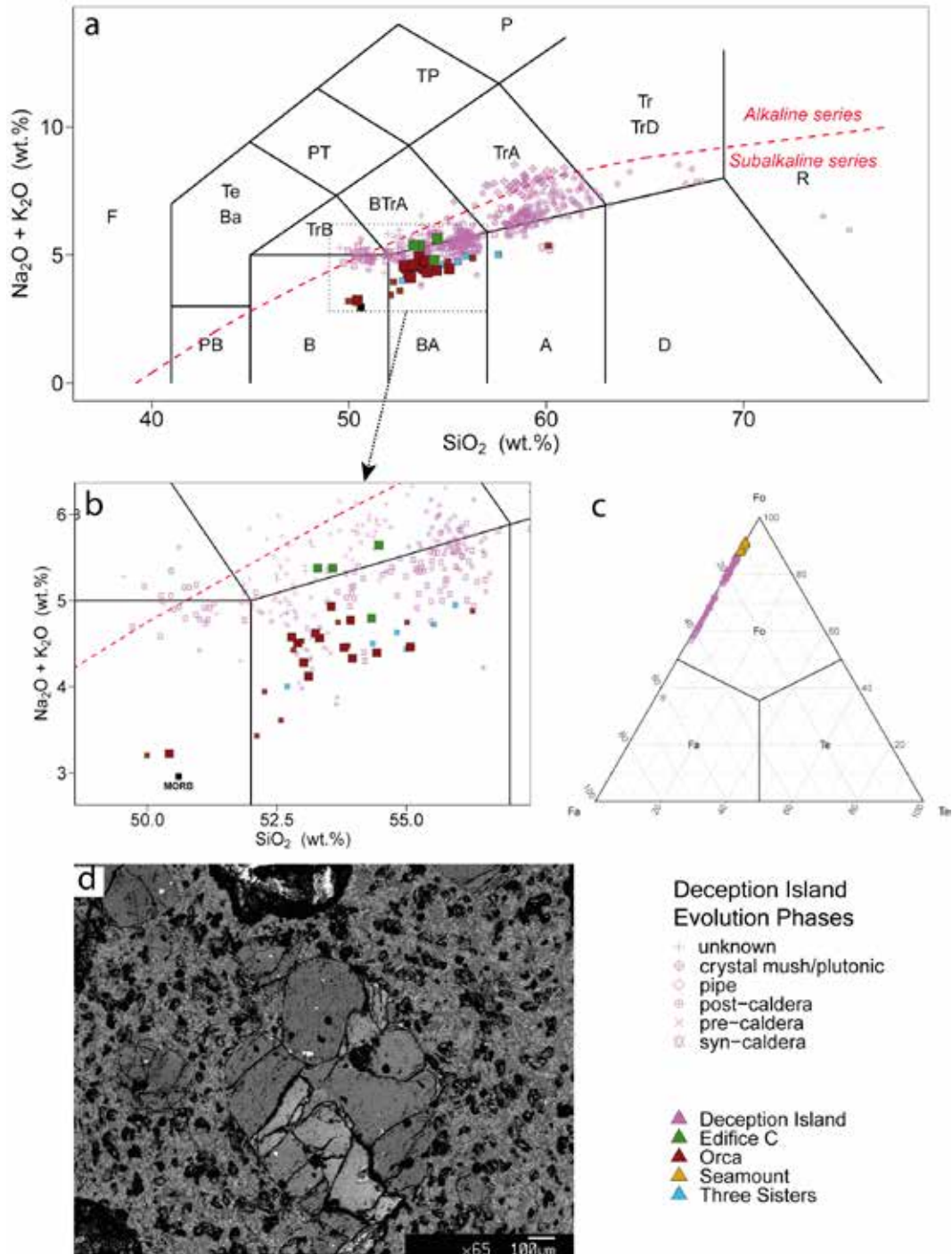


Figure 1 Central Anatolian Volcanic PGlass shards compositions according to the TAS diagram (a,b). Olivine compositions (c). Back Scattered Electron (BSE) image of an olivine phenocryst (d). Deception Island data from Geyer et al., (2019).

ZONING PATTERNS OF CLINOPYROXENE AND MAGMA CHAMBER NUMERICAL SIMULATION RECORD DYNAMICS AND TIMESCALES OF MAFIC-SILICIC MAGMA INTERACTION IN THE PLUMBING SYSTEM OF ZARO (ISCHIA ISLAND, ITALY)

Pelullo C., Arienzo I., Brown R.J., Chakraborty S., D'Antonio M., de Vita S., D'Oriano C., Mark D.F., Montagna C., Nazzari M., Pappalardo L., Petrosino P.

In the framework of the “Tifeho project”, aiming at reconstruct the structure, growth and evolution of the magmatic feeding system/s of some eruptions originated from the Campania Volcanic area, the WP3 focuses on the quantification of timescales of magma chamber processes before eruptions. For this purpose, detailed mineral compositions of major and minor elements (Si, Ti, Al, Fe, Mg, Mn, Ca, Na, K, Ni and Cr) have been acquired along core-to-rim transects of zoned clinopyroxene crystals of products belonging to the Zaro lava complex (<7 ka; Ischia island, South Italy; Fig. 1a-b). The data were collected at the HP-HT Laboratory of Experimental Volcanology and Geophysics of the Istituto Nazionale di Geofisica e Vulcanologia in Rome (Italy), using a Jeol-JXA8200 electron microprobe equipped with five wavelength dispersive spectrometers. Chemical and isotopic characteristics of the Zaro lava and hosted mafic, intermediate and felsic enclaves suggest mixing/mingling processes occurred before eruption. This finding is supported by both the zoning pattern of Zaro clinopyroxene crystals and numerical simulation of magma chamber dynamics. Three distinct compositional populations, named ME0 to ME2 at decreasing Mg#, have been recognized, with significant differences among clinopyroxene of the various lithotypes (Fig. 1c). The relationships among the compositional populations detected in the zoning pattern allowed reconstructing the sequential growth of crystals at different T-P conditions and record the growth of crystals during the mixing between a shoshonitic and a trachytic magma.

Results of numerical simulations of a single magma input show efficient mingling dynamics between the two magmatic components in the Zaro plumbing system occurring on relatively short timescales of some hours (Fig. 1d). Moreover, the modeling results predict accumulation of mafic magma at the top of the plumbing system, giving rise to typical mingling patterns very similar to those observed in the field. Lastly, the application of diffusion modeling (Fig. 1b) allowed estimating the duration of the whole magma recharge processes that may have occurred several times in the timespan from decades to months preceding the eruption.

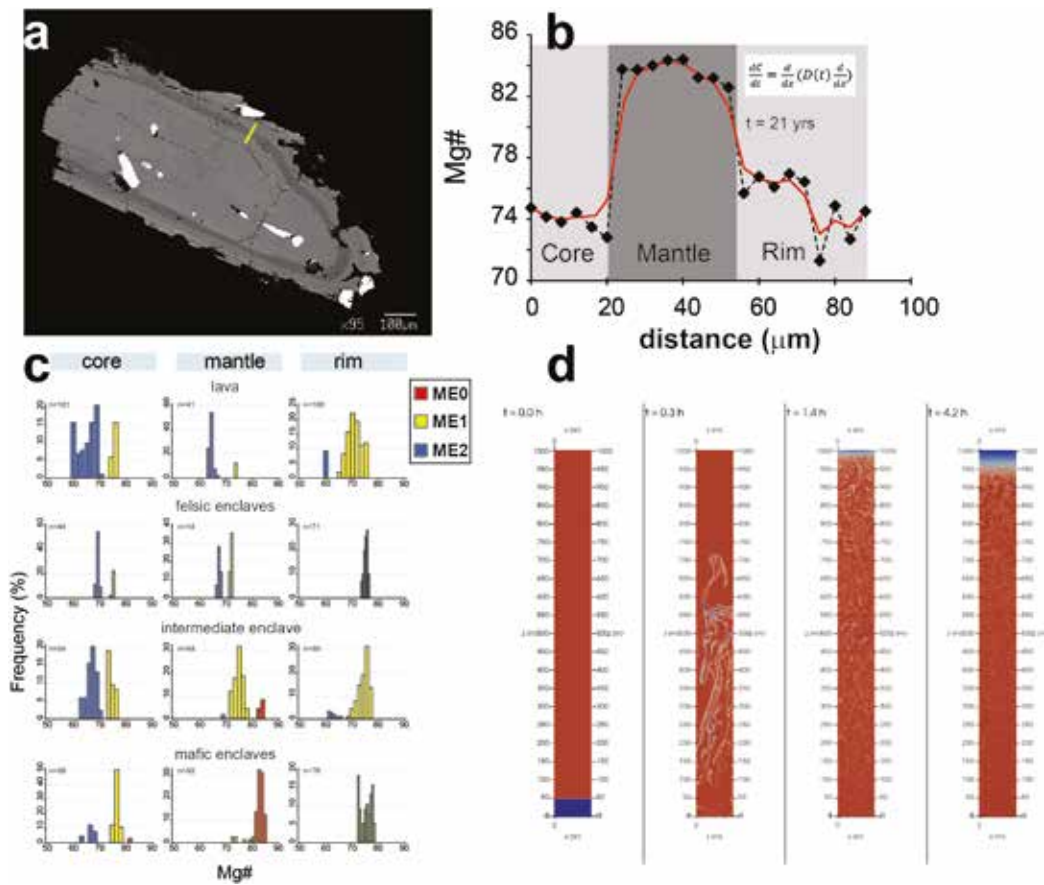


Figure 1
 a BSE image of a zoned clinopyroxene crystal from the Zaro lava complex; b Mg# [molar $Mg^{2+}/(Mg^{2+}+Fe_{tot})$] concentration profiles from core to rim of the clinopyroxene shown in Fig. 1a. Black diamonds are points measured along the crystal traverse. Black dashed lines indicate the inferred initial profile shapes. The modeled profiles (red lines) show the diffusive smoothing that the concentration gradient have experienced; c Mg# frequency histograms of core, mantle and rim of the clinopyroxene crystals from the various Zaro lithotypes; d Results of the numerical simulation of the evolution of composition (in terms of end-members weight fractions) in time in the simulated Zaro plumbing system.

GEOCHEMICAL CHARACTERIZATION OF OLD (>100 KA) TEPHRA OUTCROPPING AT BAIA DEGLI INFRESCHI (SALERNO, SOUTH ITALY)

Pelullo C., Arienzo I., Doronzo D., Sparice D., de Vita S., Di Vito, M.A., Zanchetta G.

The Campania Plain (South Italy) has been the site of volcanism for at least 300 kyrs with occurrence of many large-volume ignimbrite eruptions. Despite this significant activity, most of the knowledge about past volcanic activity of the Campania Plain is based on studies of products recognized in distal marine and terrestrial successions as key tephra markers (C-22, X-5 and X-6) of the Mediterranean MIS 5 period, attributable to several high magnitude oldest events originated in Campania.

In the framework of the TIFHEO project, aimed at investigating the activity of Campi Flegrei before the Campanian Ignimbrite eruption (CI; 39.88 ± 0.17 ka) eruption, a field survey focused at collecting samples of volcanic units older than the CI was performed at Baia degli Infreschi (Cilento coast, Salerno). In this locality, a tephra layer from a sedimentary succession has been sampled and according to its stratigraphic position, the age of the tephra is older than 100 ka. The Sr isotopic composition of feldspar crystals from this sample has been analyzed at the Radiogenic Isotope Laboratory of the Istituto Nazionale di Geofisica e Vulcanologia (INGV)-Osservatorio Vesuviano, while the juvenile fraction of pumice fragments extracted from the tephra have been analyzed for major elements at the HP-HT Laboratory of Experimental Volcanology and Geophysics of the INGV-Roma 1. The "Infreschi" sample has a composition overlapping the boundary between phonolite and trachyte fields of the Total alkali vs Silica classification diagram. SiO_2 content of the tephra pumices are in the range 64.8-60.2 (wt%), CaO content varies between 2.5 and 1.3 (wt%). Na_2O and K_2O contents range from 7.9 to 4.3 (wt%) and from 9.2 to 5.6 (wt%), respectively. Al_2O_3 and TiO_2 range between 19.5 and 18.2 (wt%) and between 0.9 and 0.2 (wt%), respectively. FeO content is in the range 3.8-2.7 (wt%) and MgO content is in the range 0.94-0.2 (wt%). The pumice sample displays a low $\text{K}_2\text{O}/\text{Na}_2\text{O}$, typically ≤ 1.8 and a CaO/FeO ratio in the range 0.4-0.7.

The "Infreschi" tephra can be attributed to the Campi Flegrei volcanic activity and its major elements content well match the composition of the X-6 tephra marker recognized in distal marine and terrestrial successions of the Mediterranean area.

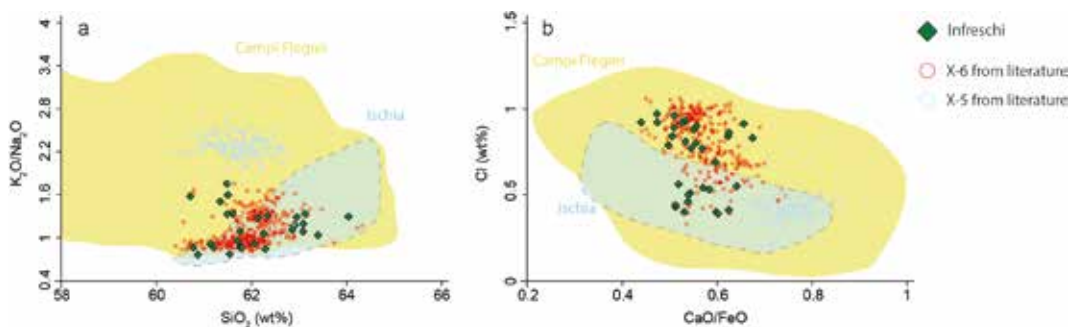


Figure 1

a) $\text{K}_2\text{O}/\text{Na}_2\text{O}$ vs SiO_2 and b) Cl (wt%) vs CaO/FeO variation diagrams of glass juvenile fraction of the analyzed tephra from Baia degli Infreschi compared to the pre-CI tephra markers (X-5, X-6) and to Campi Flegrei and Ischia glass compositional field.

TEPHROCHRONOLOGICAL STUDY OF THE LACUSTRINE SUCCESSION OF THE CASTIGLIONE MAAR (CENTRAL ITALY) AND EVALUATION OF THE POSSIBLE IMPACT ON THE CLIMATE OF THE EXPLOSIVE ERUPTIONS OF THE PERITHYRRENIC VOLCANOES

Di Roberto A., Scateni B., Re G.

The research activity is part of the multidisciplinary project AMUSED: A MULTidisciplinary Study of past global climatE changes from continental and marine archives in the Mediterranean region (Environment Department Project-INGV). The project has as its ultimate goal to reconstruct climate variability in the central Mediterranean region during the middle-late Quaternary, with a special focus on the Holocene.

The activity carried out concerns the tephrochronological study of a continental sediments succession sampled in the Castiglione maar (Central Italy), located 20 km east of Rome along the ancient Via Prenestina where two parallel 120 m-long cores, one 15-m long core were drilled, spanning last ~280 kyr and ~12 kyr respectively and two 12 m-long and 3 m-long cores at the edge of the basin were performed.

In the last 20 years, "tephrochronology", ie the use of volcanic ash (tephra) as an isochronous (ie as a time marker), has been shown to provide high temporal and stratigraphic resolution information crucial for the dating, correlation and synchronization of archaeological, geological, paleoecological and paleoclimatic records. In fact, the main feature of tephra is to deposit almost synchronously over large areas, forming a level that has an almost identical geological age in all the sites where it is identified (isochronous). The age of the eruption that produced the tephra can be determined in various ways, the most common of which include the dating of some minerals contained in the tephra (e.g. potassium feldspar) with methods such as $^{40}\text{Ar} / ^{39}\text{Ar}$ and K / Ar . The age obtained is then transferred to the succession in which the tephra are interspersed. Tephrochronology, therefore, can implement or sometimes replace the classic dating methods that have time limitations (for example the ^{14}C method can be used for materials no older than ~ 50,000 years).

The study of tephra provides very important information also from the volcanological point of view. By studying the physical characteristics of tephra (granulometry, texture, etc.), their mineralogy and in particular the chemical composition of the volcanic glass (major elements, trace elements and isotopes) it is possible to identify the volcanic source and the eruption that produced the tephra. Tephrochronological studies therefore allow for information on the eruptive frequency of a given volcano, on the eruptive dynamics or on the geochemical evolution of the source.

Due to its geodynamic structure and the great abundance of active volcanoes, the Mediterranean area has always been considered an ideal area for the development and application of tephrochronology. The intense explosive activity of the perithyrrenic volcanoes and the Hellenic arc produced a large number of tephra levels that are interspersed in the continental and marine sedimentary sequences.

Within the project, the major-element glass compositions were determined on 40 tephra layers bearing fresh volcanic glass at INGV HPHT Laboratory in Rome, using a JEOL JXA 8200 electron microprobe (EPMA) equipped with five wavelength-dispersive spectrometers.

The major elements glass compositions of tephra from the Castiglione maar sequence were compared with literature data including the composition of proximal pyroclastic deposits erupted during the explosive activity of volcanoes from central Italy and the composition of the tephra markers identified in other records of central Italy as the Fucino basin, the Lago Grande di Monticchio and marine sediment cores from the Tyrrhenian sea.

For most of the studied tephra, the volcanic source was identified; these resulted in the Alban Hills (last two eruptive cycles), Sabatini, Vico, Ischia and Latera-Vulsini volcanic complexes. Some tephra layers remain still undetermined even if their general geochemical affinity indicates the volcanoes of central Italy as the most probable source.

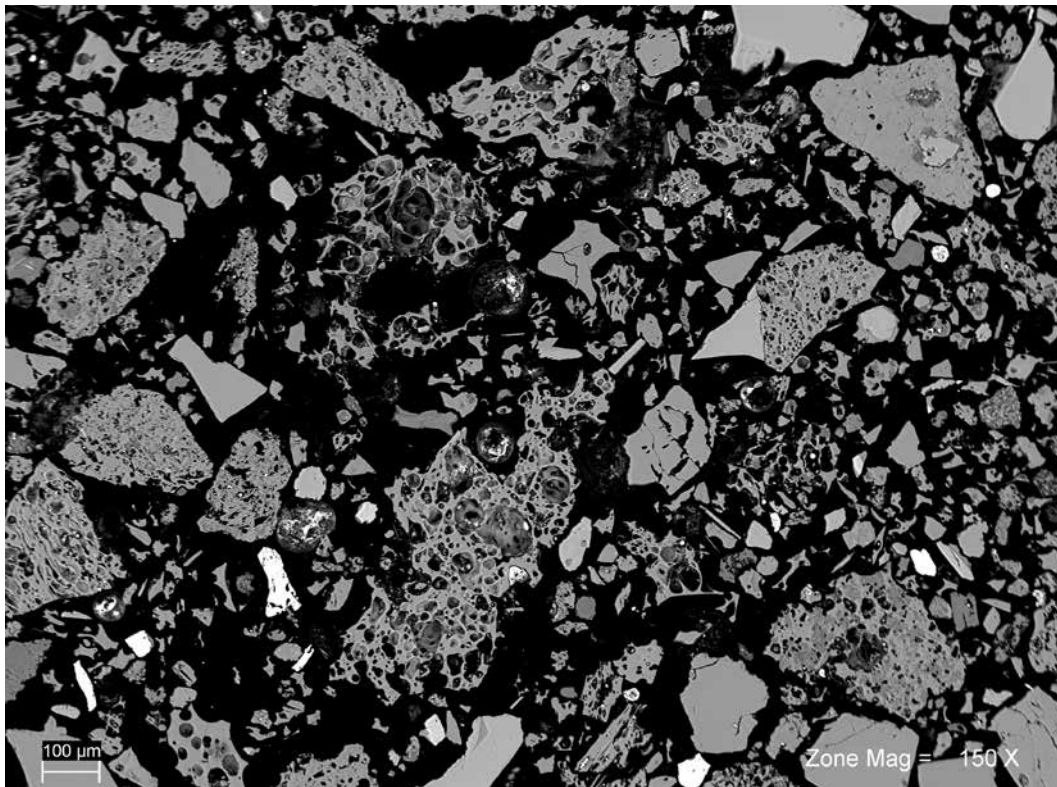


Figure 1
Image in back-scattered electrons (BSE) mode of tephra layer collected with a scanning electron microscope (SEM) Zeiss EVO MA at the INGV of Pisa.

PRELIMINARY BUBBLY FLOW ANALYSIS FROM A 2D ANALOGUE SETUP AND HIGH-SPEED SCHLIEREN SHADOW PHOTOGRAPHY

La Spina G., Spina L., Pennacchia F., Scarlato P., Taddeucci J.

For low viscosity magmas such as basalts, rapid and unpredictable transitions between effusive and explosive activity may occur. These transitions dramatically alter the impact of an eruption and pose a real challenge to policymakers tasked with mitigating the risks associated with basaltic eruptions. Mechanisms controlling these transitions, however, are not well understood, mainly due to the lack of a clear understanding of basaltic magma fragmentation.

The new Marie Skłodowska-Curie Individual Fellowships ENDGAME (started on 09/2022) aims to investigate transitions in eruptive styles at basaltic volcanoes by studying fragmentation of basaltic magmas through a combination of targeted cutting-edge fluid dynamics experiments, new holistic numerical modeling of magma ascent and brand-new field observations collected during a basaltic eruption.

One of the objectives of ENDGAME is to define new constitutive equations for basaltic magma fragmentation by implementing and performing 2D/3D jet flow and shock-tube experiments with a bubble- and particle-bearing analogue material in combination with high-speed Schlieren shadow photography.

We performed preliminary tests aimed to prove out the configuration of the under-construction large 2D apparatus in combination with the Schlieren shadow-photography and high-speed cameras. We created a small 2D setup using either 2 parallel glass sheets (3 mm thickness, 20 cm length) or 2 parallel Plexiglas sheets (10 mm thickness, 20 cm length) separated by rubber seals and filled with a viscous liquid (Fig. 1a). The liquid was obtained by mixing hair gel (Grafic Gel Aqua Extraforte, Garnier) and distilled water with different proportions. We also used a small spherical mirror (7.5 cm diameter, 75 cm focal length, Fig. 1b) and a high-speed camera (Fig. 1c). Air was injected into the 2D setup through a capillary tube connected either to a syringe or to a continuous gas supply and a flowmeter to control the air flow (Fig. 1d). We investigated several flow rates of air, between 5×10^{-3} and 15×10^{-3} l/s.

Preliminary results show that we can see density perturbations within both water and a viscous liquid, using either the 3 mm glass sheets or the 10 mm Plexiglass sheets. Furthermore, we can observe shock waves propagating inside large bubbles when coalescence is occurring (Fig. 2), likely due to the rupture of the bubble wall. Our results demonstrate that we can properly set up the Schlieren shadow photography in combination with a high-speed camera and see the density perturbation within a viscous fluid and shock waves propagating within large gas bubbles. Starting from this setup, we implemented the new large apparatus for the 2D jet flow and shock-tube experiments, which will be tested soon. By adopting at first a 2D geometry we will simplify the visualization of the phases within the fluid, allowing a better understanding of the fragmentation process. As a result, the quantification of the internal properties of the fluid will become more accessible, allowing us to formulate an initial set of equations for basaltic magma fragmentation, that will be then adjusted/validated using the 3D setup.

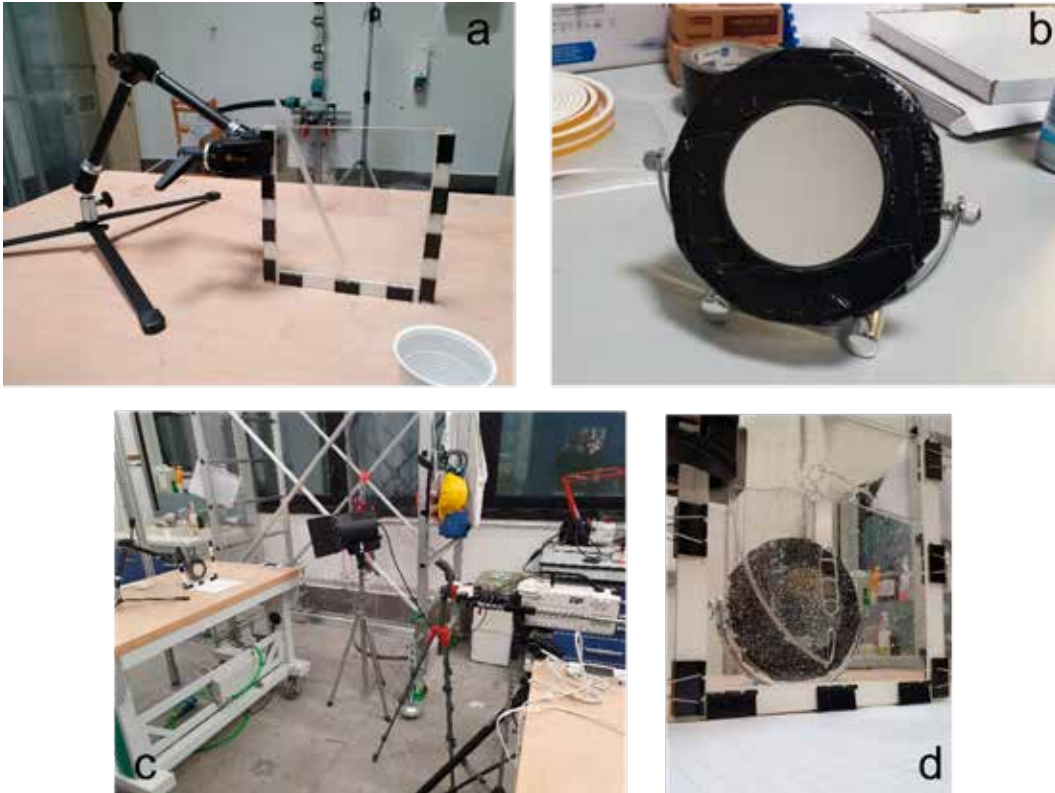


Figure 1
Preliminary setup of the small 2D apparatus with the high speed Schlieren shadow photography: a) 2D setup obtained using 2 parallel glass sheets (3 mm thickness, 20 cm length) separated by rubber seals; b) spherical mirror (7.5 cm diameter, 75 cm focal length); c) complete setup with the high speed camera on the right and the 2D analogue setup on the left; d) picture of the 2D setup during while injecting air into a viscous fluid.

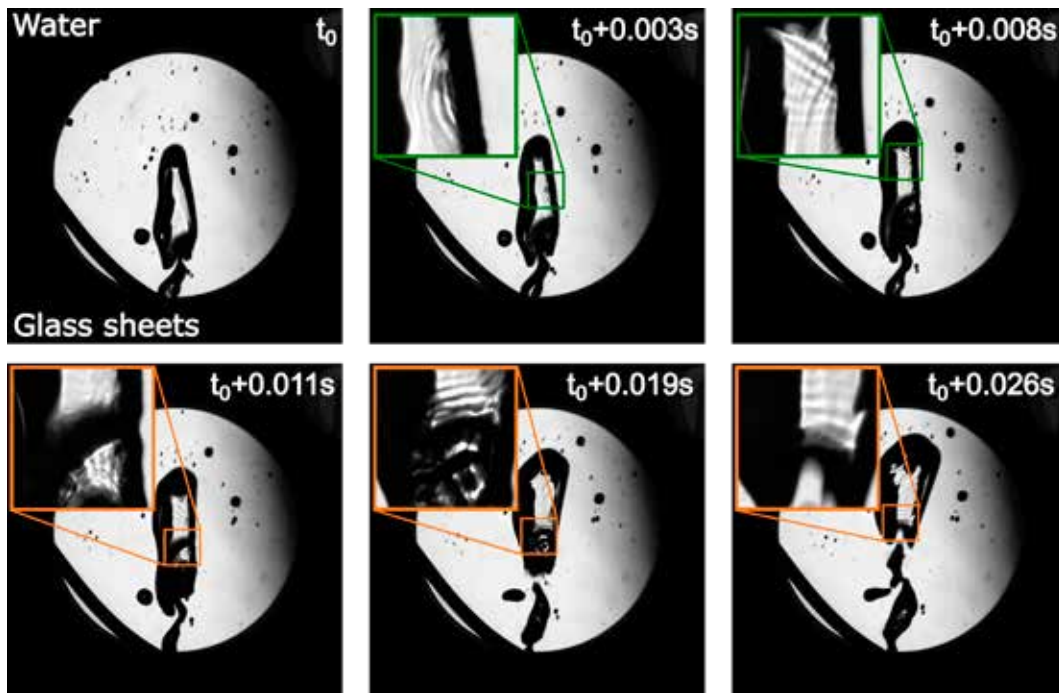


Figure 2

Images collected during an experiment with the 2D setup and the high-speed Schlieren shadow photography. Within the large bubble we can observe the formation of shock waves, propagating inside the bubble (top panels). We can also observe the shock waves resulting from the coalescence of two bubbles, likely due to the rupture of the bubble walls (bottom panels).

GEOCHEMISTRY OF ASH LEACHATES DURING THE 2021 ERUPTION OF CUMBRE VIEJA VOLCANO, LA PALMA, CANARY ISLANDS

Bagnato E., Cinti D., Pennacchia F., Del Bello E., Ricci T., Scarlato P., Taddeucci J.

On September 19, 2021, a new eruption began at the western flank of Cumbre Vieja volcano (La Palma, Canary Islands; Fig. 1a), after an inter-eruptive period of 50 years from the previous one (Teneguía, October 1971). The new event was classified as a basaltic fissure type eruption, dominated by strombolian activity and episodic phreatomagmatic pulses. During the most explosive phases, fine ash particles (less than 2 mm in size) were frequently dispersed for greater distances from the eruptive center. Adsorption onto ash particles is an important sink for volcanic volatiles released during eruptions. Ash leachates are key sources of information on eruptive plumes as their compositions are thought to reflect, at least to some extent, the composition of itself. Consistently, their volatile ratios (e.g., S/Cl, Cl/F, S/F) are used to identify changes in eruptive style. In this report we briefly present the leachate analyses of volcanic ashes from the beginning of the 2021's Cumbre Vieja eruption, aimed at determining the relationship between chemical composition of water-soluble components adhering to volcanic ash and the volcano's activity episodes. Ash samples have been provided by the colleagues of INVOLCAN (Instituto Volcanológico de Canarias) who posed a few ash-collecting stations at different distances from the main eruptive vents. In detail, we leached ash samples from the AS2 and AS5 stations, sited at about 1 km from the vents, in the West and East side, respectively. Water-extractable concentrations of the ash samples leached at 1:25 for 2 hours were analyzed by ion chromatography for major ions (Cl⁻, SO₄²⁻, F⁻, Na⁺, Ca²⁺, Mg²⁺, K⁺). The most abundant components in ash leachates are SO₄²⁻ for the anions and Na⁺ for the cations, with mean concentrations of 782 and 317 microg/g_{ash} and 473 and 315 microg/g_{ash} for the stations AS2 and AS5, respectively. Fluoride is an element of primary concern for human and animal health, showing a mean composition in ash leachates of 150 microg/g_{ash}. Indirect information on the chemicals deposited as mineral films on the surface of ash grains can also be derived from scatterplots correlating the molar abundances of cation and anion species in ash leachates. In particular, our data demonstrate that Na and Cl in Cumbre Vieja's ash leachates correlate strongly ($r_2 = 0,72$) (Fig. 1b), as do Ca and SO₄ ($r_2 = 0,82$) (Fig. 1c), suggesting that the higher the availability of acidic gases (SO_{2g} and HCl_g) in the plume, the more favorable is the extraction of cations from dissolving ash fragments, followed by precipitation of CaSO_{4(s)} (Anhydrite or Gypsum) and NaCl_(s) (Halite) on ash surfaces. However, an additional input from the sea spray has not to be excluded. The S/Cl molar ratio in the ash leachates from the 2021 eruption ranges from 0.14 to 5 and the observed values > 3 suggest to be related to ash-rich phases of the eruption. Besides, S/Cl and S/F molar ratios measured in the Cumbre Vieja's ash leachates fall in the range proposed for the divergent volcanism's bulk gas signature (i.e. volcanological origin of the detected chemicals) (Fig. 1d).

This supports a prevalent volcanogenic origin of the two elements and confirms that adsorption of plume acidic gas species (e.g., SO_{2g} and HCl_g) onto volcanic ash is among the key controlling factors on ash leachate chemistry, as also documented at other volcanoes. These preliminary results show significant temporal variations in ash leachate compositions, revealing changes in the eruption dynamics.

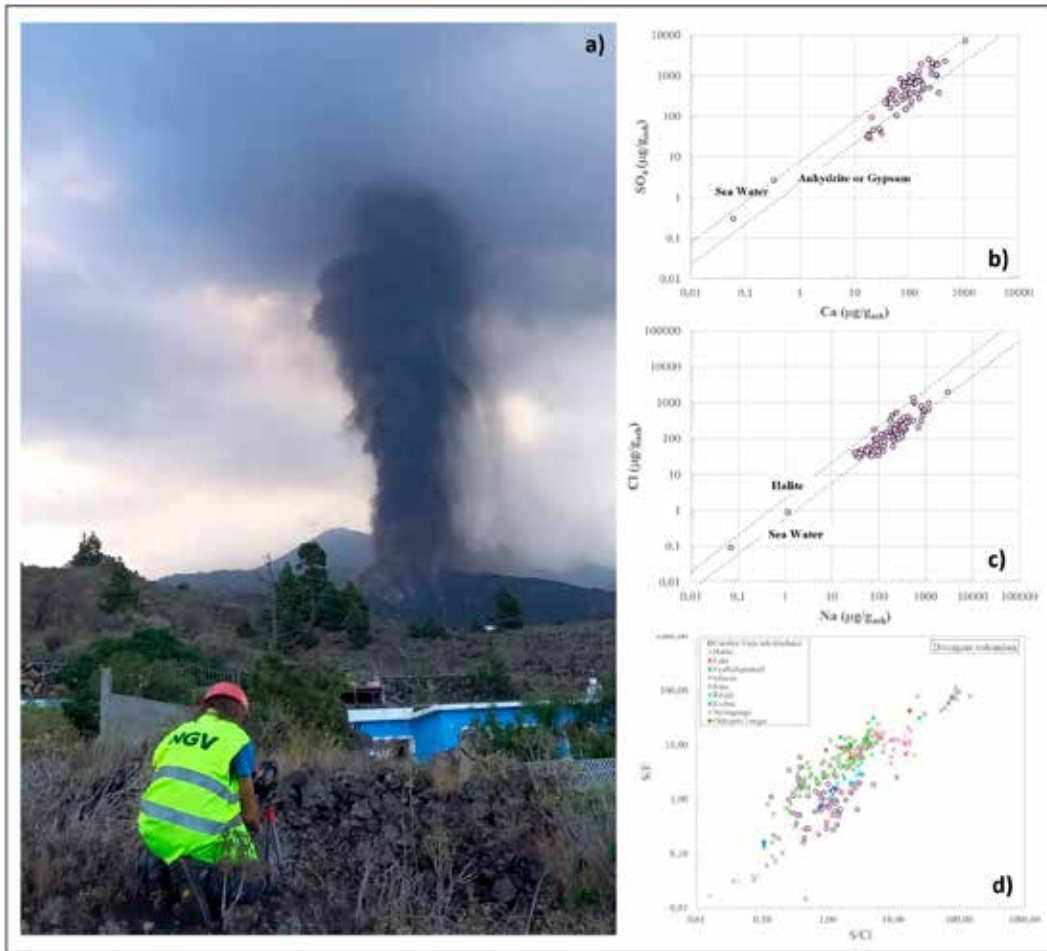


Figure 1

a) Ash-rich eruptive plume of the 2021's Cumbre Vieja volcano (photo credit: P. Scarlato, INGV, Roma1); b) and c) Scatterplots correlating the molar abundances of cation and anion species in ash leachates from the 2021's Cumbre Vieja volcano; d) S/Cl variation with S/F molar ratio for leachate solutions from Cumbre Vieja volcano compared with the divergent volcanism's bulk gas signature.

THE ROLE OF IRREGULAR CONDUIT GEOMETRY ON THE DYNAMICS AND SEISMO-ACOUSTIC RADIATION OF SCALED VOLCANIC JETS

Spina L., Taddeucci J., Pennacchia F., Morgavi D., Scarlato P.

With the aim of investigating the effect of conduit roughness on volcanic jet dynamics and on the related seismo-acoustic radiation we performed a series of laboratory experiments on scaled volcanic jets using the Fractal Burster setup. Compressed air with pressure of 2, 4, 5, 7 and 8 bar was instantaneously released through an electrovalve into home-build epoxy pipes (length 80 cm, mean inner diameter: 3 cm; Spina et al. 2019; 2022 for details) with fractal dimension D of the internal surface (proxy for conduit surface irregularity) of 2 (smooth), 2.18 and 2.99, used as analogue conduits. The dynamics of the resulting subsonic to supersonic jets were observed using a high speed camera (50 KHz) synchronized with two monoaxial accelerometers (0.5 to 10 KHz) and one triaxial accelerometer (2 to 7 KHz) located along the conduit outer surface, at 7 or 40 cm from the vent. An array of microphones (0.5-40 KHz), was distributed at the experimental conduit vent to cover different azimuthal and zenital directions.

A window of 0.045 seconds of acoustic and accelerometric signal was selected for each experimental run. We investigated different amplitude parameters, such as RMS and peak-to-peak amplitude, and spectral features like peak frequency and mean frequency, that is the center of mass of the spectrum. The temporal evolution of the spectral properties of the signals were evaluated using a wavelet periodogram. For each column of the periodogram, i.e. for each time-step, we extracted the frequency at which the maximum spectral amplitude was observed (Fig. 1, Panel I, a,b,c). Then, we computed the average frequency corresponding in the full signal window and using two non-overlapping time-windows of 0.02s. This allowed us to investigate different processes dominating initial or late stages of jet dynamics. Finally, for the experiments performed with synchronized accelerometric and acoustic sensors, we also evaluated the amplitude ratio (RMS and peak-to-peak amplitude) among the signals, as a proxy for energy partitioning.

The results of the above-described investigation of the elastic features of the experimental jets were compared against the observation and kymographs from shadowgraph of high-speed video images.

Experiments performed at pressure above 6 bar show evidence of supersonic jet structures. We observed that shock-cell spacing progressively decreases with increasing fractal dimension, i.e. conduit roughness of the analogue conduit surface, that implies a decrease in Mach number (Fig. 1, Panel IIa,b). Acoustic and accelerometric signals are also affected by the interaction between the jet structure and rough walls. This is clear by looking at i) the higher wavelet maximum frequency (especially in the waveform coda) observed for fractal conduits and ii) the increasing accelerometric to acoustic amplitude ratio with increasing fractal dimension, implying an increased energy transfer to the surrounding medium at the expense of the atmosphere.

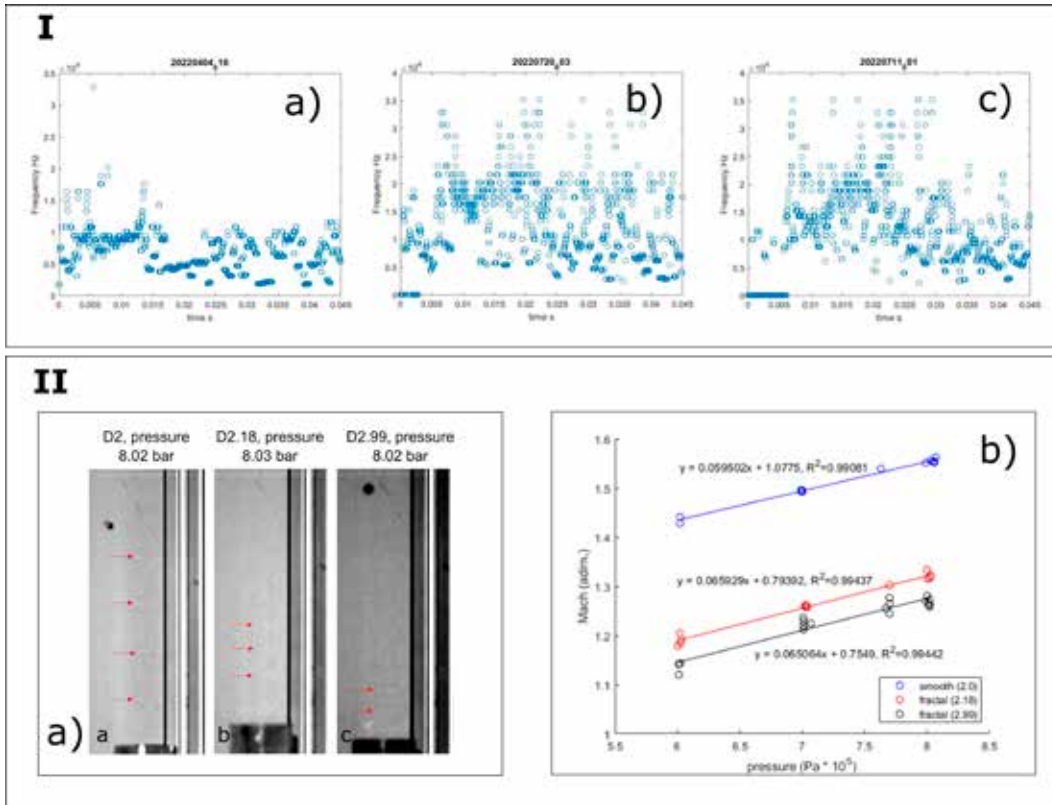


Figure 1

Panel I: Frequency corresponding to the maximum value of the wavelet periodogram computed for each time step for acoustic signals of experimental jets with starting pressure of 8 bar and smooth ($D=2$; a) and fractal ($D=2.18$ and $D=2.99$, (b) and (c) respectively) conduits.

Panel II: Still frames from shadowgraph high-speed videos of the experiments. Shock cells in the under-expanded supersonic jets (red arrows at boundary) are less defined and closer spaced as pipe fractal dimension increases.

Mach number computed from shock-cells spacing (measured from high-speed videos) against pressure of the gas reservoir for smooth ($D2$, green dots) and fractals ($D2.18$ and $D2.99$, blue and red dots respectively) conduits. For each set of experimental data, the linear fit is shown as a solid line.

MULTIDISCIPLINARY CHARACTERIZATION OF THE EXPLOSIVE DEGASSING AT STROMBOLI VOLCANO FROM HIGH-FREQUENCY UV, THERMAL, VISUAL AND ACOUSTIC TIME SERIES

Del Bello E., Bagnato E., Tamburello G., Spina L., Ricci T., Taddeucci J., Scarlato P., Andronico D., Pennacchia F.

Stromboli volcano offers a rare opportunity to study active volcanic processes using a multitude of techniques, such as UV camera, thermal and visible imagery and acoustic signals. These integrated approaches enable high-frequency acquisition of volcanic phenomena, providing insights into rapid processes, such as Strombolian explosions, and quantification of several parameters, including mass or volume flow rates of gas and pyroclasts, output rates, onset, duration and energy of explosions.

We recorded high-frequency, multi-parametric measurements of the ongoing explosive activity in October 2020, when discrete ordinary Strombolian events occurred, and in May 2021, when we observed a peculiar spattering activity. Daily, we acquired 2-5 hours-long continuous time series of UV, thermal infrared and visible imagery, and acoustic data. UV images were processed to calculate SO_2 fluxes along sections perpendicularly oriented to the plume transport direction. Thermally, we integrated the frame-by-frame maximum brightness temperature obtaining the time variation of the explosions-related temperature anomaly. Visually, we applied an optical flow algorithm obtaining the plume and pyroclast ejection speed variations. From acoustic signals we obtained the temporal evolution of the spectral properties of the different eruptive styles. Wavelet analysis of a subset of ordinary events also provided information on the dynamics of volcanic jets.

The integrated analysis of the datasets allowed us to identify different active and passive degassing patterns occurring at the summit vents, and to discriminate between the observed activity styles (Fig. 1). A correlation of the thermal and SO_2 signals is observed both in terms of frequency and amplitude of mean peaks, particularly at the onset of each explosion. In some cases, the mean vent-specific masses and fluxes emitted by individual explosions were also determined. The high acquisition rate of our data provided more refined quantitative eruption parameters than those obtained by standard, low-frequency methodologies, further constrained by the estimates obtained using independent methods.

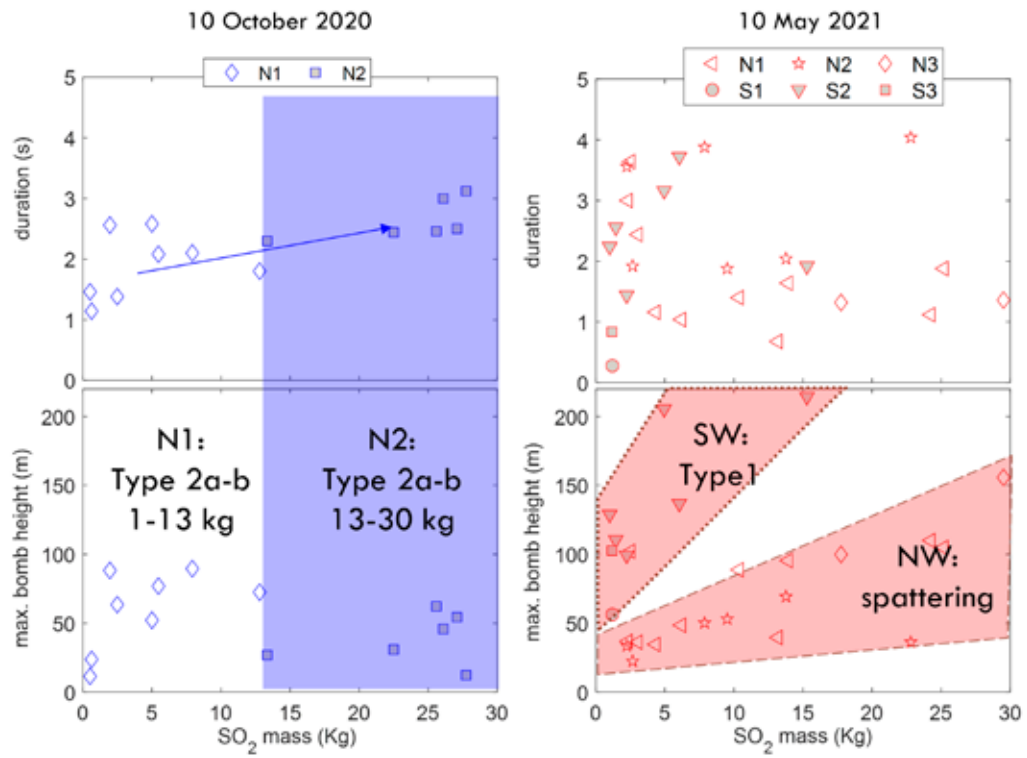


Figure 1
 Main stratigraphic section of the Tajogaite eruption (center). On the left, grain size distribution of samples representative of the deposits. On the right, sample componentry analysis and d.

THE TEPHRA OF THE 2021 TAJOGAITE ERUPTION AT CUMBRE VIEJA VOLCANO (LA PALMA, CANARY ISLANDS): DISTRIBUTION, STRATIGRAPHY, TEXTURAL AND PETRO-COMPOSITIONAL VARIATIONS

Andronico D., Del Bello E., Taddeucci J., Rodriguez L., Pontesilli A., Scarlato P., Civico R., Pennacchia F., Ricci T., Coldwell B., Gadys Melián G., Pankhurst M.J., D'Auria L., Hernandez P. , Perez N.

The long-lasting Tajogaite eruption (La Palma, Canary Islands; 19 September-13 December 2021) was one of the most attractive in recent years, with several vents opening along a ~1 km-long eruptive fissure and simultaneous explosive and effusive activity forming a complex pyroclastic cone and a wide lava flow field.

To reconstruct the magma processes within the volcanic conduit that controlled the eruptive dynamics, we performed detailed and repeated surveys on tephra fallout deposits at more than 120 sections, identifying stratigraphic units and measuring the deposits thickness. A proximal section, ~1 km SW of the active vents and along the main dispersal axis, was sampled and studied in detail. In addition, samples from two (out of seven) “ash-stations” located around the growing cone allowed daily collection of samples during the eruption, providing an additional high-frequency set of samples. Grain-size, ash componentry, SEM and EMP analyses were then conducted on selected samples.

Three main stratigraphic units were identified, associated with key eruptive phases: a lower unit, mainly composed of lapilli-bearing layers, a middle unit prevalently made of ashy beds alternated to minor coarse-lapilli layers, and an upper unit still lapilli-dominated. SEM-derived componentry, based on morphological and textural basis, allowed identification of transparent and fluidal (A), blocky and shiny (B), and blocky opaque (C) particles, plus less abundant crystals and blocky red particles, with relative percentages being correlated with changes in intensity and style of the activity observed during different eruption phases. Groundmass glasses have basanitic to tephriphonolitic compositions, with markedly sodic character. A general trend of decreasing melt differentiation towards the upper stratigraphic levels suggests an increase in the fractionation of olivine relative to clinopyroxene with time, which may relate to changing magma plumbing dynamics. Finally, we preliminarily associated temporal variations of magma compositions and textural features within the stratigraphic sequence.

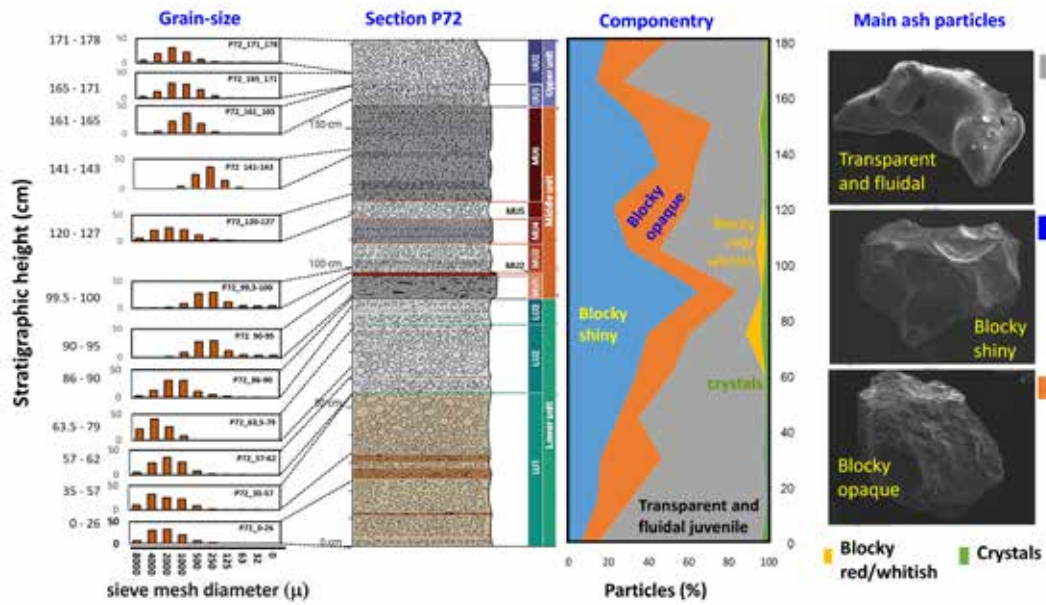


Figure 1
 Main stratigraphic section of the Tajogaite eruption (center). On the left, grain size distribution of samples representative of the deposits. On the right, sample componentry analysis and distribution along the stratigraphic height.

SOLIDIFICATION OF CICIRARA LAVAS FROM MT. ETNA

Casarin A., Marcucci L., Gennaro E., Nazzari M., Lanzafame G., Scarlato P., Ferlito C., Iezzi G.

The morphology of a lava flow is determined by the viscosity of the molten fraction, the rate of deformation and the textures of minerals and pores. At Etna, aa morphologies are very common, while pahoehoe are rare since the former ones are relative SiO²- and crystal-rich lavas. Here, 9 samples of pahoehoe lavas emplaced from prehistoric to last centuries are investigated; these lavas are locally named "cicirara" due to their high content of millimetric size phenocrysts of plagioclase (plg) and clinopyroxene (cpx). This textural attribute strongly contrasts with their pahoehoe crusts.

To solve this apparent paradox, the bulk compositions of these lava samples were first analysed via X-ray fluorescence (XRF, Catania University); then, the micro-chemical compositions of minerals and glasses were determined by EMPA-WDS at the HPHT lab (INGV-Rome). Finally, textural characteristics were obtained at variable and representative magnifications by: i) high-resolution scanner (HRS, INGEO Dept.), ii) transmission optical microscope (TOM, INGEO Dept.) and iii) scanning electron microscope in back-scattered mode (BS-SEM, HPHT lab of INGV-Rome); large images of rocks sampled by TOM and SEM were obtained by capturing micro-photographs in sequence and then merging them into one. The following 2D quantitative textural features were measured: size, abundance, shapes, number of crystals per surface, size frequencies and orientation (Figs. 1a, 1b). The three methods were used in a complementary way to measure phases having size > 1 mm.

In the 9 lava samples, plg phenocrysts (# 800 points) have homogeneous composition: CaO = 9.9-12.8 wt%, Na₂O = 3.4-4.6 wt% and K₂O <1wt%. Cpx phenocrysts (# 380 points) are present only in 7 lava samples and again display homogeneous composition MgO = 13.4 ± 0.3 wt%, CaO = 21.6 ± 0.2 wt%, Na₂O <0.6 wt%. The equilibrium vs dis-equilibrium solidification of phenocrysts was obtained by comparing mineral and bulk compositions. Only a small part of cpx are in equilibrium and then useful to retrieve T and P conditions of crystallization by thermo-barometer models. Preliminary results reveal that the T and P ranges of cpx crystallization is between 1153±13 °C and 6 ± 1 kbar, i.e. they crystallised in a narrow and deep region. All these "cicirara" lavas have a limited content of bubbles (9.3 ± 3.6 area%, except sample SDA, 25,3 area%) and a high content of mm-sized plg and cpx (plg > 1 mm = 26.6 ± 6.8 area%, cpx > 1 mm = 4,7 ± 3.0 area%). The 2D long and short dimensions allow to model the 3D crystal habit (Fig. 1c); plg are prismatic, with short size between 0.2/0.3 and intermediate one between 0.55/0.89, while cpx shows more variability and a more pronounced similarity between short and intermediate lengths (Fig. 1c).

The textural and chemical outcomes allow to simulate the viscosity of these lavas, either under anhydrous and hydrated conditions. These rheological models point out that only a minor amount of plg and cpx are actual phenocrysts, i.e. large crystals present before the eruption. Consequently, a significant portion of them grown or coalesce during post-eruptive conditions. At the same time, minerals with sizes < 1 mm mainly solidified during the emplacement of these lavas. The proposed solidification path allows to develop the typical pahoehoe crust of "cicirara" lavas. In general, the presence of mm-sized minerals is not unequivocally interpretable like phenocrysts.

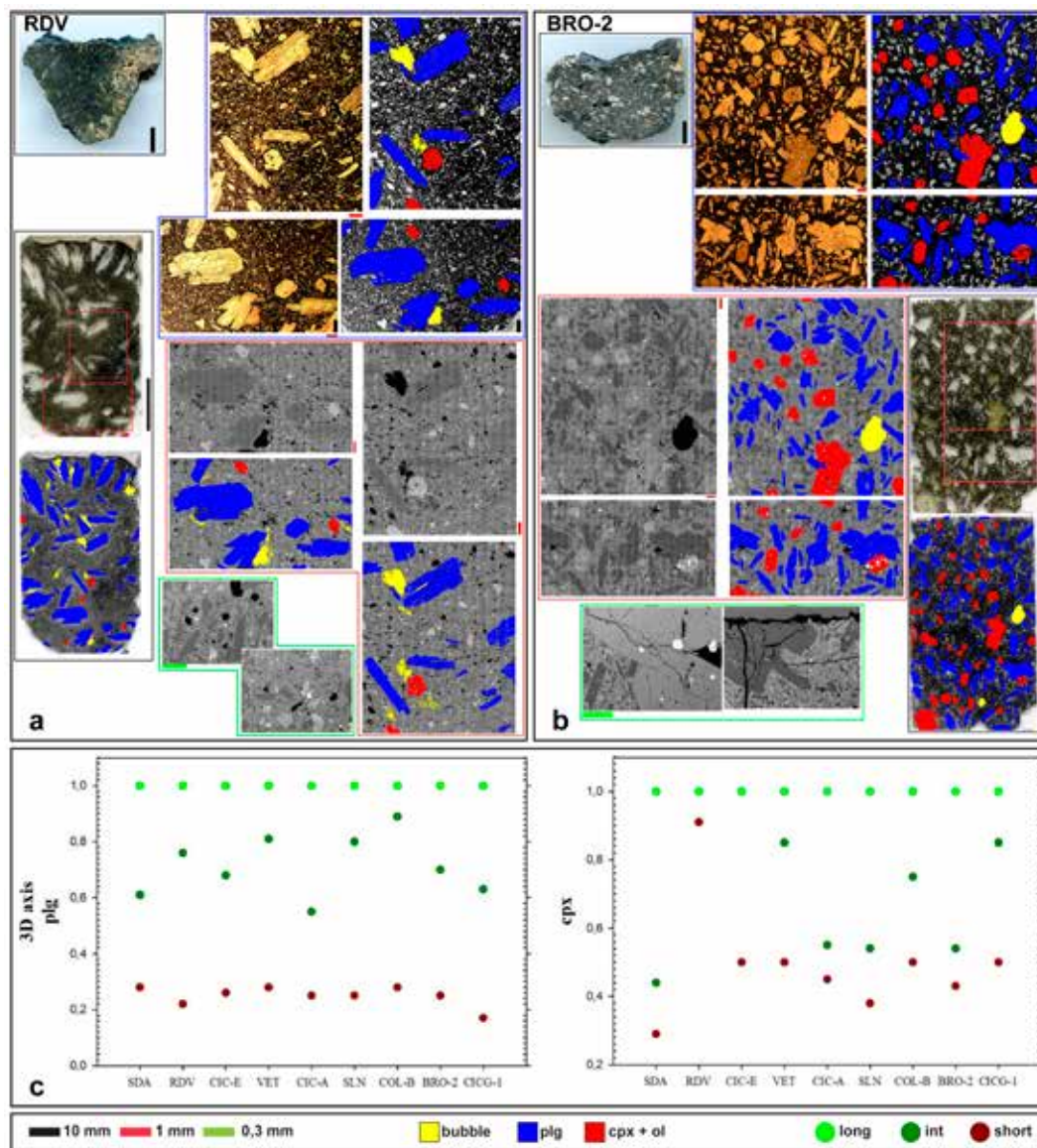


Figure 1

a) b) Textural characteristics of two of the analysed samples: RDV (prehistoric, a) and BRO-2 (1651, b). Black, red and green bars correspond to 1 cm, 1 mm and 0.3 mm, respectively. Red squares on thin sections indicate acquired areas. False colours represent bubbles (yellow), plg (blue) and cpx+ol (red). Contours of boxes indicate the image analysed by SEM and by TOM (red and blue, respectively), while green contours are for single BS-SEM images; c) 3-D shapes of plg (left) and cpx (right) crystals obtained for 9 samples. Light green, dark green and brown dots indicate long, intermediate and short axes respectively.

PETROGRAPHY OF MORTARS WITH VIRGIN AND RECYCLED AGGREGATES (CDW)

Radica F., Iezzi G., Monaco A. P., Bravo M., Cruciani G., de Brito J., Galderisi A., Nazzari M., Scarlato P.

Construction and demolition waste (CDW) are non-hazardous solid waste deriving from construction, renovation and/or dismantling of buildings, as well as from natural adverse events (earthquakes, landslides, etc.). CDW are mainly composed of ceramic-like inert materials such as concrete, mortars, cements, masonries (tiles, roof-tiles and/or bricks) and natural/ornamental stones. These huge amounts of end-of-life (EoL) waste necessitate a full recycling and reusing, limiting further extraction of raw materials for the production of aggregates, cements and/or masonry. However, the upcycling recycling of CDW as secondary raw materials for new construction materials is limited to low performance applications. This is mainly attributable to their heterogeneity. Contrarily to homogeneous virgin materials, the presence of different materials in CDW with variable crystalline and non-crystalline phases with peculiar chemical, mineralogical and textural attributes prevent the fabrication of secondary construction materials with high and constant physical-mechanical properties. The determination of phases and their features in CDW is thus mandatory to separate them in different classes with constant petrography.

In this work we determine the petrography of two mortars: i) a classical mortar prepared with natural virgin sand aggregates (VS) and ii) a recycled mortar produced with recycled natural stone (NS). This latter aggregate was manually selected in the post-earthquake rubbles of the Marche region that occurred after the seismic events of 2016 and 2017. The type and content of crystalline phases in these two mortars were performed by XRPD measurements. The VS aggregates contain 80, 15, 5 wt.% of quartz, alkali-feldspar and sheet-silicates, respectively, whilst the NS one is composed of 58, 19, 11, 12 wt.% of calcite, quartz, plagioclase and sheet-silicates. These two aggregates were used to prepare 12 standard mortar specimens per type to determine their physical-mechanical properties. The compressional and flexural behaviors, as well as the density and porosity of VS-mortar is slightly higher than the NS-mortar. To further constrain these differences, we prepare one thin section per mortar to quantify their textural attributes.

These thin sections were analyzed by i) high-resolution scanner (HRS), ii) transmission optical microscopy (TOM) and iii) scanning electron microscopy (SEM-EDS). HRS, TOM and SEM analyses identify the various crystalline and non-crystalline phases and especially their textures (size, shape, distribution, etc.). The image analysis performed on VS- and NS-mortars by HRS, TOM and SEM allow to quantify the amount of phases (area%), plus their sizes and shapes (Fig. 1a). The 2D image analysis results agree with XRPD outcomes and with the fraction of materials with different sizes used to prepare the mortars. HRS images can be obtained rapidly and economically but allow to discriminate only some phases with size > 0.5 mm; SEM images are instead able to capture any attribute of phases but is extremely time consuming and expensive.

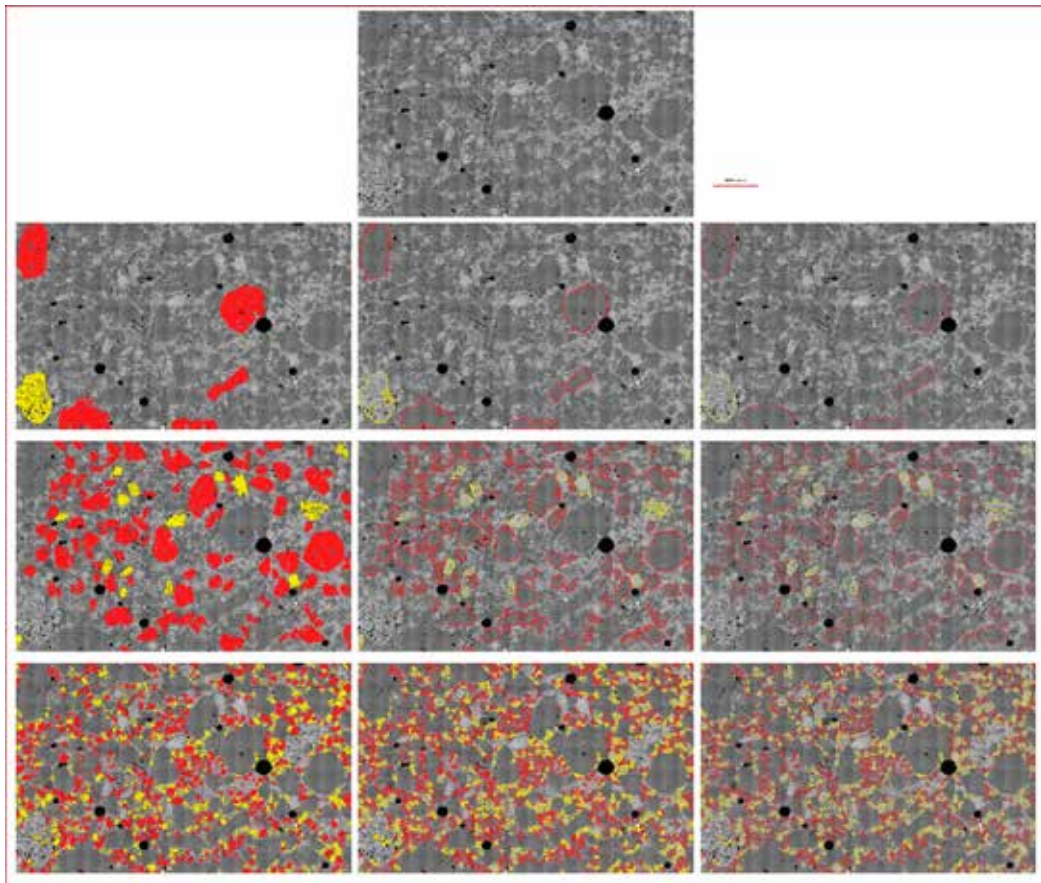


Figure 1
SEM image analysis for the VS mortar. Red areas are quartz and yellow areas are feldspar+biotite. From top to bottom selected size ranges are displayed: > 2 mm, from 2 to 0.5 mm and from 0.5 to 0.125 mm. The amount (area%), size (length, width, perimeter), shape (aspect ratio, roundness) can be accurately measured.

ASSESSING THE SURFACE REACTIVITY OF AMORPHOUS MATERIALS: RELATIONS WITH IRON OXIDATION STATE

Gianchiglia F., Stagno V., Ballirano P., Tomatis M., Turci F., Bardelli F., Pacella A.

Preliminary studies conducted on mineral fibres have shown that the reactivity of iron centres play a key role in fibres toxicity (Fantauzzi et al. 2010). In addition to the amount, the structural coordination and the oxidation state of iron on the surface is also considered crucial (Turci et al., 2011). However, the surface of the fibres appears often amorphous, but no data exists on the reactivity as a function of Fe^{+2} and Fe^{+3} .

This research project aimed to investigate the effect of Fe oxidation state on surface chemical reactivity of amorphous materials.

A total of 6 glasses of clinopyroxene-like composition with different contents of Fe^{2+} and Fe^{3+} were synthesized in the HP-HT laboratory using the high-temperature furnace, with the aim to investigate the effect of the iron oxidation state on the physical and chemical properties of glasses. More in detail, anhydrous Fe-bearing glasses with nominal composition such as diopside, jadeite, hedenbergite and aegirine were synthesized using a mixture of oxides and carbonates as starting material, prepared from high-grade reagents like $CaCO_2$, Na_2CO_3 , MgO , SiO_2 , Al_2O_3 , Fe and Fe_2O_3 and melted between $1400^{\circ}C$ and $1500^{\circ}C$ within a time interval of 45 min to 5h. These glasses were chosen to be representative of the simplified analogue of natural magmas with variable polymerized structure.

The synthesized glasses were observed under an optical microscope, the chemical composition was determined by EPMA, while the oxidation state was determined by conventional Mössbauer. The synthetic glasses were also used to conduct glass structure measurements by XAS at ESRF (Grenoble, France). To assess the surface reactivity of the investigated glasses, the production of hydroxyl radicals ($HO\bullet$) via Fenton reaction was analyzed through the spin-trapping technique and the acquisition of EPR spectra. The obtained results show that all glasses are reactive in radical release, with increasing kinetics in the first 30 min. The most reactive samples are aegirine and hedenbergite, while diopside and jadeite with higher iron content are slightly more reactive than the corresponding solids with lower iron content (Fig. 1).

OH release after 30

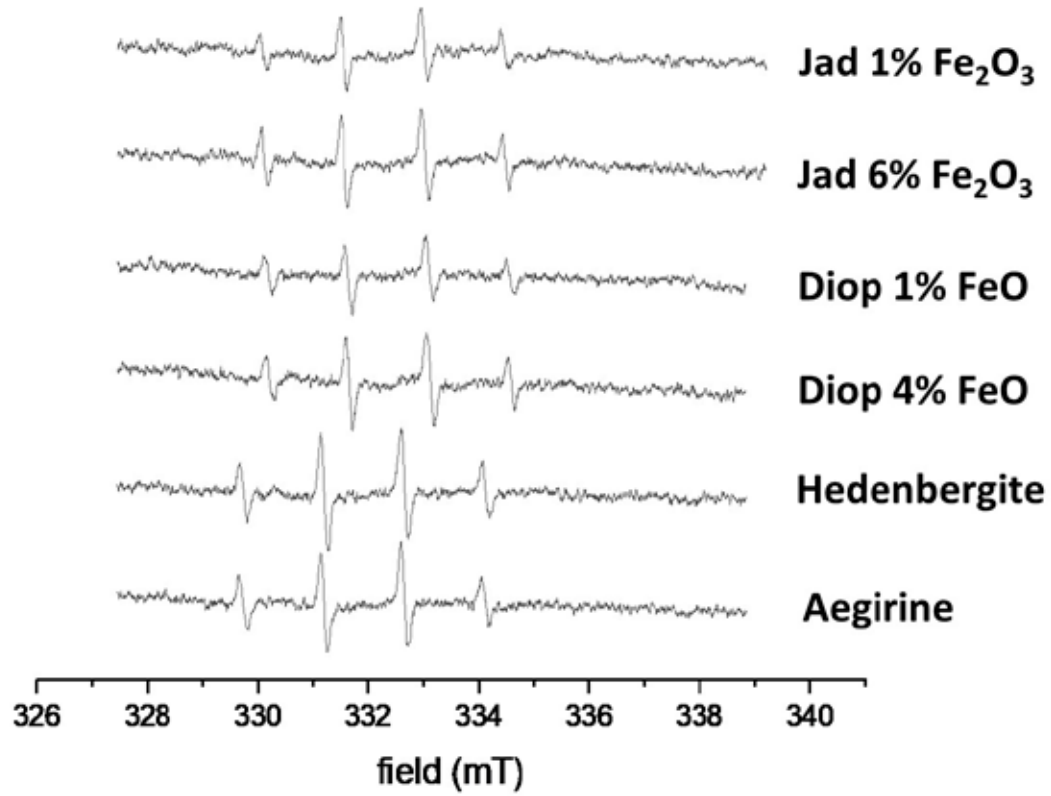


Figure 1

EPR spectra of the [DMPO-OH]• adduct obtained after 30 min of incubation with H₂O₂. The intensity of the spectra is proportional to the amount of radical species released.

CHEMICAL COMPOSITION OF OLIVINE HOST AND SPINEL INCLUSIONS COMBINED WITH IN SITU MÖSSBAUER SPECTROSCOPY MEASUREMENTS: IMPLICATIONS FOR THE MANTLE REDOX STATE

Marras G., Carnevale G., Caracausi A., Rotolo S.G., Stagno V.

The redox state of the Earth's upper mantle links to the oxidation state of peridotite rocks; this can be calculated using oxy-thermobarometric equilibria representative of the mineral assemblages where Fe³⁺-bearing spinel and garnet are involved and their Fe³⁺/ΣFe known to be redox sensitive. To date, accurate measurements of Fe³⁺/ΣFe in peridotites is limited to those rocks where spinel (or garnet) crystals can be easily separated and measured by conventional ⁵⁷Fe Mössbauer spectroscopy. No data exist on spinel inclusions commonly observed as entrapped in olivine due to analytical challenges in extracting and measuring tiny inclusions.

The aim of this study is to retrieve the f_{O_2} of the mantle beneath Mt. Vulture (Italy) through the study of wherlitic lapilli that contain olivines with multiple tiny spinel inclusions.

Measurements of the Fe³⁺/ΣFe ratios were performed on the olivine (host) and extracted spinels (inclusions) with size of 20-30 μm using in situ synchrotron Mössbauer spectroscopy at the beamline ID18 of the European Synchrotron Radiation Facility (ESRF) in Grenoble (France). The chemical composition of the investigated olivine host and spinel inclusions was analyzed at Istituto Nazionale di Geofisica e Vulcanologia (Rome, Italy) using the JEOL JXA-8200 Superprobe.

Olivine has Mg# [Mg/(Mg+Fe) mol ratio] of about 0.90, while spinel shows Cr# [calculated as Cr/(Cr+Al) mol ratio] > 0.40, both in agreement with previous available data for wehrlitic xenoliths from Vulture. Our Mössbauer data show that the Fe³⁺/ΣFe ratio for olivine is ~0.04, overlapping with literature data, while the Fe³⁺/ΣFe of the tiny spinels ranges between 0.38 and 0.40 (Fig. 1), hence, among the highest values measured in literature for mantle spinel-peridotites.

Figure 2 shows a back-scattered electron image of olivine (dark) and several spinel inclusions (bright) with variable size (≤ 50 μm) and (sub)euhedral habits.

Data of Fe³⁺ and chemical composition can be combined with thermodynamic predictions of the Fe³⁺ content expected at a given P-T- f_{O_2} to test the possibility to use spinel inclusions for oxy-thermobarometric calculations with implications for the speciation of volatiles in depth.

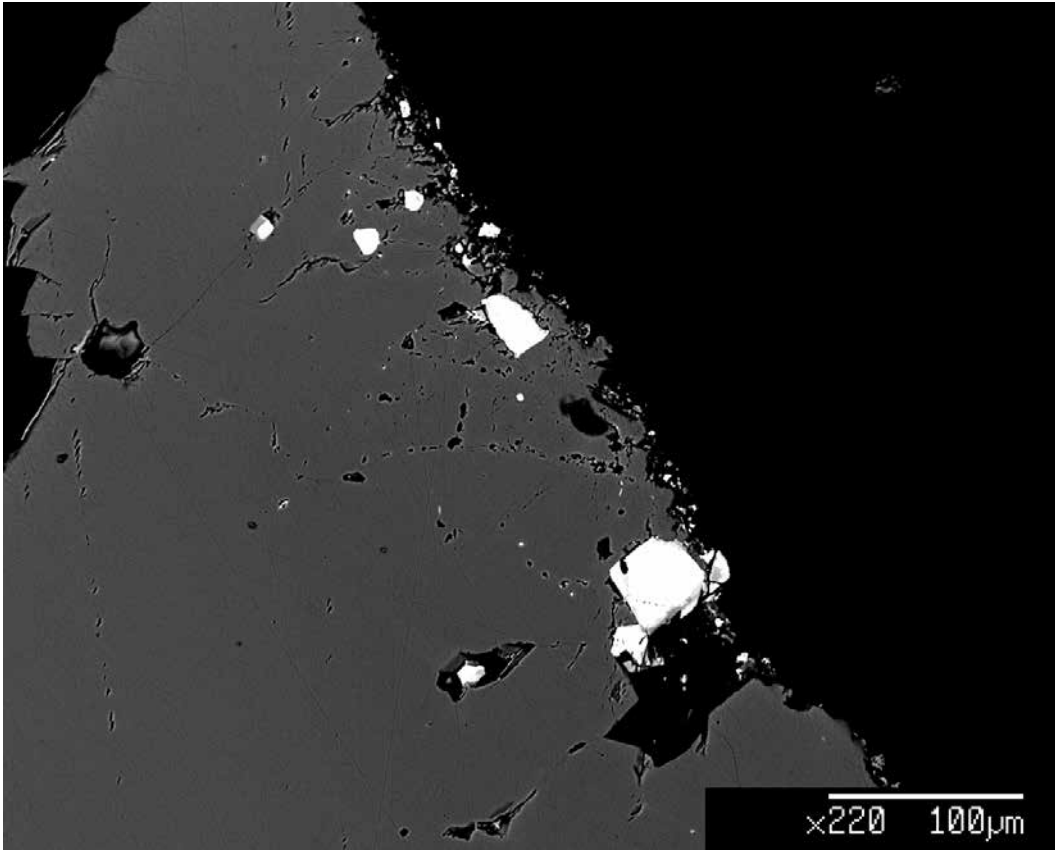


Figure 1
Mössbauer spectrum of a spinel inclusion in olivine (<20 µm) fitted with two doublets for Fe²⁺ and one doublet for Fe³⁺.

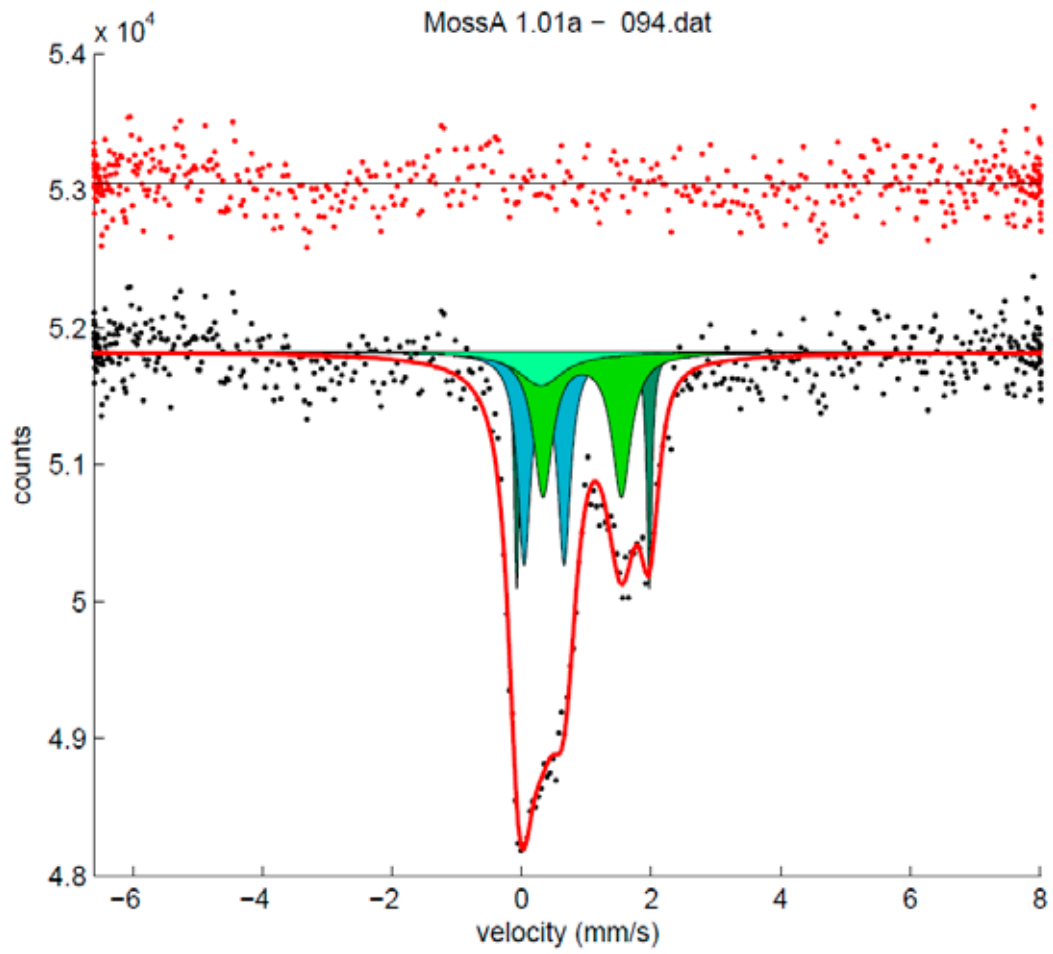


Figure 2
Back-scattered image of the Vulture olivine (dark) with spinel inclusions exposed after polishing (bright).

CHARACTERISATION OF ERUPTIVE PRODUCTS FROM GLACIAL/SUB-GLACIAL ERUPTIONS IN THE MOUNT MELBOURNE AREA (NORTHERN VICTORIA LAND, ANTARCTICA)

Rocchi I., Di Roberto A., Masotta M., Rocchi S.

In the frame of the PNRA project, several expeditions in Antarctica sampled a wealth of volcanic products during the field seasons 2005-2006, 2011-2012 and 2014-2015. The last project, which started in 2018, focussed on the MAGma-ICe interaction (MAGIC), with the objective to reconstruct the ice cover evolution and the effects of variable ice load on the eruptibility and composition of magma. Therefore, a particular attention was addressed to the volcanic products that can give insight on the type and distinguishing features of the eruptions. For this reason, in this study two types of samples were analysed: hyaloclastites (a volcanoclastic deposit formed by the explosive interaction between magma and water) and lapilli tuffs.

The samples were prepared and preliminarily selected at INGV, Pisa, using a scanning electron microscope equipped with an energy-dispersive system (SEM-EDS). Then, they were analysed for their chemical content using the electron microprobe provided by the INGV, Roma. The samples show a variable texture, both in vesiculation and for the presence of microlites in the glass, with different degrees of alteration (Fig. 1a, b). The EPMA analyses were performed with the objective to achieve a good overview of all the different type of samples and to select the most representative ones to perform further chemical analyses (e.g. LA-ICP-MS). The preliminary results show a general homogeneity of the analyses performed in each sample; however they also permit discriminating between samples deriving from different sites (Fig. 1c).

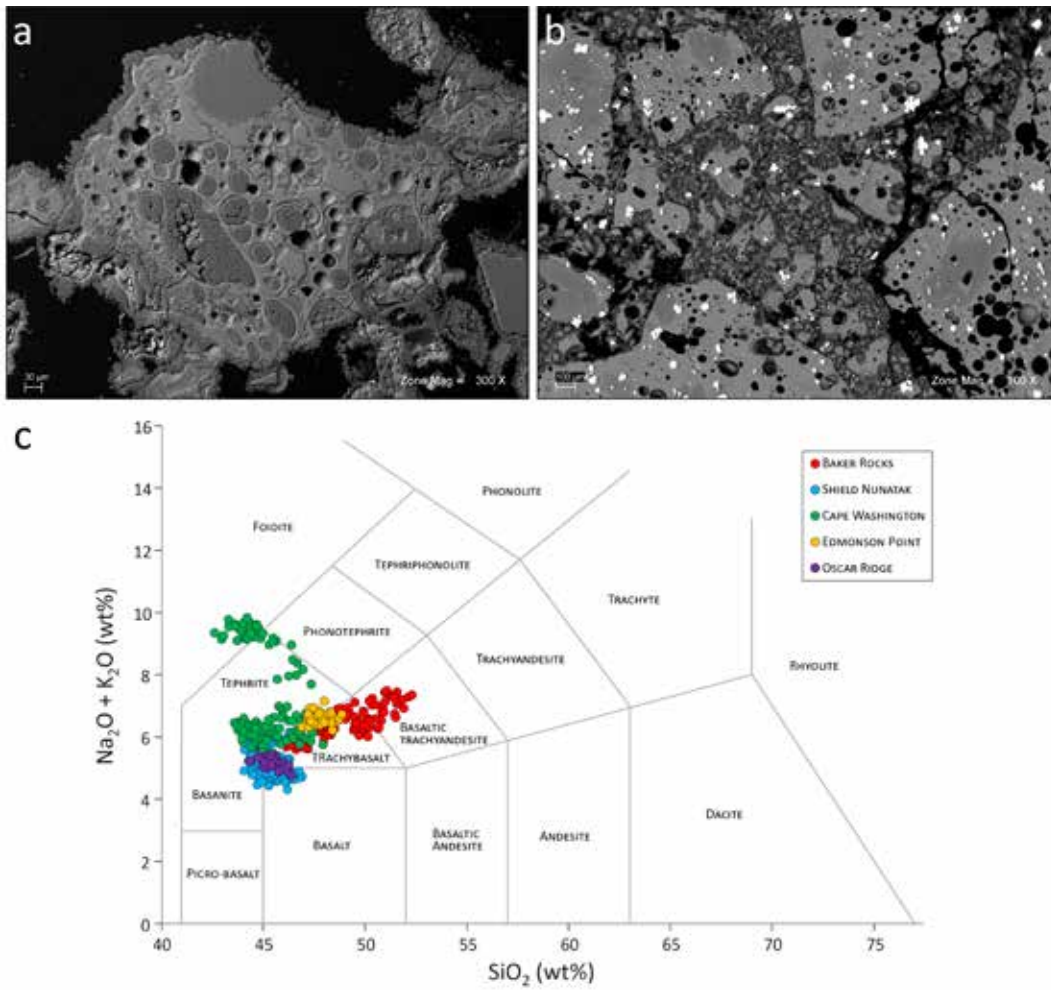


Figure 1
 SEM microphotographs of: a) a sample from Baker Rocks showing moderate vesiculation, with the vesicles filled by calcite, and glassy fragments showing a microlite-poor glass; b) a hyaloclastite sample from Cape Washington showing glassy fragments in a fine-grained matrix formed by completely altered fragments (<100 μm) and a micritic phase composed of zeolite, smectite and calcite. c) Results from the EPMA-WDS analyses reported on the TAS diagram.

PAIMGSPGAASVZ - PETROLOGICAL APPROACH FOR IDENTIFYING MAGMATIC GAS SOURCE OF POST-GLACIAL ERUPTIVE ACTIVITY IN THE SOUTHERN VOLCANIC ZONE (SVZ CHILE)

Robidoux P., Moussalam Y., Koga E., Pontesilli A.

The project goal is to identify pre-eruptive magma storage depths and mantle sources from magmatic fluids beneath Holocene-to-contemporaneous stratovolcanoes in populated regions of Araucania, Chile (Central Chilean Volcanic Arc). Those areas enclose abundant large communities (Concepcion, Los Angeles, Temuco, Villarrica, Pucon, etc.) closely settled near to giant stratovolcanoes (Villarrica, Tolhuaca, Lonquimay, Llaima, among others). In this project, the team gives emphasis on magmatic fluid characterization. The dissolved volatiles and silicate melt compositions are keys to determine if each magmatic recharge comes from the same origin in the crust-mantle regions below the stratovolcanoes in the Andes Cordillera. To support the measurements of major volatiles and noble gases as inert gas tracer of volcanic fluids (INGV-Palermo), the major element composition is measured in glass rims and glass inclusions from olivine as pyroxene minerals sampled at Villarrica and Tolhuaca volcanoes. The volcanic pyroclastic samples were examined to determine the major element composition of primitive melts at the HP-HT Laboratory of Experimental Volcanology and Geophysics of the Istituto Nazionale di Geofisica e Vulcanologia (INGV) in Rome (Italy), using a Jeol-JXA8200 field-emission electron microprobe equipped with five wavelength dispersive spectrometers.

Olivine and pyroxene minerals were selected and prepared (inclusion intersection, polishing) then pressed in five distinct indium mounts. The major element composition of each crystal with core vs. rim spots is measured with glass inclusion surfaces to determine pre-eruptive magma conditions (Fig. 1 a-b). The targeted eruptive sequences mainly correspond to paroxysmal eruptions, explosive in the case of Villarrica, but effusive in the case of Tolhuaca. According to our main results processed from EMPA (major oxide wt. %), the major elements were used to track the composition of primitive magmas feeding Villarrica and Tolhuaca volcanoes and verify if melts have been in equilibrium with the first generation of phenocrysts (Fig. 1 c-d). The results indicate large ranges of Forsterite contents (Fo%) observed on olivines in Minor Eruptive Vents from Villarrica (Mg# crystal in Fig. 1c; reaching 88%), which generally comes superior to Tolhuaca (Mg# crystal in Fig. 1d; reaching 84%). The composition of glass vs. mineral hosts acquired with EMPA were also used to correct for post-entrapment diffusion of FeOT-MgO between the inclusion and its mineral host. In such circumstances, the equilibrium was reached after using models based on expected K_d of olivine (0.30 ± 1) and pyroxene (0.26 ± 1). We discovered that the Tolhuaca volcanic system records glass compositions and glass inclusions far from the equilibrium in terms of FeOT-MgO. At Villarrica, the equilibrium was reached in several samples, but many required post entrapment corrections (PEC) to recast MgO and FeOT contents of the original MI system.

Preliminary conclusions: While the data are under process for the volatile contents, we observed impressive consistency in the composition of magmas that have fed each paroxysmal event at Villarrica volcano (few basalts and dominating basalt andesites). Impressive changes in composition are observed through the central Tolhuaca magma system (basalt andesites to andesites extremes) which produced outpouring of lava fields on NE flanks. Differentiation processes of residual melt are stronger for crystallization processes at Tolhuaca. Inclusion entrapment and solidification of olivine-host rims testify liquid melt compositions of Tolhuaca far from equilibrium according to distribution coefficient “Kd”.

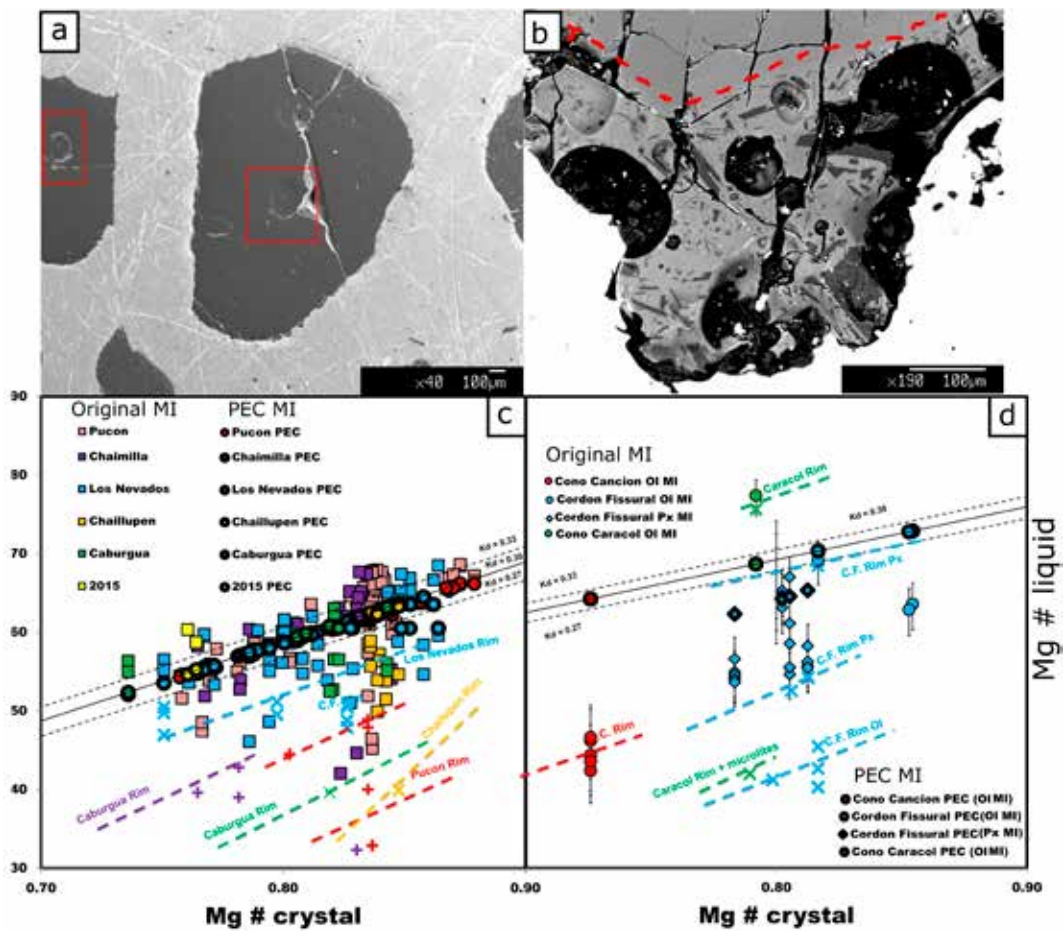


Figure 1
 a): Mineral photography with BSE (back-scattered electron) photomicrographs on Villarrica glass inclusions and b) Tolhuaca Matrix Groundmass. c) Results of EMPA analyses with molar ratios of Mg is calculated in mineral hosts (Mg# crystal) and primitive melts (Mg # liquid). The Mg# are compared with model of original distribution coefficient “Kd” before and after post-entrapment corrections on MI according to Petrolog applied over Villarrica glass inclusions, then d) Tolhuaca glass inclusions and mineral glass rims.

PETROCHEMICAL ANALYSES OF TEPHRA PRODUCTS FROM THE RECENT ERUPTION OF CUMBRE VIEJA VOLCANO (LA PALMA, CANARY ISLAND)

Rodriguez F. et al.

On September 19, 2021, a new eruption began at the west flank of Cumbre Vieja volcano (La Palma, Canary Islands) after an inter-eruptive period of 50 years from the previous eruption (Teneguía, October 1971). The 2021 event was a fissure and powerful strombolian eruption with a magnitude VEI=3 and this eruption was considered the most important of Europe during the last 75 years in terms of the significant amount of SO₂ released and the serious damage caused by the lava flows. The eruption officially ended on December 13, 2021. After 85 days of eruption, several tephra samples were collected at tephra-collecting stations almost on a daily basis. In addition, field tephra-collecting surveys were developed during and after the eruption. From January 17 to 21, 2022, an INGV-INVOLCAN team (Istituto Nazionale di Geofisica e Vulcanologia and Instituto Volcanológico de Canarias) carried out a field survey, aimed at mapping tephra deposits and collecting representative samples. More than 100 observation points were made, being one of them, the stratigraphic section P72, excavated 1km away from the vents to the southwest, with a total thickness of 184 cm. Representative samples were collected at 11 different heights and layers: From 0 to 26 cm, from 35 to 57 cm, from 57 to 62 cm, from 63 to 79 cm, from 79 to 80 cm, from 86 to 90 cm, from 90 to 95 cm, from 120 to 127 cm, from 143 to 144 cm, from 165 to 171 cm and from 171 to 178 cm. These samples were studied and compared with the control sites or tephra-collecting stations installed during all the period and picked up almost on a daily basis, in order to obtain a better picture of the stratigraphic series and the deposit times.

The chemical composition of matrix glasses and mineral phases of polished epoxy mounts of these tephra samples collected were analysed through the JEOL JXA-8200 electron microprobe (EMP), located at INGV-RM1. Almost 300 observation points were made with EMPA, in the 11 different heights and layers of the main stratigraphic section P72. This was during 7 days of this Excite TNA access in May 2022. Having a lot of samples available, we started the work in the first round of access, and a second Excite TNA proposal was submitted and accepted for a second round to finish/continue the work. A complementary TNA project (EXCITE_C1_2022_41) developed in July 2022, 'Textural analyses of tephra products from the recent eruption of Cumbre Vieja volcano (La Palma, Canary Island)', was carried out with the same collected samples.

As preliminary conclusions we can say that, glass compositions ranged between basanites/tephrites (mostly) and tephriphonolites, with markedly sodic compositions. A general trend of decreasing melt differentiation towards the upper stratigraphic levels was identified (Fig. 1), where stratigraphic level is the mid-point of each stratigraphic interval considered. In particular, this is clear by looking at SiO₂ and Na₂O+K₂O, while minimal variations are observed in Mg#, FeO/MgO. This differentiation trend is also associated with an increase in CaO/Al₂O₃ towards the upper stratigraphic levels. Overall, scatter at each stratigraphic level seems to relate to varying degrees of groundmass crystallisation.

These trends could suggest an increase in Olivine/Clinopyroxene fractionation with time, which represents the two main phenocryst phases controlling melt evolution in these magmas. Changes in their relative abundances may relate to changing physico-chemical conditions (e.g. tapping of magmas slightly differing in storage pressure and/or water content) and/or different magma compositions in the first place. Both these processes may potentially be related to tapping of a zoned reservoir while eruption proceeds. Groundmass crystallisation alone isn't likely to control melt differentiation, since glass $\text{Na}_2\text{O}/\text{K}_2\text{O}$ is almost constant and plagioclase is a main groundmass constituent (no phenocrysts). In order to better constrain what drives melt compositional changes with stratigraphy, a future investigation of crystal compositions and zoning patterns will extend the results of this work and provide further insights on the magmatic processes underlying the eruptive patterns observed during the 2021 Cumbre Vieja volcanic eruption.

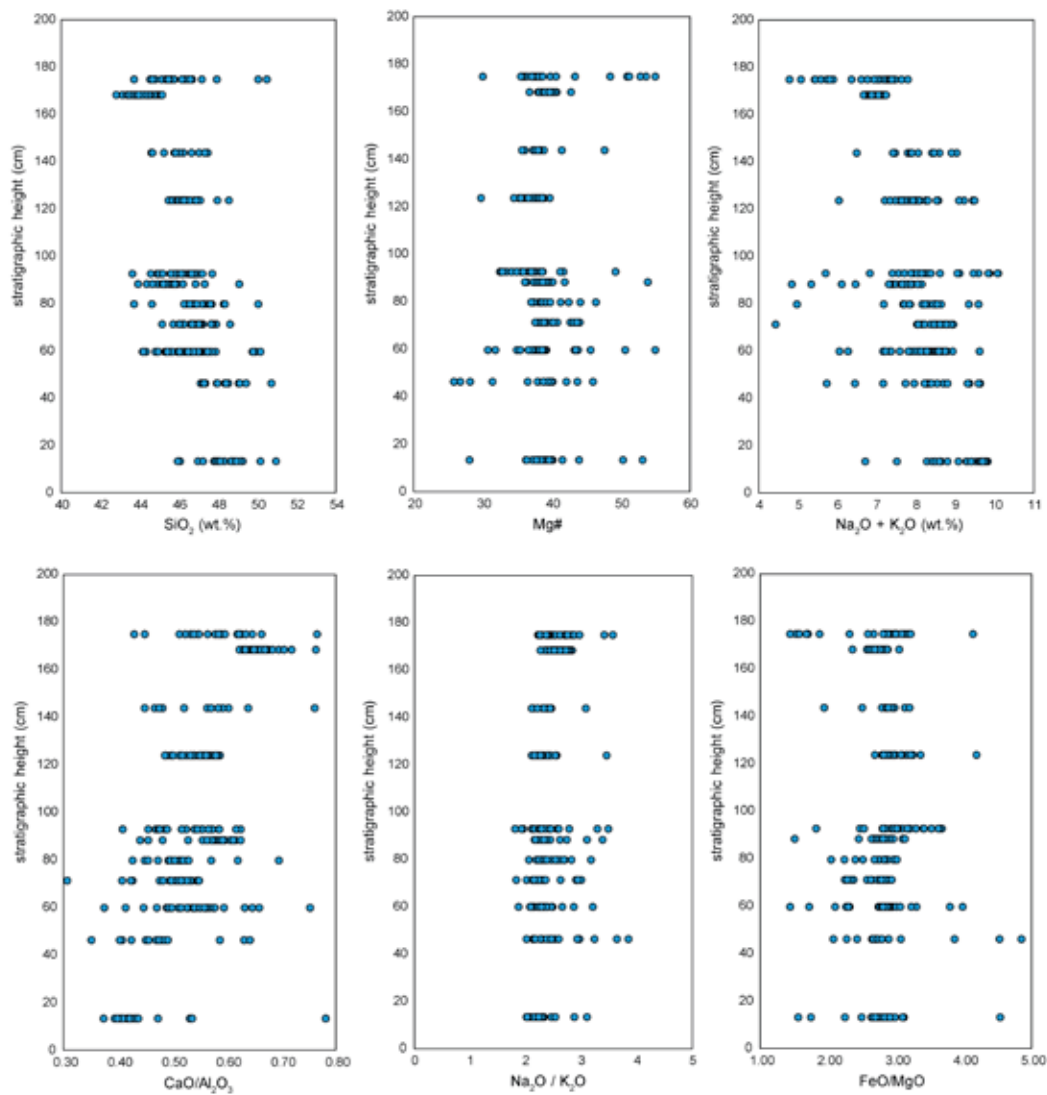


Figure 1
Chemical compositions at the studied stratigraphic levels of P72 section.

TEXTURAL ANALYSES OF TEPHRA PRODUCTS FROM THE RECENT ERUPTION OF CUMBRE VIEJA VOLCANO (LA PALMA, CANARY ISLAND)

Martin Lorenzo A. et al.

On September 19, 2021, the Cumbre Vieja volcano (La Palma, Canary Islands) erupted after 50 years of dormancy, the last eruption having occurred in 1971 when it formed the Teneguía cone. The historical volcanism of La Palma typically produced explosive-effusive eruptions associated with tephra cones, cinder deposits and lava flow fields. The 2021 eruption was characterized by an almost continuous tephra emission along a ~ 1 km long fissure, with only a few phases of quiescence lasting no more than a few hours. The main goal of this Excite TNA project was the study of the textures and morphology of tephra deposits of this eruption. The outcomes of this research were complementary with another TNA Project: Petrochemical analyses of tephra products from the recent eruption of Cumbre Vieja volcano (La Palma, Canary Island), thereby analysing different aspects of the same volcanic products.

During 85 days of eruption, several tephra samples were collected at tephra-collecting stations almost on a daily basis. In addition, field tephra-collecting surveys were developed during and after the eruption. From January 17 to 21, 2022, a collaborative fieldwork of Istituto Nazionale di Geofisica e Vulcanologia (INGV) and Instituto Volcanológico de Canarias (INVOLCAN) mapped tephra deposits and collected representative samples. More than 100 observation points were made, being one of them, the stratigraphic section P72; excavated ~1km away from the vents to the southwest, with a total thickness of 184 cm. Representative samples were collected at 11 different heights and layers: From 0 to 26 cm, from 35 to 57 cm, from 57 to 62 cm, from 63 to 79 cm, from 79 to 80 cm, from 86 to 90 cm, from 90 to 95 cm, from 120 to 127 cm, from 143 to 144 cm, from 165 to 171 cm and from 171 to 178 cm. These samples were studied and compared with the control sites or tephra-collecting stations (AS2 and AS5, in this case) installed during all the eruption period and picked up daily. These samples were investigated for characterisation first by optical microscopy for a first component analysis, and then studied (morphological and textural analyses) with the high-resolution Scanning Electron Microscopy, SEM.

First, different ash class-sizes from a few samples were initially observed under binocular to select the ash-size class to analyze. The best range of particles allowed to better distinguish the different components of particles at Cumbre Vieja volcano resulted in the class 0.25 mm. The ash componentry was carried out on 48 samples by counting 300-500 particles at steps of 100 particles each for evaluating the representivity of the analyzed particles during each step.

Five types of components were recognized (Fig.1): Crystals, transparent and fluidal juvenile, blocky shiny, blocky opaque and blocky red. The morphological and textural features of the different particles were studied in more detail with the SEM. In general, the transparent and fluidal particles appear elongated to vesicular; in the case of blocky shiny and opaque particles, appeared irregular morphology with shapes that vary from rounded-vesicular and the presence of microlithic matrices is very frequent.

Regarding the componentry analysis of the 48 analyzed samples reported, it's evident a variation in the proportions of the five components that can be correlated with the explosive styles that alternated during the eruption phases. The results of this study will be relevant to define and classify the explosive processes that dominate the rise of magma and its fragmentation, helping to improve hazard mitigation strategies at basaltic volcanoes where the explosive activity is similar to Cumbre Vieja.

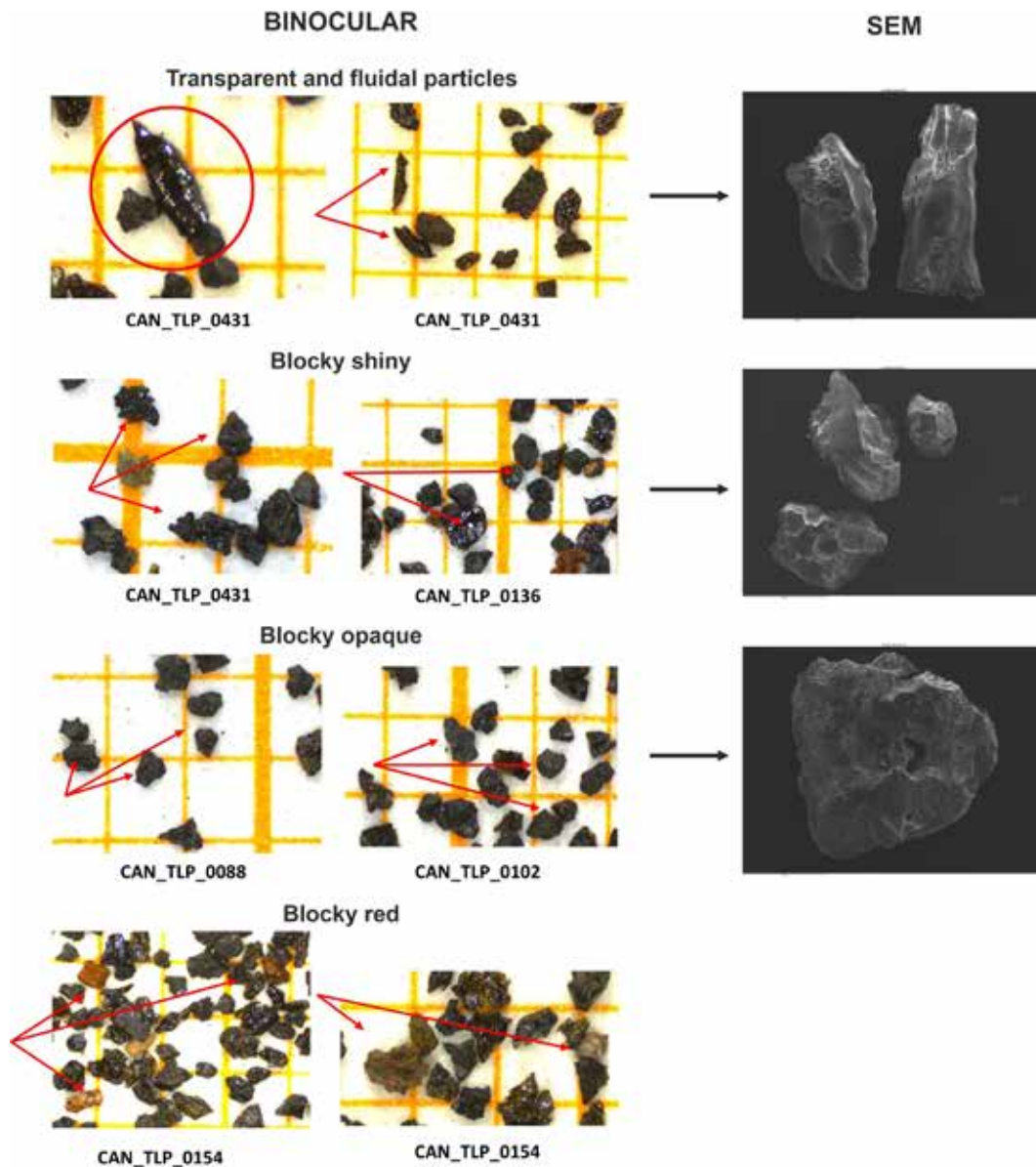


Figure 1
Different types of components were recognized. On the left, images taken from the binocular; on the right, images taken from the high-resolution Scanning Electron Microscopy (SEM).

THE EFFICACY OF HIGH FREQUENCY PETROLOGICAL INVESTIGATION AT OPEN-CONDUIT VOLCANOES: THE CASE OF MAY 11TH 2019 EXPLOSIONS AT SOUTHWESTERN AND NORTHEASTERN CRATERS OF STROMBOLI

Pontesilli A., Del Bello E., Scarlato P., Mollo S., Ellis B., Andronico D., Taddeucci J., Nazzari M.

Petrological monitoring studies typically focus on eruptive phenomena occurring over long timescales of the order of days to years, aiming at identifying major changes in the physico-chemical state of magma during ascent towards the surface. Exceptionally, we present results from an integrated petrological and statistical approach based on the compilation of ~5300 major and trace element data for glass and crystals, in combination with volcanological data on eruptive events over very short timescales of minutes to hours at Stromboli volcano (Sicily). On May 11 2019, we had the rare opportunity to collect individual fresh fallout ash products from eighteen mostly consecutive explosions, erupted in a 2-hour time span and, at the same time, to acquire continuous high frequency (50 Hz) infrared thermal data of the same explosions. Through video analysis, we observe that explosions were more frequent and ash-dominated at the southwestern crater area (SCA, 8–10 events/hour) than at the northeastern crater area (NCA, 3–5 events/hour), where coarser material was ejected. The statistical analysis of glass and plagioclase compositions reveals differences in the products erupted from the two crater areas. SCA explosions tapped less differentiated magmas (Mg#~42–46, ~257–365 LaN, ~0.7–0.9 Eu/Eu*) in equilibrium with more anorthitic plagioclase cores (An~72–88), whereas NCA area explosions are more differentiated (Mg#~40–44, ~286–387 LaN, ~0.6–0.8 Eu/Eu*) and in equilibrium with less anorthitic plagioclase cores (An~68–82) (Fig. 1a, b). Thermometric calculations based on major and trace element clinopyroxene-plagioclase-melt equilibrium modeling highlight that the SCA explosions were fed by hotter magmas in comparison to NCA explosions. Plagioclase-based diffusion modeling also indicates longer timescales for the dynamic ascent of NCA magmas (Fig. 1c), leading to preferential groundmass crystallization at the conduit walls and transition from sideromelane to tachylite groundmass textures. The final emerging picture is that in May 2019, concurrent normal eruptions from different crater areas at Stromboli were heralds of compositionally and thermally diverse magmas rising at different rates within the uppermost branched part of the conduit region. High frequency petrological monitoring approaches have the potential to constrain dynamic conduit processes related to transient, explosive eruptions in persistently active volcanoes, thereby offering new insights on the interplay between magma dynamics, ascent timescales, and eruptive behavior

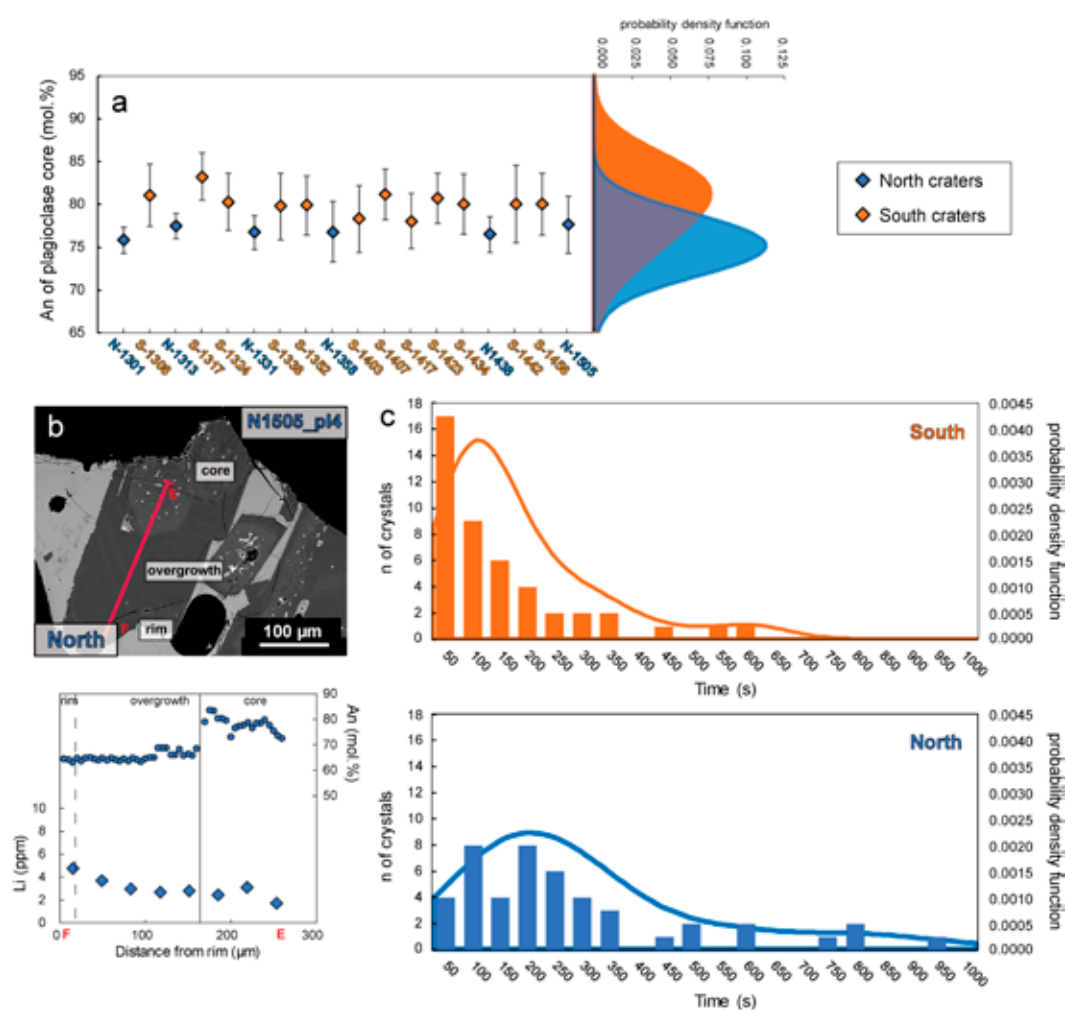


Figure 1
 (a) Anorthite (mol.%) content of plagioclase cores from North and South craters and related Kernel density estimates. (b) Back-Scattered Electron (BSE) image and compositional profile showing the Anorthite (mol.%), Li (ppm) and textural change of a representative plagioclase phenocryst, from core to overgrowth and rim. (c) Histograms and Kernel density estimates for the ascent timescales calculated by the diffusion modeling of Li in plagioclase overgrowths and rims from South and North craters.

TRACKING ALKALINE MAGMA EVOLUTION THROUGH CUMULATE ROCKS

Pontesilli A., Mollo S., Brenna M., Masotta M., Scarlato P., Nazzari M.

The importance of amphibole-clinopyroxene assemblage in arc magmas is widely acknowledged and has been shown to control on magma differentiation and the generation of a hydrous lower crust. This fractionation is often referred to as “cryptic” because the amphibole does not represent a common phenocryst phase in arc magmas. Lower crustal “hot-zones” have been identified on the basis of amphibole-rich cumulates produced by reaction-replacement of antecrystic clinopyroxene. Conversely, the role of amphibole in intraplate settings, where hydrous input through active subduction is missing, is still poorly understood. Amphibole-bearing cumulates are nonetheless a common feature of intraplate composite volcanoes such as the extinct Dunedin Volcano (New Zealand) or the active Cumbre Vieja (Canary Island). Amphibole often coexist with clinopyroxene in mafic to intermediate magmas (alkali basalts to mugearite and phonotephrite), and form cumulate rocks, represented by gabbros, clinopyroxenites, and amphibolites. Although the two phases generally crystallize under equilibrium conditions, some cumulates show evidence of clinopyroxene resorption and amphibole overgrowth. These cumulates are heralds of magma differentiation driven by hydrous magma batches that ascend and interact with crystalline mushes in the lower crust. Cumulates from more differentiated magmas (syenites) are instead characterized by crystal remnants which indicate resorption of Mg, Ti-rich amphibole and clinopyroxene. Overgrowth textures resulting from Fe-rich amphibole and clinopyroxene indicate fractionation from more evolved magmas (benmoreites, tephriphonolites, phonolites) at shallow crustal levels.

Here major and trace element compositions from natural amphibole-clinopyroxene assemblages are compared with those obtained via temperature-gradient experiments reproducing the textural features of crystalline mushes (Fig. 1). Results are then integrated with equilibrium melt compositions estimated by means of published partitioning schemes for amphibole and clinopyroxene. This approach allows reconstructing the original melt compositions in equilibrium with natural cumulate parageneses and the crystallization sequences resulting from crystal replacement reactions.

We observe that cumulate rocks can be used to track the evolution of melts from which cumulate crystals are segregated, thus offering new physicochemical constraints on cumulate-forming processes operating in alkaline magmatic systems. Clinopyroxene-amphibole phase relationships in magmas interacting with cumulates representing the heralds of previous crustal intrusions may act as a chemical buffer to melt differentiation in alkaline magmatic provinces, and hence help to explain trends in melt compositions observed at intraplate, polygenetic magmatic provinces

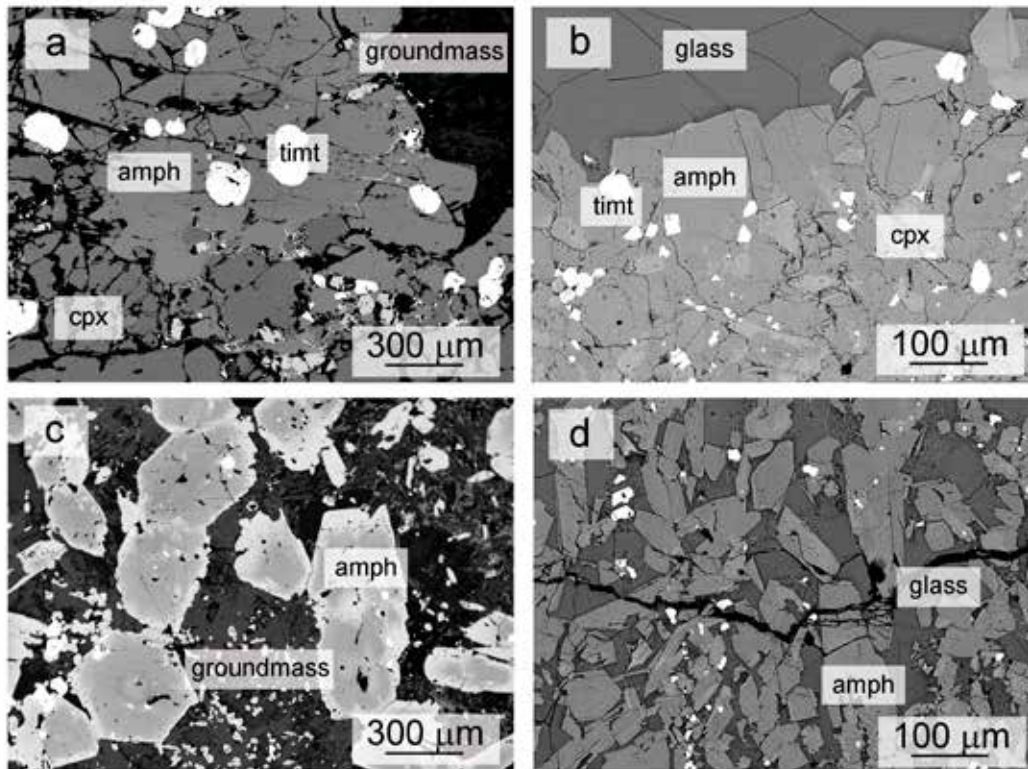


Figure 1

Back Scattered Electron (BSE) images of amphibole-clinopyroxene bearing cumulate rocks and experimental equivalents. a) amphibole-clinopyroxene cumulate with abundant titanomagnetite inclusions; b) experimental equivalent of cumulate in (a) produced via thermal-gradient experiments, with amphibole-clinopyroxene intergrown and abundant titanomagnetite inclusions; c) amphibole-rich cumulates hosted by a microcrystalline lava; d) experimental equivalent of (c) produced in thermal-gradient experiments, and constituted by amphibole-rich cumulate and residual glass preserved in the interstices of the crystalline network.

READING THE MINERAL RECORD OF REE ENRICHMENT IN ALKALINE-SILICATE MAGMATIC SYSTEMS

Soderman C., Beard C.

Rapid growth in the demand for critical metals, including the rare earth elements (REE), is driving expansion and diversification in their supply chains. The majority of the world's REE resources are found in alkaline igneous rocks and carbonatites. We used the EPMA instrument to analyse the compositions and zoning (a proxy for the degree of disequilibrium during crystallisation) of mineral phases from a range of alkaline-silicate systems, which is important to understand the processes controlling REE enrichment. There were two broad scientific aims to this visit. Firstly, to further quantify the nature of zoning in clinopyroxene samples from alkaline-silicate systems; secondly, to determine how widespread these disequilibrium crystallisation textures are across a global suite of alkaline-silicate complexes. All samples studied during this visit have already been characterised for their major and trace elements, and basic petrographic information was already known. Samples were selected based on their mineralogy (containing clinopyroxene, whether optically zoned or not; and containing phases which can be modeled using a thermodynamic dataset being developed for THERMOCALC software as part of this project). The SEM was used as part of a sister project (DREAMSa) to help with phase identification to complement the EPMA work, and help prioritise samples for EPMA. Quantitative point analyses and transects were measured on six samples, covering a range of bulk compositions and tectonic settings: Gardar, Greenland; the Erongo and Etaneno Complexes, Namibia; and NW Scotland. Generally, only subtle compositional zoning was identified in clinopyroxene, with some notable exceptions in samples from the Erongo Complex where pyroxenes showed both sector and concentric zoning (Fig. 1). Both the overall lack of disequilibrium textures, and the characterisation of the zoning in samples where it is present, provide constraints on the applicability of the equilibrium models we are developing to predict REE enrichment in alkaline-silicate systems.

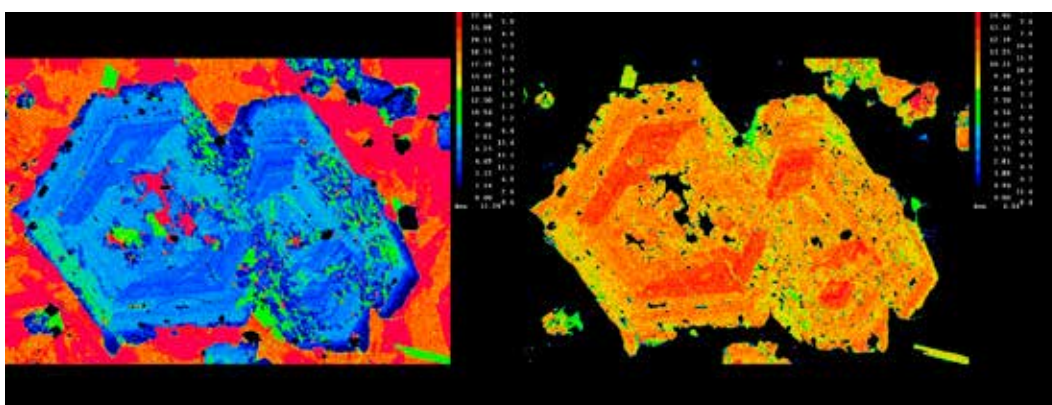


Figure 1
Aluminium (left) and magnesium (right) maps of a sector and growth zoned clinopyroxene glomerocryst in a tephrite sample from the Erongo Complex, Namibia.

UNRAVELLING THE PETROGENESIS OF THE NORTHERN MAKRAN (SE IRAN) PERIDOTITES AND HOSTED CHROMITITES THROUGH THE CHEMISTRY OF THEIR PRIMARY ASSEMBLAGES

Lucci F., Saccani E., Nazzari M., Delavari M.

Ophiolites and related peridotites massifs are outcropping mantle sections and therefore are priceless archives of information on oceanic basins evolution from seafloor spreading stage to final closure. They clearly represent a key for the understanding of geodynamic scenarios and major geological processes. Furthermore, since these ultramafic complexes could host valuable chromitite deposits, no wonder about the relevance of understanding their petrogenesis. In this running project we focus on different ophiolitic units from Sorkhband to Kanuj and Band-e-Zeyarat hosting chromitite layers and ponds, part of the Northern Makran Domain of Iran. The Makran of Iran extends from SE Iran to SW Pakistan for ca. 450 Km and it is near 200 km wide from the Gulf of Oman to the Jaz Murian depression to the north. From south to north the Makran has been divided in three sectors: i) the Makran accretionary prism, ii) the Jaz Murian depression and iii) and the Cenozoic volcanic arc developed on the southern border of the Lut block. Concerning the accretionary prism, it is one of the largest one exposed on Earth and it comprises from south to north the Makran flysch zone, the outer Makran ophiolite belt, the Bajgan-Durkan metamorphic complex and the inner Makran ophiolite belt. The Makran is developed above the northward dipping subduction of Indian oceanic crust under Iran resulting from nearly N-S convergence between Arabia and Eurasia. This subduction environment is believed to have started during Late Jurassic or Early Cretaceous and it is still working. A vigorous debate exists on the geodynamic scenario responsible for the genesis of the different ophiolites units within the accretionary prism sector and above all for the related and diffuse large peridotites and chromitites bodies. The aim of this ongoing work is to unravel the tectono-magmatic framework of these Iranian ultramafic rocks and in general to better understand the genetic environments of chromitite- hosting peridotite massifs. The scientific rationale behind this study, is based on a multidisciplinary approach that integrates petrographic observations, textural characterization and detailed (large and statistically significative) chemistry database of the primary olivine- clinopyroxene-orthopyroxene-spinel assemblages. Chemical indexes such as Cr#, Mg#, X_{Fo}, Al#, X_{Aeg} integrated with opportune classic and forward thermobarometry models will be also applied to explore the petrogenesis of these ultramafic rocks belonging to the Persian sector of the Neo-Tethys realm.

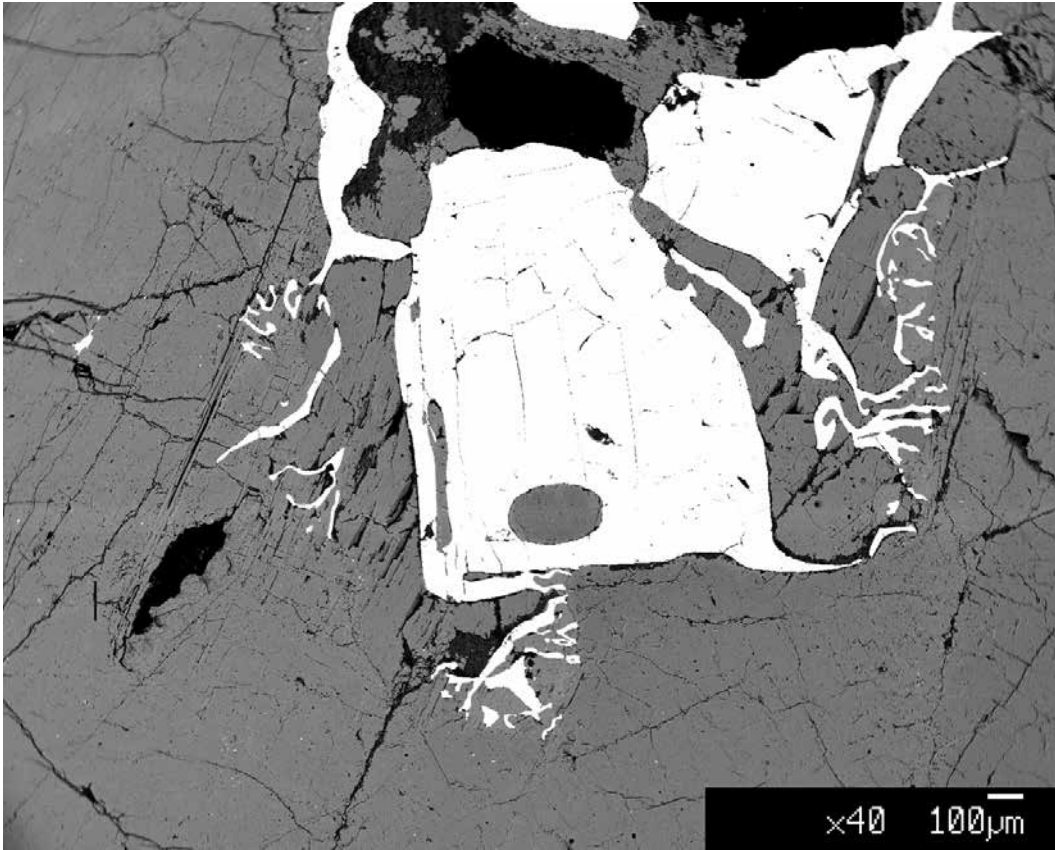


Figure 1
Back-scattered electron (BSE) image showing the typical texture of a Cr-bearing spinel from a massive peridotite sample. In particular it is possible to observe the symplectite textures developed between the spinel and the surrounding clinopyroxenes.

PETROLOGICAL CHARACTERIZATION OF NWA 12800 CARBONACEOUS CHONDRITE

Vitrano A., Foresta Martin F., Nuccio P.M., Lucci F., Bernardini S. , Della Ventura G., Tortora L. , Graziani V. , Nazzari M. , Rotolo S.G.

Carbonaceous chondrites consist of agglomerated primitive components and preserved the history of primordial dust aggregations in the protoplanetary disk. An investigation of NWA 12800 carbonaceous chondrite has been carried out on a thin polished section by means of optical microscopy, backscattered electron imaging, X-ray elemental mapping, EDS and electron microprobe analysis. The meteorite clearly shows chondritic texture, with well-defined chondrules normally ranging in size between 60 μm and 3 mm in diameter embedded in abundant dark grey, fine-grained matrix. Sulfides and metals, like troilite and FeNi alloys, are present as blebs or spherules inside and out of chondrules. Mesostasis glass inside chondrules show no mosaicism, indicative of nearly 3 petrologic types. A fluffy calcium-aluminum rich inclusion (CAI) displays a core-mantle structure. The core has a gehlenitic melilite composition while the mantle is composed of diopside-grossmanite. This kind of CAI texture could be interpreted as a primary nebular condensation sequence by transport in different regions of the protoplanetary disk. Another CAI displays an Al-diopside core enveloped by a sequence of mono-mineralic rims, having a spinel rim and an external diopside rim. This sequence has been interpreted being a record of melting episodes during a high-temperature event in the solar nebula, generated by "flash heating". Compact CAIs, that originated as molten droplets, were also observed. The observed chondrules show several textures as complex and different thermal histories: barred olivine, porphyritic olivine pyroxene, granular olivine, isolated olivine grain, and radial pyroxene. Frequently, chondrules are surrounded by dust-accretionary rims, more rarely by igneous rims. Functional groups of organic compounds were detected in the matrix by means of micro-FTIR. In a large sharp-edged area, characterized by a whitish matrix, only a few not well-defined chondrules are present. The properties of this area appear very similar to CI carbonaceous chondrites. The collected data already obtained suggest a complex petrogenetic scenario of the meteorite. NWA12800 is therefore a polymict breccia, with marked heterogeneity of the distribution of its components and possesses valuable and interesting information to be deeply investigated.

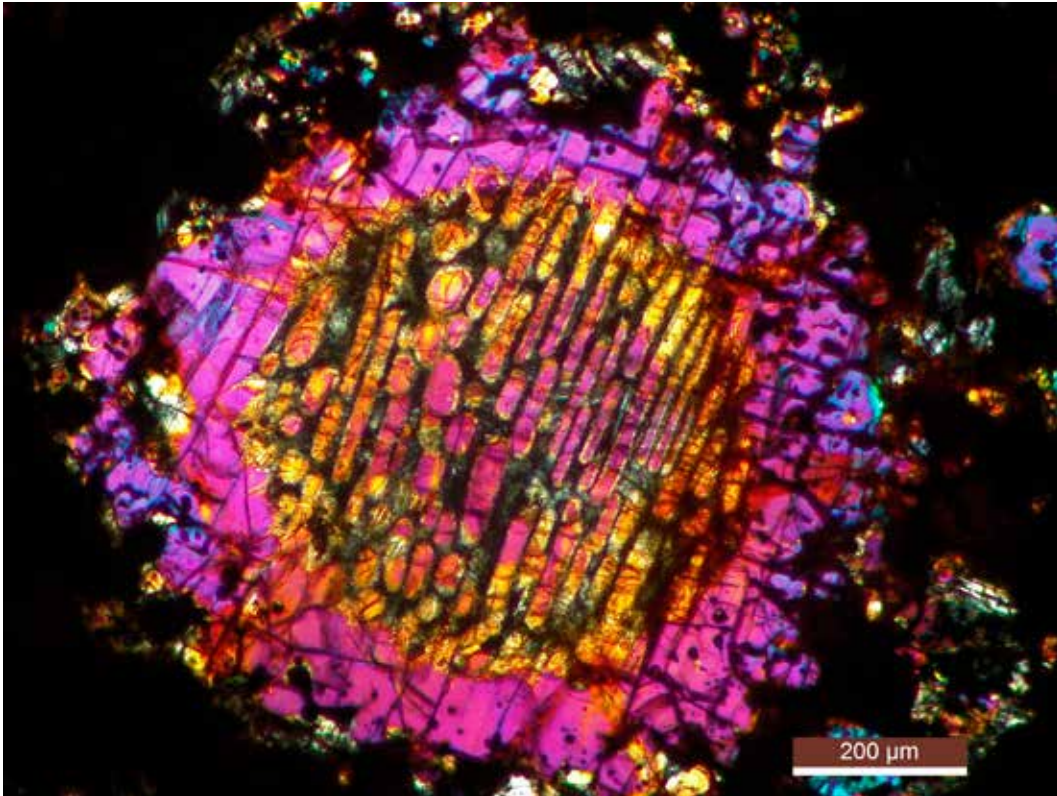


Figure 1
Barred olivine, crossed nicols. This chondrule is the result of the cooling of a melted droplet silicate precursor in microgravity.

8.2 ROCK PHYSICS AND EARTHQUAKES

FAULT REACTIVATION BY FLUID INJECTION: INSIGHT FROM LABORATORY FRICTION EXPERIMENTS WITH MULTIPLE REACTIVATION STEPS

Aretusini S., Cornelio C., Volpe G., Pozzi G., Spagnuolo E., Di Toro G., Cocco M.

One type of fault reactivation is by means of fluid injection. This process consists in the stepwise increase of pore fluid pressure or flow rate. Usually, the need of injecting fluids into rocks is related to anthropic activities which need to dispose of wastewater related to hydrocarbon production. However, the style of fault reactivation, whether seismic or aseismic, with or without any sudden release of elastic strain energy from the body of rocks surrounding the fault, needs to be studied to assess the hazard related to anthropic activities. At the same time, the possibility of performing fluid injection experiments in an underground laboratory, such as the Bedretto laboratory (BULGG, Switzerland) will enhance the understanding of the fault reactivation processes and extend it to the larger and deeper natural earthquakes. In BULGG, small and accessible faults are to be instrumented to monitor all the activity during both fluid injection and fault reactivation (FEAR project).

Here we reproduced fault reactivation by stepwise pore fluid pressure increase in the laboratory via rotary shear experiments performed on fault gouge layers from the MC fault, to be reactivated by fluid injection in the BULGG laboratory. First, we imposed the stresses equivalent to those at depth but scaled by two: 12 MPa normal stress, 7.5 MPa confining pressure, 1.5 MPa pore fluid pressure. Second, we impose slip at 10^{-5} m/s for 0.01 m to have an equally compacted and textured layer. Third, we applied a shear stress so that an equivalent slip tendency of 0.35 is achieved (ca. 2.7 MPa), and kept it constant. Then we stepwise increase pore fluid pressure by 0.1

MPa every 150 s. After reactivation, the maximum slip velocity was set to 0.1 m/s. In the friction experiments, this sequence was performed once (1-sequence) or twice (2-sequence). Our experiments show the radically different frictional behavior and style of reactivation between the 1- and 2-sequence experiments. The 1-sequence experiments have an abrupt reactivation leading to the main event. The 2-sequence experiments have in the second reactivation an “oscillatory” style in which slip rate is accelerating and decelerating just before the main event is triggered by the last step of pore pressure increase. This suggests implicitly a role of the shear fabric developed during the first reactivation stage, in which extensive grain size reduction might have led to stiffening of the fault, responsible for the oscillatory slip. This frictional behavior suggests the importance of the effect of texture development during multiple cycles of seismic slip. The generalization of our data and observations will contribute to shed light on the mechanics of faults and induced earthquakes by fluid pressure increase.

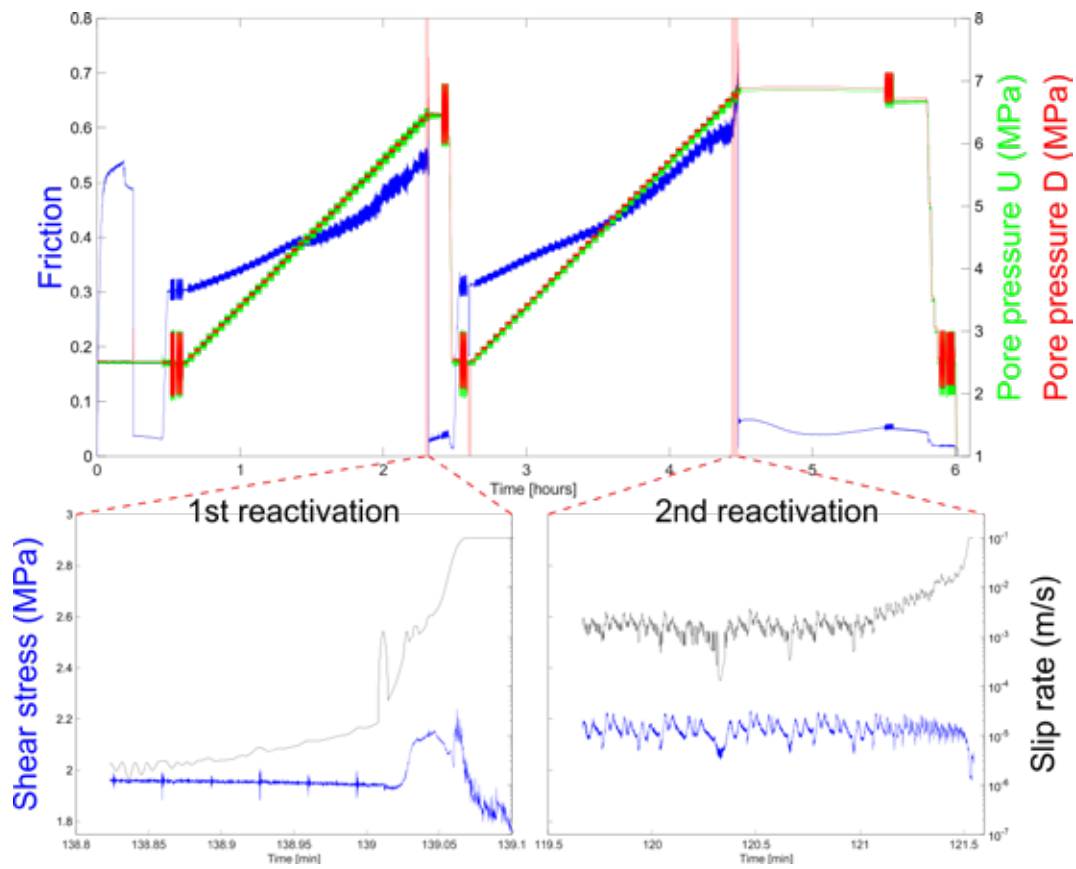


Figure 1
 Reactivation experiment with two subsequent fault reactivations. a) The full experimental sequence: the two reactivations are indicated by red boxes. b) First reactivation is abrupt, linked to a pore pressure increase, b) Second reactivation is oscillatory for several minutes, and then accelerates further with a second pore pressure increase.

DYNAMIC WEAKENING PROCESSES IN THE SLOCHTEREN SANDSTONE FAULT GOUGE CONTROLLING EARTHQUAKE SLIP IN THE GRONINGEN AREA

Hung C.C., Aretusini S., Spagnuolo E., Niemeijer A.R.

In the Groningen area, induced seismicity was related to the extraction of methane gas. Induced earthquakes were typically small (i.e., M3). Laboratory high velocity friction experiments allow to reproduce the slip and slip velocity occurring during these events. In particular, arbitrary slip velocity functions allow better similarity of laboratory experiments with natural earthquakes.

Here, we aim to determine how much frictional heating and weakening can be generated at small scales (grain-grain contact) and resulting dynamic weakening mechanisms during a small and fast slip event. To address this issue, we performed friction experiments using SHIVA on Slochteren sandstone gouge (material from Groningen) with Indian sandstone forcing blocks. All experiments were performed at normal stresses of 12 MPa, confining pressure of 2.5 MPa, under water-saturated and pressurized conditions at pore pressure of 1 MPa, with a novel experimental setup. After applying the stresses and letting the sample compact, we applied a preshear at 5 mm/s for 0.4 m of slip under drained (pressure-constant) conditions, then we applied the seismic slip event under undrained (volume-constant) conditions. To simulate the seismic slip we parameterized triangular and regularized Yoffe functions with large accelerations (15-30-60 m/s²), velocity (1.2-1.7 m/s), and short slip (0.075-0.15 m). To investigate the efficiency of the generation of the frictional heat and its effect on weakening, we performed experiments at low and high normal stresses (8 to 18 MPa). From the measured friction (i.e., the ratio of shear stress and normal stress) we obtained the peak, minimum friction coefficient, the slip weakening distance and show that they vary weakly in all the tested experimental conditions. This suggests that under undrained conditions, seismic slip in the quartz-rich fault gouge hosting earthquakes in the Groningen area appears to be independent of the dissipated frictional power. Future work will focus on numerical modeling and microstructural analysis to investigate the dynamic weakening processes that drive earthquake slip.

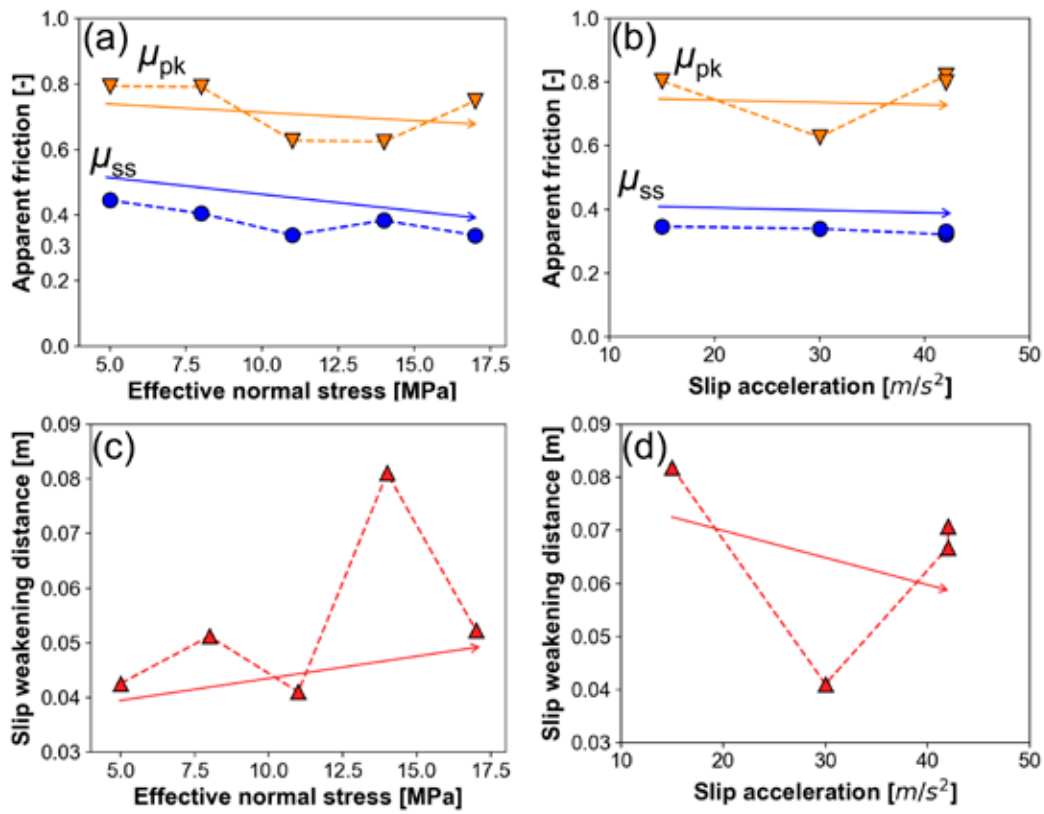


Figure 1
 Compiled constitutive parameters obtained from the experiments. Peak and steady state friction versus: a) effective normal stress, and b) slip acceleration. Slip weakening distance versus: c) effective normal stress, and d) slip acceleration. All the water-saturated gouges show minor dependence of weakening and weakening distance on normal stress and slip acceleration.

LANDSLIDES TRIGGERED BY RAINFALL: INSIGHT FROM LABORATORY EXPERIMENTS

He X., Aretusini S., Spagnuolo E., Di Toro G.

Landslides triggered by rainfall are a serious problem in southeastern China, where highly altered basaltic rocks are affected by slope instability. In the past, laboratory high velocity friction experiments allowed us to replicate the landslide collapse. On top of this, combining a novel experimental setup (Aretusini et al, 2021) and stress-stepping experiments (Giacometti et al., 2018), we can replicate the evolution before and during the collapse on saturated gouges representing the landslide decollement. Here, we performed experiments by loading the altered basalt gouges at normal stress and confining pressure of 5 MPa and initial pore pressure of 2 MPa. Then, sliding at 10⁻⁵ m/s for 0.01 m established an initial microstructure. After this, shear stress was set constant and equal to 90% of the one achieved at the end of preshear. At this point, pore fluid pressure was incremented by 0.1 MPa every 5 minutes from 2 to ca. 3.5 MPa where instability and sliding up to 0.1 m/s occurred. The entire stage of fluid injection and pore pressure stepping was interested by dilatancy events which could be either correlated to normal stress decrease or pore pressure increase. The last dilatant event was the largest and correlated with an increase of slip and slip rate, leading to the landslide collapse. Future work on this matter will focus on explaining the mechanical correlation between dilatancy, slip, and shear stress evolution leading to nucleation of landslides by increase of pore fluid pressure representing rainfall.

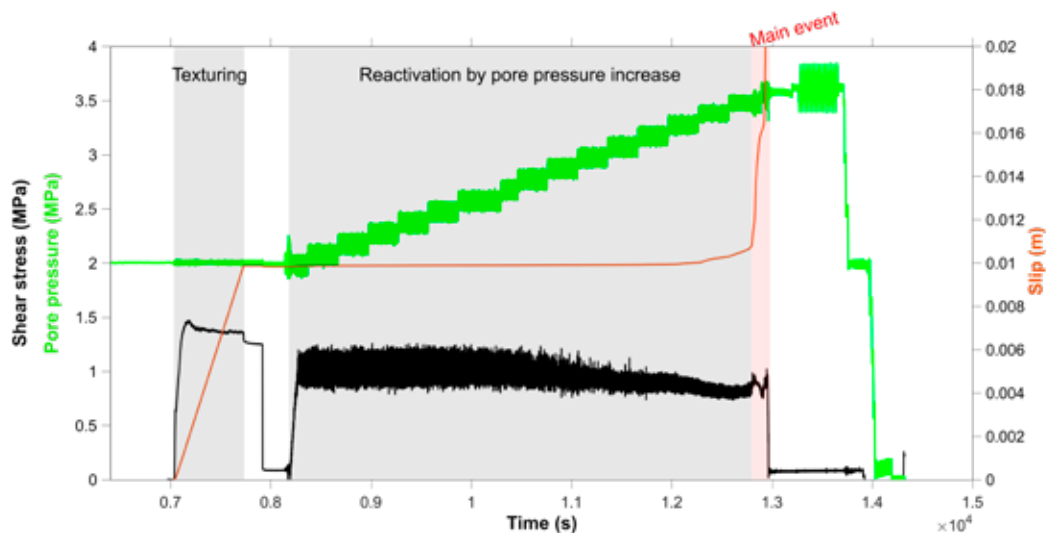


Figure 1 Reactivation experiment by pore fluid pressure increase. The subsequent stages are indicated by gray and red boxes. First, the texturing stage at low velocity (first gray box), then the reactivation stage by pore pressure increase at constant shear stress (second gray box), and finally the main event (red box).

CO₂ ABSORPTION AND HYDRATION TESTS IN BASALTS

Buono G., Cornelio C., Pappalardo L., Spagnuolo E., Procesi M., De Min A., Marzoli A., Etiope G.

This work is a task of the Petrobras (CENPES) / INGV project in “Igneous rocks as source and sink of abiotic hydrocarbons and CO₂”. In task 4 we tested the potential for mineral carbonation of the basalts drilled from the Petrobras sites in Paranà, Campos Basin. We combined two approaches to investigate both the amount of sources for divalent cations in the basalts of interest and the changes in flow path geometries that expose the surface to mineral carbonation. Our approach consisted in (i) measuring in continuous the permeability of sample PTSZ-9 during CO₂-rich water flow-through experiments in a permeameter (ii) performing 3D textural analyses using X-ray computed tomography before and after the mineral carbonation experiments. The permeameter is installed at INGV HPHT lab of Rome and was equipped with a furnace designed on purpose to reproduce reservoir conditions on 20 mm diameter cylindrical samples. The micro-CT is installed at INGV OV of Naples and was used to perform multiscale images of samples PTSZ-7, PTSZ-9, PTSZ-12, PTSZ-18 and CBF. CBF is a fresh basalt recovered from the same district in Campos basin but including the subaerial volcano-sedimentary sequence (Badej and Pampo area) here used for a comparative test. Tests of induced reactive transport of CO₂-rich fluid via CO₂-rich water flow-through experiments on basalt core PTSZ-9 showed that saturation was achieved after 24 days suggesting a low initial permeability (e.g. lower than 10⁻²² m²). At 22.5 MPa of fluid pressure, at the full saturation of the sample resulting in a 36 MPa effective normal stress, measured permeability was $k = 6.1445 \times 10^{-20} \pm 3.2422 \times 10^{-21}$.

Comparison of tomographic slices before and after reaction with CO₂-rich samples on sample PTSZ-9 fluids suggests that, at the condition of the reservoir, mineral carbonation is limited. Our results show that during the experiment dissolution and precipitation were identified mainly on freshly opened fractures (Figure). A possible explanation is that the tested basalts were emplaced during the rifting of the South Atlantic Ocean, over sediments enriched in volatiles, in a basin with attenuated crustal thickness. These basalts suffered extensive seawater interaction which caused enrichment in MgO, FeO total, K₂O, Rb and Ba and depletion in SiO₂ and CaO. At the in-situ conditions, given the rock permeability, the low degree of divalent cations due to previous hydrothermal alteration mineral carbonation is hindered. Moreover, the available data of the reservoir suggest that the site is characterized by a very low storage capacity due to the high degree of mineral carbonation. This means that, in terms of CO₂ storage, the investigated site represents an ideal natural analog where the storage process has reasonably come to completion.

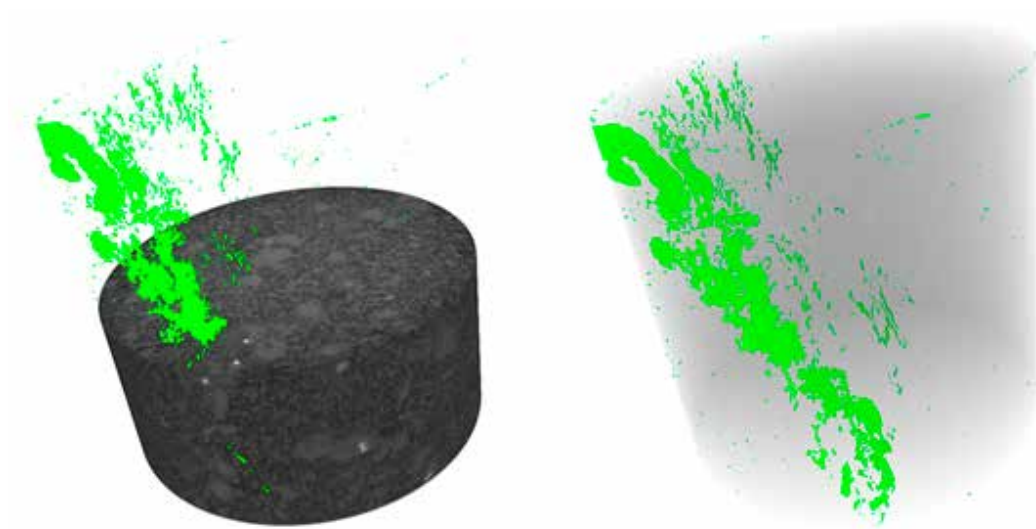


Figure 1
Volume rendering of a sharp, low-density, planar structure with a variable thickness in the basalt sample scanned after the CO₂ hydration test.

MULTIPLE SLIP VELOCITY PULSES ON GOUGE LAYER: MECHANICAL RESPONSE EVOLUTION

Cornelio C., Aretusini S., Spagnuolo E., Di Toro G., Cocco M.

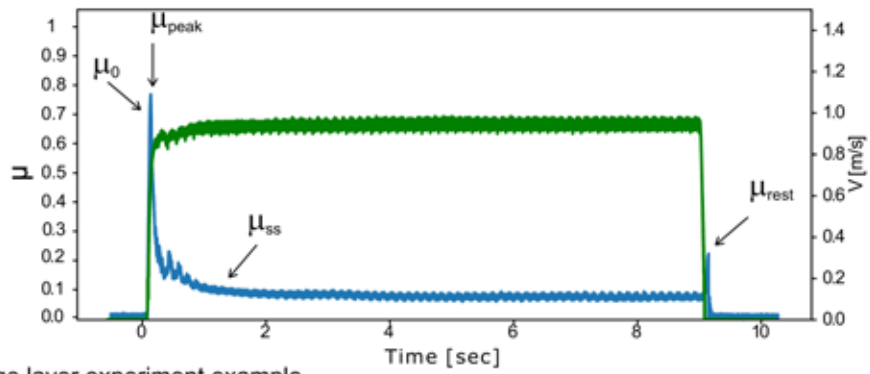
Geological faults are complex systems composed of a fault core, a damage zone and an intact protolith. The fault core is the portion of the fault zone where most of the displacement is accommodated and it can include individual slip surfaces (thin principal slip zones, PSZs), unconsolidated gouge volumes (thick principal slipping zone), or, more often, a complex geometry with different slipping zones with gouges. Geological evidence showed that mature faults, which experience long displacement in their slip history, are richer in gouge, while immature faults, which experience small displacement, are more similar to bare rock surfaces.

Various laboratory experimental techniques aimed to reproduce at small scale the rock deformation during a seismic event. The fault is usually represented as a surface discontinuity (bare rock surface experiments) or as a thick gouge layer. While various studies have been performed to characterize the gouge or bare rock surface behavior under high slip-rate deformation conditions, few studies focused on the evolution of a gouge layer, which undergoes multiple slip-pulses. Here, we present friction experiments that reproduce seismic slip conditions on both gouge and bare rock surface material. The aim of this study is to analyze the evolution of the mechanical behavior of a Carrara marble gouge layer undergoing multiple slip pulses (i.e., four trapezoidal slip pulses at 1 m/s for 1 m of slip, with hold time of 120 s between each pulse) and to compare it with the mechanical behavior of a bare rock surface sample of the same material sheared at 1 m/s for 1 m of slip. All experiments were performed at normal stress of 10, 20, and 30 MPa under room humidity conditions.

Our experimental results show that despite the static and dynamic friction coefficients being higher in gouge than in bare rock surface experiments, the frictional work to achieve the dynamic weakening decreases at each slip pulse in gouge experiments and becomes comparable with the bare rock experiments after the second pulse. Microstructural evidence suggests that most of the energy in the first two pulses is spent for strain localization in a PSZ and bulk grain size reduction within the gouge layer. After the second slip pulse, slip in a one or more well-developed PSZ in the now fine grained gouge layer makes the mechanical behavior analogue to the one of the bare rock surface.

We imply that during the seismic slip history (or earthquake cycle) in a gouge-bearing carbonate fault, which are widespread in the Mediterranean region, the occurrence of repeating earthquakes is energetically favorable, assuming that the PSZ undergoes limited weathering during each interseismic stage.

a. Bare surface experiment example



b. Gouge layer experiment example

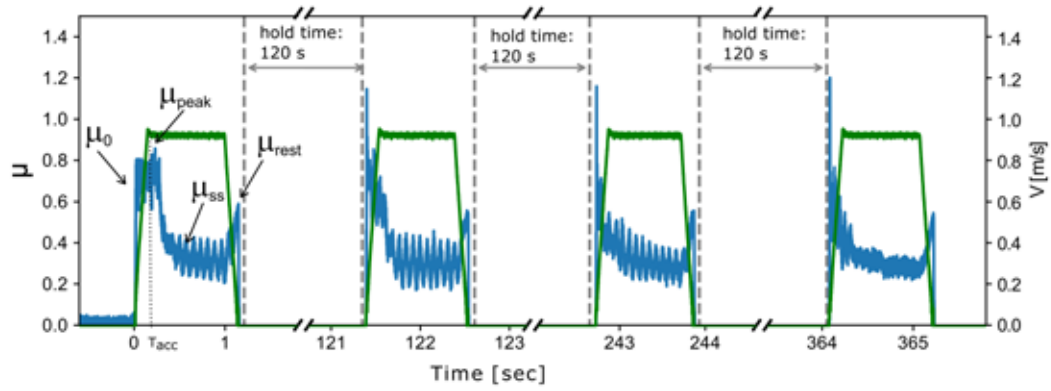


Figure 1

Recorded apparent friction μ and slip rate V for a) bare surface experiment and b) gouge layer experiment. a) for bare surface experiment a single impulse of slip rate was imposed, while b) for gouge experiments, four impulses of slip-rate were imposed with a holding time of 120 second between each seismic pulse. For each experiment, μ_0 , μ_{peak} , μ_{ss} , μ_{rest} are represented.

FRictional PROPERTIES OF QUATERNARY FAULT CORES FROM THE ATACAMA FAULT SYSTEM, NORTHERN CHILEAN FOREARC: ACTIVE FAULTS OR WEAKNESS ZONE OF THE UPPER PLATE?

Gonzalez Y., Pozzi G., Aretusini S., Spagnuolo E., Jensen E., Gonzalez G.

Several geophysical evidences have documented that the most recent normal fault reactivations in the Coastal Cordillera of northern Chile have occurred at least since the late Quaternary. Recently, micrometer-scale permanent deformation has been recorded in the main faults of the Atacama Fault System (AFS) triggered by seismic wave propagation of near-field subduction earthquakes (Victor et al., 2018). Fault reactivation has mostly occurred along the pre-existing trench-parallel faults of the Atacama Fault System located above the down-dip of the seismogenic subduction zone of northern Chile (Figure). Coseismic surface ruptures in this study area are characterized by meter vertical surface offsets of alluvial surfaces cross-cutting Quaternary deposits. These huge structures were formed during early Cretaceous as sinistral faults and reactivated as normal faults during Neogene around 20-10 Myr ago. Geophysical observations suggest that, on the one hand, the AFS seems to be capable of accumulating stress slowly over thousands of years behaving as potentially active faults and, on the other hand, the structures that make up the AFS could be considered as a weak fault zone, where the stress load occurs instantaneously as a consequence of subduction earthquakes. In the last condition the AFS behaves sympathetically in response to nearby or distant earthquakes. However, the deformation mechanisms and the internal structure of these faults remain poorly understood. In this work, we present a methodological proposal in order to understand the role of the internal structure and the mechanical properties of fault zones in the Quaternary reactivations processes of the AFS. We specifically intended to quantify the mechanical properties of fault cores and damage zones of five study sites (site 4 and 8, Fig. 1) using two pioneering apparatuses installed at INGV, BRAVA and SHIVA.

To this end we performed XRD analysis on five major faults to identify mineralogical composition of the fault cores. The fault gouges are composed of phyllosilicates (25-70 wt. %), silicates, and carbonates-sulfates.

Experiments are addressed to (i) build the reactivation envelope by stepping up and down the normal stress from 25 MPa to 125 MPa under water saturated conditions (ii) characterize the rate and state behavior of these gouges (iii) constrain the dynamic parameters under low to high velocities in SHIVA and (iv) test the slip behavior during fault reactivation under a stepping down (unloading) of normal load at constant shear stress. Mechanical results (Fig. 2) indicate that all fault materials are velocity strengthening, the frictional value for reactivation ranges between 0.15 and 0.43 mainly as a function of the phyllosilicate content. All fault materials undergo dynamic weakening with peak friction between 0.35- 0.52 and dynamic friction as low as 0.15 – 0.25. Moreover, reactivation by unloading is abrupt only for low-phyllosilicates gouges. Results suggest that the reactivated segments of the AFS are conditioned by the occurrence of frictionally weak fault cores representing a structural weakness zone of the upper plate region located above the seismogenic subduction zone.

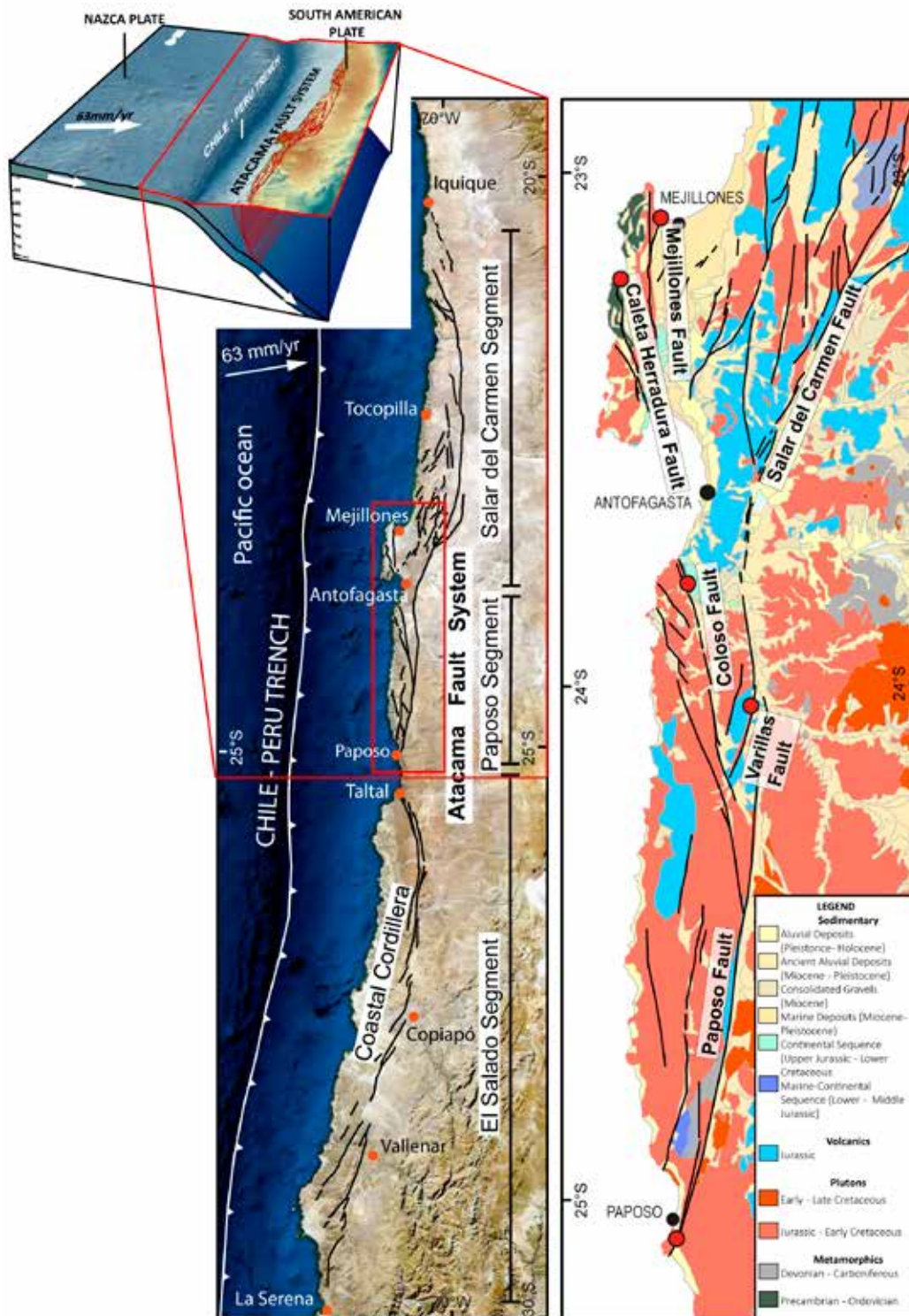
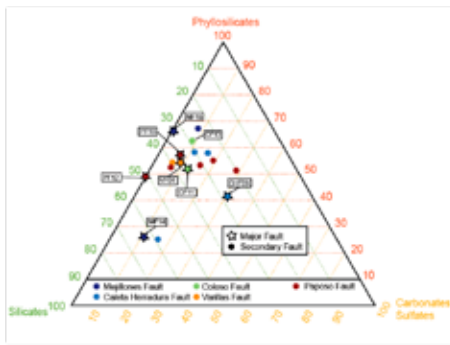
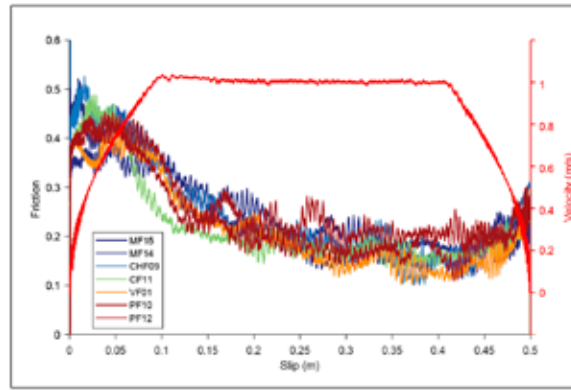


Figure 1
 Block diagram of the geological setting of northern Chile between 19-25°S. The subduction zone was modeled from Hayes (2018). b) Map of northern Chile showing the Atacama Fault System (black lines indicating fault traces). c) Location of the selected study sites (red circles) at the Paposo segment and southernmost part of the Salar del Carmen segment. The hillshade image was generated by ArcGIS 10.5.1 based on the 12.5m DEM provided by AlosPalsar.

- **Water Saturated (10 MPa)**
- **Preshear stage (10 $\mu\text{m/s}$)**
- **High velocity (1 m/s)**



a)



b)

Figure 2
 (a) Mechanical data represented in a ternary phase diagram as a function of phyllosilicate content (b) dynamic weakening and dynamic parameters from high velocity experiments on the five major fault gouges.

IDENTIFYING WHETHER (AND WHEN?) RADON CHANGES IN EXPERIMENTALLY LOADED LABORATORY FAULTS

Benà E., Spagnuolo E., Piersanti A., Sassi R.

The aim of this experimental study is to evaluate if radon is affected by rapid changes in the stress field in the four lithologies sampled in the area of Pusteria/Pustertal Valley (north-eastern Italy). The distribution and the magnitude of radon, thoron and CO₂ soil gas anomalies was previously analyzed in this area at 278 sites according to a regular grid and along three N-S profiles crossing the aseismic Pusteria fault system, over an area of about 60 km². The area is characterized by the Periadriatic fault system which is the aseismic tectonic boundary between the Austroalpine orogenic wedge and the Southalpine indenter in the Eastern Alps. The outcropping crystalline basement is composed of orthogneiss and paragneiss (Austroalpine domain) to the north of the PF, and phyllites intruded by granites (Southalpine domain) to the south of the PF. With the aim of testing the behavior of radon in the presence of pre-existing faults and fracture in a natural and amply monitored setting, we performed 14 experiments on the four lithologies using non conventional creep tests in SHIVA on pre-cut cylindrical samples. Pre-cut samples are put in friction under a constant normal load (5 MPa) and a constant stepwise increase in shear stress until sample slip. The pre-cut simulates the presence of a pre-existing fault, the assembly was closed in a vessel designed for fluid confinement. Radon was continuously recorded during the loading stage using a Lucas cell connected to the vessel. Air was forced to circulate from/to the cell using a pump. The time series of radon was analyzed using change points analysis designed to detect significant changes in the radon time series. Main results of this study are: (i) radon is sensitive to rapid changes in the shear stress (ii) the temporal variation and the amount of these variations depend on lithology (iii) the detected change points in the radon time series correlate with significant changes in the mechanical data either in the shear stress and/or axial dilation (Figure). This correlation is significant since the mechanical data and radon data are independent measures. This study suggests that radon is effective to monitor temporal changes in the state of stress exerted on the sample.

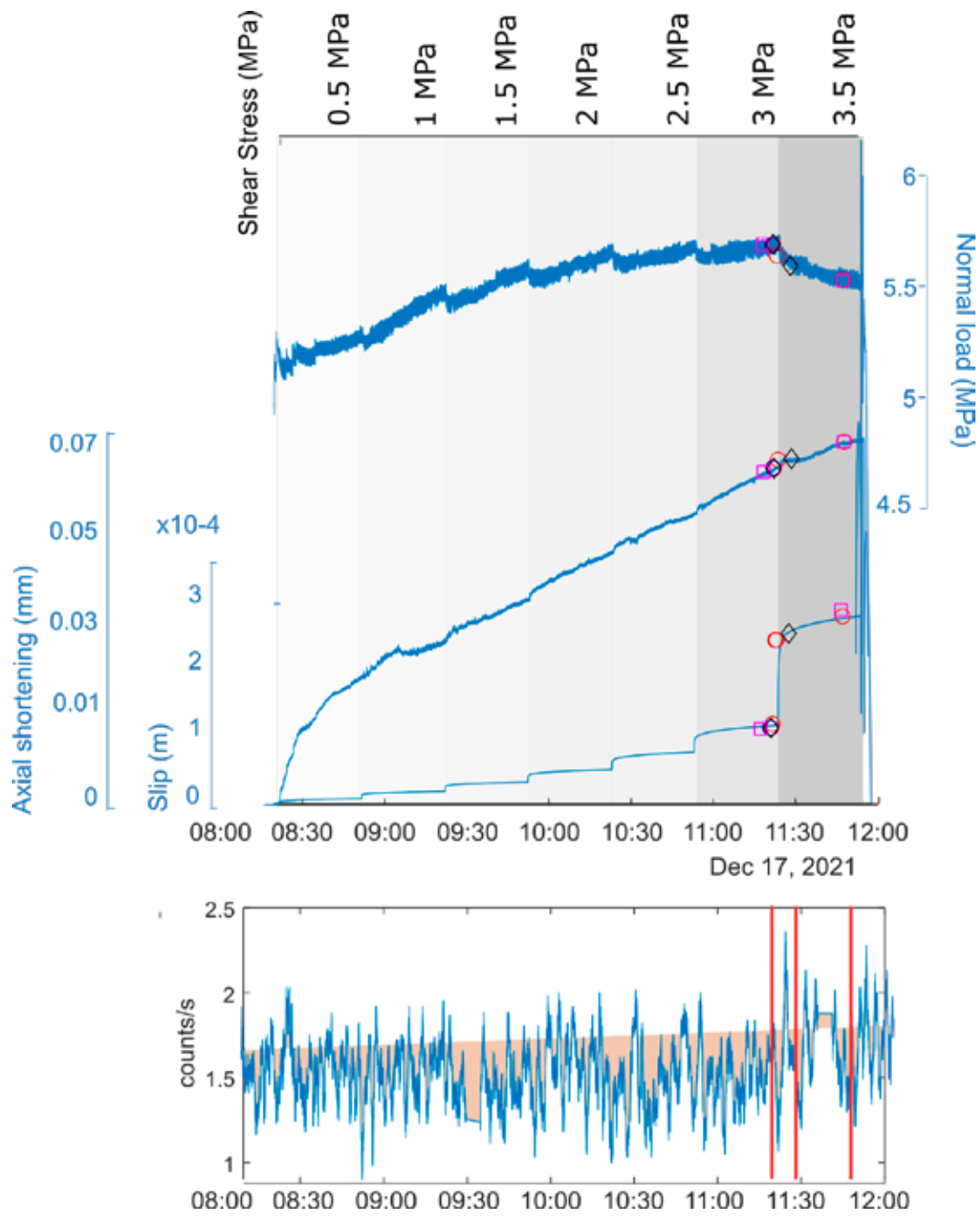


Figure 1

Experiment s1897 in granite. Mechanical data (upper panel) versus radon time series (lower panel), filtered with a moving time window of 1 minute, with change points. Change points were calculated using: mean (red circles), rms (blue circles), std (squares magenta), lin (black diamonds). Mechanical data are: shear stress represented by a stepwise increase in gray shaded rectangles, normal load, axial shortening and slip. The change point analysis for radon time series evidences significant points in the mechanical data. The radon time series for granite appears with an increasing trend.

MIRROR-LIKE SURFACES IN BITUMINOUS DOLOSTONES (CENTRAL APENNINES, ITALY)

Chinello M., Fondriest M., Tesei T., Spagnuolo E., Schito A., Bowden S.A., Germinario L., Mazzoli C., Cornelio C., Di Toro G.

Mirror-like surfaces (MSs) are ultra-polished fault surfaces that reflect visible light thanks to their low surface roughness (nm-scale). These ultra-polished surfaces are often found in seismogenic fault zones cutting limestones and dolostones. Both natural and experimentally-produced fault-related MSs were described in spatial association with ultrafine matrix (grain size $<10\mu\text{m}$), nanograins ($<100\text{nm}$ in size), amorphous carbon, decomposition products of calcite/dolomite (i.e., portlandite, periclase) and larger in size but “truncated” clasts. However, the mechanism of formation of MSs is still a matter of debate. Indeed, experimental evidence shows that MSs can develop both under seismic (slip rate $\approx 1\text{ m/s}$), and aseismic (slip rate $\approx 0.1\text{-}10\ \mu\text{m/s}$) deformation conditions, involving various physical-chemical processes operating over a broad range of P-T conditions, strain and strain rates.

To understand how MSs form and their role in the seismic cycle, 10 samples were collected and analysed from normal faults cutting bituminous dolostones (Central Apennines, Italy). The MSs samples were from faults with increasing cumulated slip (from $< 1\text{ mm}$ to few meters) and different resolved stress.

Ultra-high resolution scanning electron microstructural investigations of the MSs and the associated slip zones, show that the mirrors consist of exposed surfaces of ultra-flat dolostone grains and dolomite nanoparticles cemented by a $<1\text{-}2\ \mu\text{m}$ thick matrix of smeared bitumen. Cataclastic flow and pressure solution aided by the presence of bitumen are the main deformation mechanisms, probably associated with aseismic creep and fault healing/sealing during the seismic cycle.

Surface microroughness measurements (White Light Interferometry) reveal that (1) the RMS microroughness is $< 500\text{ nm}$ over a lateral distance $< 1\text{ mm}$ and (2) both the profile and the areal RMS show a weak inverse correlation with increasing displacement. The Power Spectral Density (PSD) analysis shows that only in the sample with a displacement of less than 1 mm there is a dependence of roughness with slip direction is present (that is, striae are observed).

Finally, Gas Chromatography-Mass Spectrometry analyses conducted on bitumen biomarkers from a fault MS which accommodated 86 cm of slip displacement show changes in the structure of biomarkers relative to the wall rocks, possibly a consequence of frictional heating during seismic slip.

This multidisciplinary study, by investigating the mechanism of formation of MSs, show that these ultra-polished features record the main phases of the seismic cycle, including coseismic slip (changes in the biomarkers structure), aseismic creep (viscous flow of bitumen) and inter-seismic fault sealing/healing (pressure-solution and cold sintering).

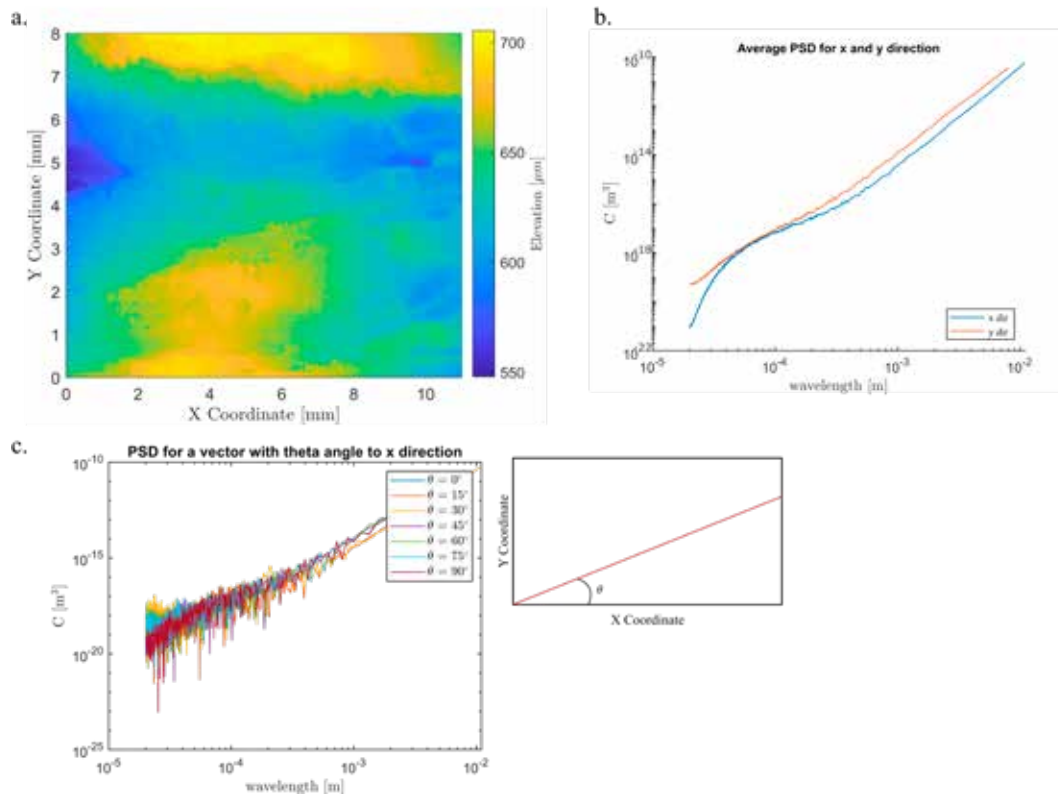


Figure 1
 Roughness measurements and PSD analysis. a) Surface microroughness measurements for sample FTW08 b) Power Spectral Density evolution with wavelength averaged in x and y direction. c) Power Spectral Density evolution versus wavelength for one vector tilted by θ respect to the x direction.

FAULT ROCKS ASSOCIATED WITH THE RESERVOIR-TRIGGERED SEISMICITY OF THE KOYNA-WARNA AREA (INDIA)

Di Toro G., Chiesurin A., Spagnuolo E., Gomila R., Roy S.

In 1962, the Koyna Dam was completed in a rural area 250 km southeast of Mumbai (India), primarily for hydropower generation. Since then, the area, which was essentially devoid of natural seismicity, has been affected by a sequence of moderate to large magnitude earthquakes, including the one of December 11th, 1967 (ML6.3, 177 casualties), the largest human-induced earthquake so far. Major earthquakes (ML>4) are modulated by basin-filling and emptying operations, which follow the monsoon regime with peak rainfall between July and September. There are two peaks of seismicity: the first between August and September (“rapid-response”), corresponding to the rainy season, and the second in February (“delayed-response”) corresponding to the dry season. The ML>3 earthquakes have normal to strike-slip focal mechanisms, reactivate steeply-dipping faults/fractures, and are located between 3 and 10 km depth in the granitoid Indian basement (2.7-2.6 Ga) buried beneath the 0.5-2 km thick Deccan basaltic lava flows (68-60 Ma). The temperature at hypocentral depths is estimated to be between 80 and 200°C. Especially the delayed-response seismicity implies poro-elastic effects, also related to the percolation of water from the surface to hypocentral depths. To study the seismicity of the area, a large deep drilling project was completed by the Ministry of Earth Sciences (India) which includes nine wells down to 1.5 km depth and a pilot well down to 3 km depth. Here we describe the fault rocks (mylonites, cataclasites, breccia and faults/fractures filled by epidote, quartz, chlorite and calcite veins) collected in boreholes KBH1, KBH6 and KBH7.

Visual analysis of the cores plus mineralogical, microstructural and geochemical investigations (X-ray powder diffraction; scanning electron microscope equipped with Wavelength-Dispersive X-Ray Spectroscopy) allowed us to reconstruct the sequence of deformation events. Steeply-dipping faults/fractures filled by chlorite and calcite are the last deformation event as they cut through all other structural features. We recognized eight types of chlorites based on optical properties, crosscutting relations and chemical composition. The temperature of formation of the chlorite spans from 350°C (or HT-chlorite found in the shear zones cut by the Deccan basaltic dykes), to 200°C<T<250°C (or LT-chlorite filling fault/fractures cut by calcite veins, but with uncertain crosscutting relations with Deccan basaltic dykes), and 130°C<T<135°C (or Very-LT-chlorite filling fault/fractures, which are also cut by calcite veins, and cut the Deccan basaltic dykes). LT- and Very-LT-chlorite formation temperatures were estimated with the Bourdelle & Cathelineau (2015) chlorite geothermometer. The range of 130°C<T<250°C for chlorite formation, which can be extended to lower temperatures considering that these faults/fractures are cut by calcite veins, overlaps

with the one ($80^{\circ}\text{C} < T < 200^{\circ}\text{C}$) estimated at the hypocentral depths of the Koyna-Warna area. Moreover, these fault/fractures found in the boreholes are hosted in steeply-dipping fault/fractures (or sub-parallel to the structures illuminated by the hypocentral distributions), and are filled by minerals precipitated from percolating fluids (i.e., consistent with the evidence of delayed-response seismicity). We conclude that the faults/fractures currently reactivated by reservoir-triggered seismicity most likely correspond to those filled by calcite and LT- to Very-LT chlorites found in the deep boreholes.

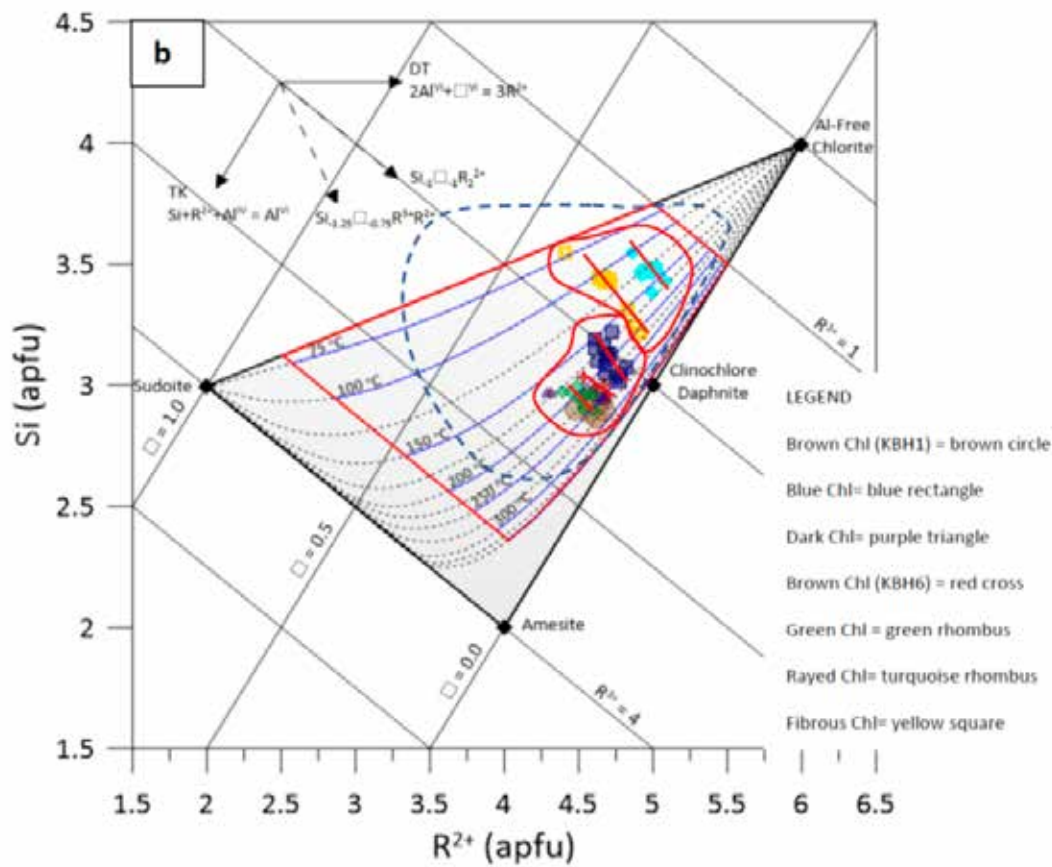


Figure 1
 Temperature of formation of the Mg-chlorites from the Koyna borehole samples. The diagram reports the isotherms calculated with the geothermometer of Bourdelle & Chatelineau (2015). In the boreholes, seven Mg-chlorite classes were found. Chlorites of KBH7, closed red curve in top right, have the lowest formation temperatures, are associated with calcite-bearing veins and belong to the faults/fractures that cut the other chlorite-bearing faults. The faults/fractures currently reactivated by reservoir-triggered seismicity in Koyna-Warna area most likely correspond to those filled by calcite and LT- to Very-LT chlorites found in the deep boreholes.

THE EFFECT OF NORMAL STRESS OSCILLATIONS ON FAULT SLIP BEHAVIOR NEAR THE STABILITY TRANSITION FROM STABLE TO UNSTABLE MOTION

Pignalberi F., Giorgetti C., Noël C., Marone C., Collettini C., Scuderi M.M.

Tectonic fault zones are subject to normal stress variations with a wide range of spatiotemporal scales, resulting in stress field alteration. These perturbations can spread over a large range of frequencies and amplitudes from the high frequencies of seismic waves generated by earthquakes to the low frequencies of solid earth tides. Because of these normal stress perturbations, critically stressed faults can be reactivated. Existing works show that complex behaviors may arise from the interplay between friction changes with slip, slip rate and stress perturbations. To shed light on the mechanics of fault dynamic triggering we performed experiments in the biaxial apparatus BRAVA in a double direct shear configuration under critically stable stiffness conditions ($K/K_c \sim 1$). We used powdered quartz gouge (Min-U-Sil) as starting material, and conducted experiments in a range of reference normal stress of $\sigma_n = 10\text{-}13.5$ MPa. After shearing the material and reaching a steady state sliding at $10 \mu\text{m/s}$, normal stress oscillations were applied with amplitudes A ranging between 0.5 and 2 MPa and periods T between 0.5 s and 50 s. In addition, we used the laboratory derived friction parameters as input for forward modeling using the rate-and-state friction law and a modified rate and state equation in order to assess if these laws can explain our data. Our results show that creeping faults, under critical stiffness conditions, are sensitive to normal stress perturbations showing a variety of slip behaviors depending on the amplitude and frequency of the oscillations:

1. Oscillation frequency has a major effect on fault stability. Low and high frequencies cause a Coulomb-like response of the shear stress accompanied by a complex frictional response with slow events and period doubling. At the critical frequency predicted by the rate-and-state friction law, we observe dynamic weakening resulting in regular stick-slip events.
2. Oscillation amplitude also plays a role with the main effect on the fault strength depending on the magnitude of the perturbation.
3. Using the modified rate-and-state equation we are able to accurately model the laboratory data.

Our results show that normal stress perturbation on a laboratory creeping fault, at critical stiffness condition, can reproduce the entire spectrum of fault slip behavior depending on the oscillation properties.

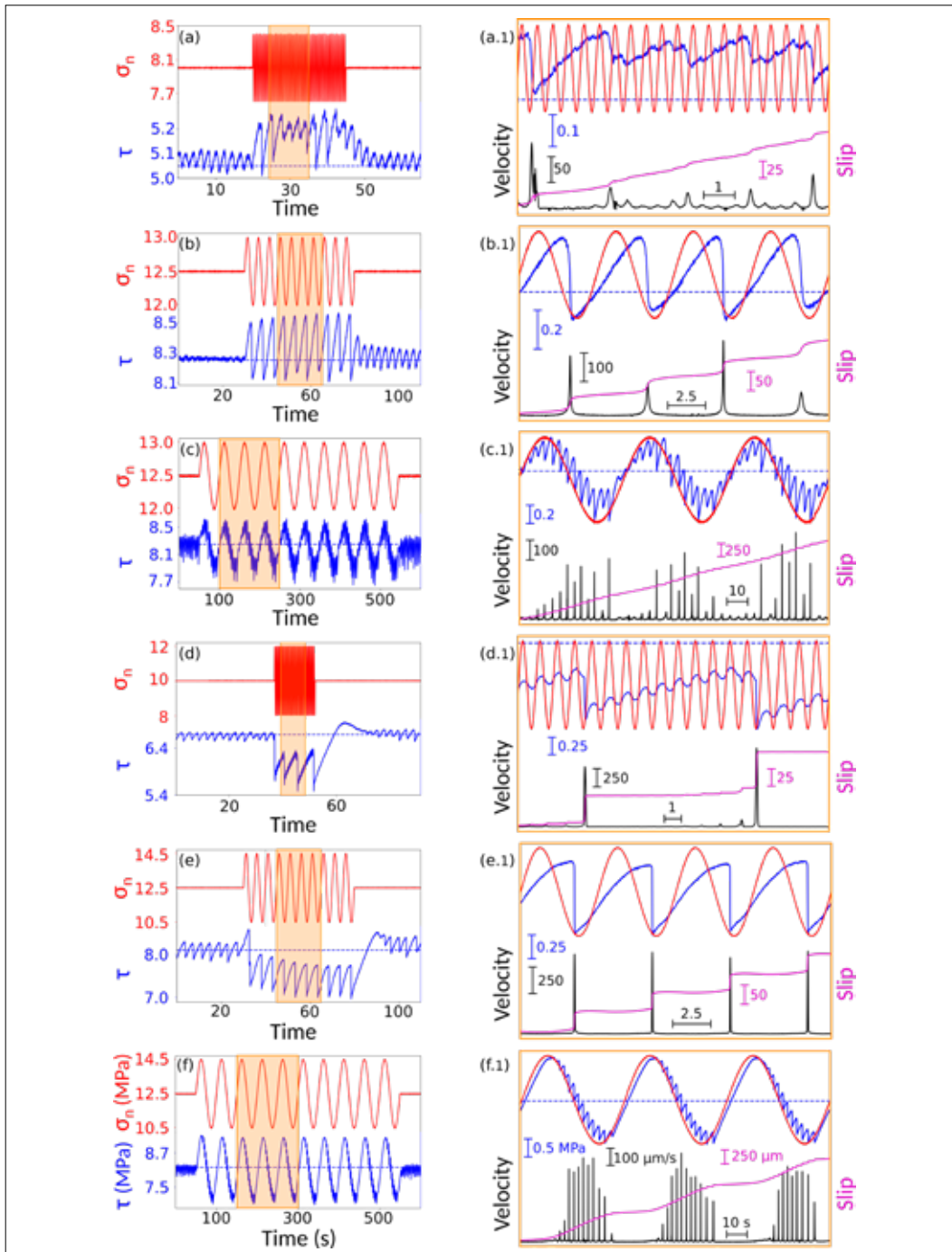


Figure 1

Mechanical data for a range of normal stress oscillations. Each panel shows the shear stress (blue) and normal stress (red) for one set of conditions. Blue dotted line shows the initial shear stress. Shaded areas in plots on left are shown as zooms on the right and include slip (magenta line) and slip velocity (black line) below the normal stress (A as on left) and shear stress (scale bar shown). (a) $A = 0.5$ MPa and $T = 0.5$ s. (b) $A = 0.5$ MPa and $T = 5$ s. (c) $A = 0.5$ MPa and $T = 50$ s. (d) $A = 2$ MPa and $T = 0.5$ s. (e) $A = 2$ MPa and $T = 5$ s. (f) $A = 2$ MPa and $T = 50$ s. Note that small stress drops are observed during normal stress reduction for $T=50$ s and more complex behavior, with large, dynamic slip events for other periods.

FABRIC-CONTROLLED FAULT STABILITY IN MONTMORILLONITE

Volpe G., Pozzi G., Collettini C.

Montmorillonite is a phyllosilicate mineral present in most of the subduction zones worldwide. This mineral is known for its low friction, null healing rate, and a strong velocity strengthening behavior, which is argued to promote aseismic, stable fault slip. However, the characterization of the frictional properties of montmorillonite has been generally conducted at deforming velocities largely exceeding the plate rate motion. In this study, we decided to test its frictional properties at deforming velocities close to the plate rate motion using the BRAVA apparatus hosted at the INGV of Rome.

We performed a systematic suite of shear experiments at different normal stresses (12.5, 25, 35, 50 and 100 MPa), 100% room humidity, and using a de-stiffened loading ram. Montmorillonite powders were deformed at velocities as low as 30 nm/s, which correspond to a velocity of around 90 cm/y, which is in the same order of magnitude of the fastest plate rates (decimeters per year). The material displayed low frictional strength (friction coefficient < 0.3) that becomes pressure insensitive at normal stresses higher than 35 MPa thus promoting a viscous-frictional behavior. Velocity strengthening behavior was recorded at all velocities and became more marked with increasing slip rate.

Our results overall agree with the results of Saffer and Marone (2003). However, at slip velocities lower than 0.1 $\mu\text{m/s}$ our samples displayed an unstable stick-slip behavior despite the velocity-strengthening property of friction. These instabilities disappear at normal stresses higher than 35 MPa, and thus in correspondence of the transition from frictional to visco-frictional rheology.

To better understand this behavior, we conducted microstructural analysis on the deformed microstructures using BSE imaging on the FESEM hosted at the INGV of Rome. Our analysis highlighted a direct dependence of the fault slip behavior to the experimental fault fabric. We observed the presence of strong localization in the unstable gouges, deformed at low normal stresses, in contrast to a pervasive and distributed deformation for the stable gouges, deformed and high normal stresses. Localized slip is associated with undulose and irregular foliation which may promote sites of stress concentration and fault jamming, allowing for build-up and periodic release of elastic energy. Distributed slip is met with regular foliation that allows for preferential stable slip on shear-parallel horizons (c-fabric). We conclude that, despite the expected stable behavior predicted by rate and state friction theory, heterogeneity of stress distribution promoted by irregular fabric dominates the macroscopic unstable fault slip behavior.

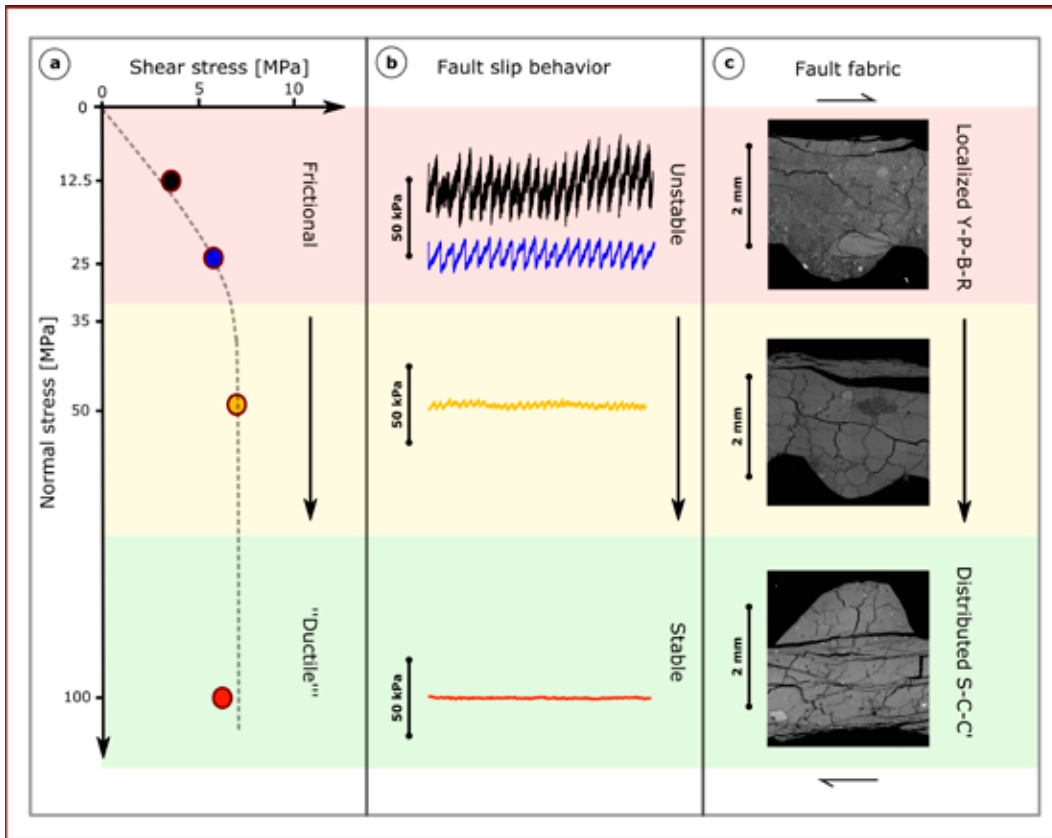


Figure 1
 Synoptic representation of the experimental results: a) Shear strength with increasing normal stress conditions. b) Evolution of friction with displacement. c) SEM back-scattered images of the cross-sections of the experimental faults.

A SYSTEMATIC STUDY OF TERNARY MIXTURES TO UNDERSTAND HOW MINERALOGICAL COMPOSITION AFFECTS THE FRICTIONAL PROPERTIES OF FAULT GOUGES

Ruggieri R., Pozzi G., Collettini C.

Natural faults are often marked by the presence of a narrow principal slip zone, characterized by fine-grained wear materials (fault gouge) produced during cumulative slip. The mineralogical composition of these fault gouges exerts a primary control on fault friction and hence on fault slip behavior. It is unclear, however, whether a systematic variation of rock composition corresponds to a systematic change of its frictional behavior. Understanding the link between fault gouge composition and frictional behavior is key to earthquake hazard assessment both for natural and induced seismicity.

For this study we selected three representative mineral phases that present severely different frictional properties and are commonly found in natural fault zones: muscovite (phyllosilicate), quartz (granular silicate) and calcite (granular carbonate). We present a systematic study of frictional properties retrieved for pure phases and their mixtures (Fig. 1a).

Thirty double direct shear experiments were performed using a biaxial rock deformation apparatus BRAVA at normal stress of 50 and 100 MPa, at room temperature, and water saturation conditions. All experiments consist of three stages. The first is a “run-in” phase of 10 mm at slip velocity of 10 $\mu\text{m/s}$ used to measure the steady-state friction. Following, a series of computer-controlled slide-hold-slide tests where the sample was maintained under quasi-stationary contact for 30 s to 1000 s and re-sheared to measure the frictional healing. Then velocity steps were performed by changing the sliding velocity from 0.3 up to 300 $\mu\text{m/s}$ to evaluate the rate and state parameters.

Increasing muscovite content results in a decrease of the frictional strength, from 0.62 for pure calcite and 0.56 for pure quartz down to 0.33 for pure muscovite powders. This effect is more marked in calcite-rich mixtures rather than quartz-rich ones, possibly due to favorable conditions for fluid-assisted pressure-solution at grain contacts. The healing ($\Delta\mu$) of the investigated materials increases linearly with hold time and reduces with increasing muscovite content (Fig. 1c). Mixtures of pure strong mineral phases (quartz and calcite) show high $\Delta\mu$ values, which range between 0.012 and 0.030, while for the pure muscovite gouge are smaller by an order of magnitude. The healing rate (linear variation of healing with logarithm of time) provides an estimate of the ability of fault to regain strength during hold periods. The strong mineral phases (calcite and quartz) show higher healing rates with a maximum value (0.013-0.014) for the 50/50 mixtures of quartz and calcite, while muscovite content severely decreases these values. The friction rate parameter $a-b$ is also strongly controlled by lithology. All mixtures exhibit velocity-strengthening behavior ($a-b > 0$), except for pure quartz at the highest sliding velocities. Pure calcite gouges show the highest values of $a-b$, 0.016-0.01, at low sliding velocities.

An increase of muscovite content in calcite-rich and in muscovite-rich gouges severely increases the values of $a-b$.

In conclusion, these experiments highlight that the mineralogical composition of fault gouges significantly affects the frictional strength, healing, and stability with a non-trivial, but consistent pattern. Calcite-muscovite interaction favors a reduction of frictional strength, frictional healing and a more marked velocity-strengthening behavior (promoting stable sliding and fault creep) in comparison to quartz-muscovite mixtures, marking the different response of the two granular phases.

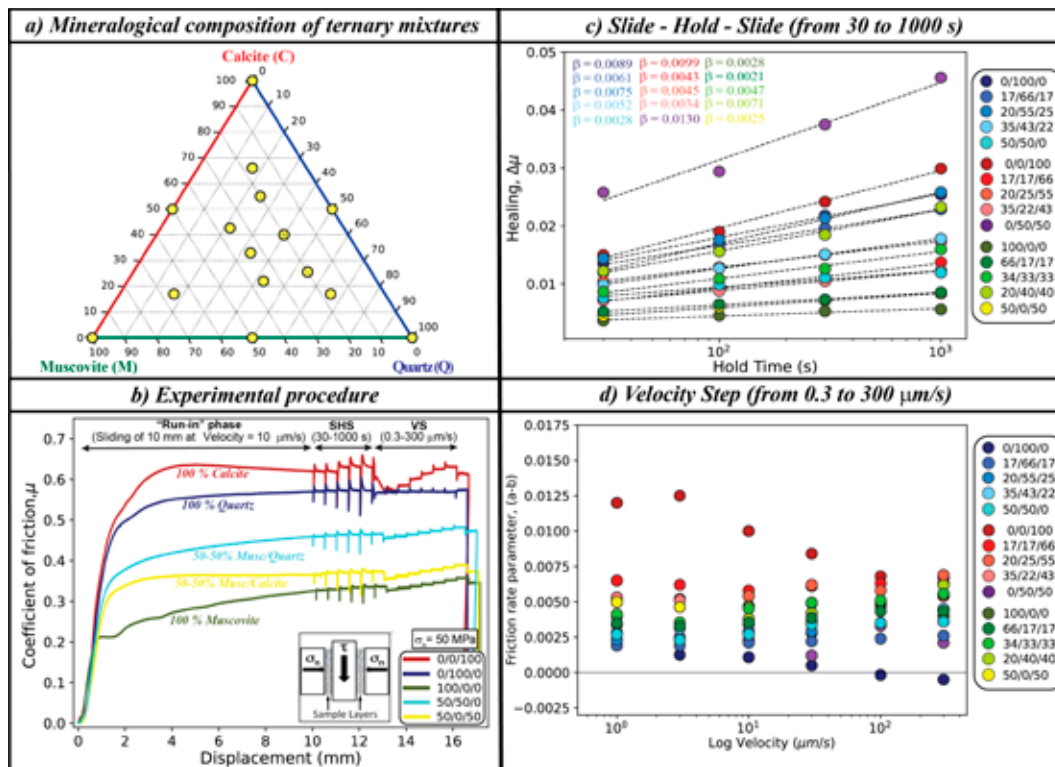


Figure 1
a) Ternary diagram of all tested mixtures composed of muscovite, quartz, and calcite mineral phases. b) Evolution of friction coefficient as a function of displacement, (c) of hold time (frictional healing), and (d) of sliding velocity (rate dependence).

8.3 TECHNOLOGY

THE HERMES PAYLOAD 2022 CAMPAIGN LAUNCH

Iarocci A., Di Stefano G., Romeo G., Vallocchia M., Mari M., Lepore A., Adobbato P., Bacci S.

The Italian payload HERMES (HEmera Returning MESsenger), a project funded and coordinated by the Italian Space Agency (ASI) and whose scientific manager is the National Institute of Geophysics and Volcanology (INGV), was launched at high altitude via a Zero Pressure Balloon last July 21, 2022 at the ESRANGE space base (Kiruna, Sweden) by the Swedish Space Corporation (SSC).

The goal was to carry out the first test for the collection of scientific data from the stratosphere and the transfer to the ground by means of a vector.

The launch of HERMES is part of the European project HEMERA, born with the aim of improving and coordinating the scientific activities aimed at creating a shared and interoperable technical-scientific platform where it is possible to carry out experiments transported by stratospheric balloons.

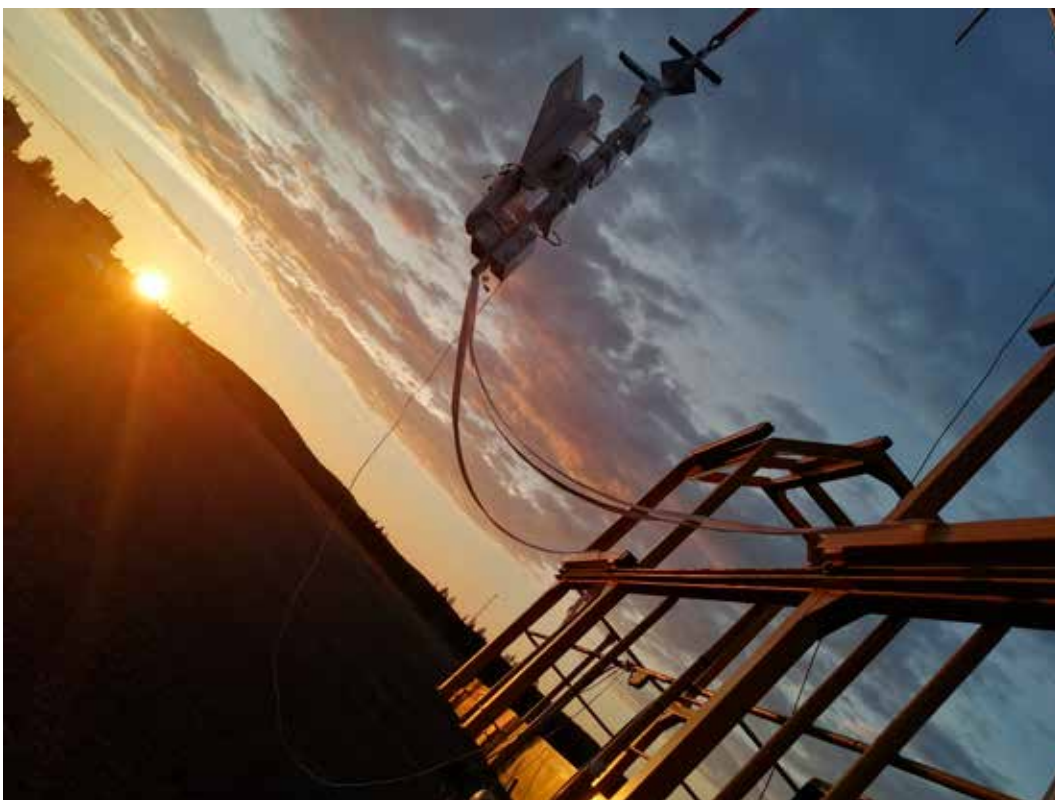


Figure 1
The payload in flight configuration.

Here the most significant data of the flight chain:

- Payload dimensions: 1.7 m (length),
- 1.2 m (glider wingspan);
- Payload mass: 16 Kg (glider 3 kg);
- Total Flight Train weight: 42.7 kg;
- Balloon (3SF ZPB 3000m3) mass: 41 kg,
- Total mass: 83.7 kg;
- Parachute: 19 ft diameter, 26.4 m2;
- Launch method: Hercules.

After launch the balloon starts to rise with an ascent speed of about 4.1 m/s. After about 1 hour and 40 minutes the balloon reached an altitude of about 23.000 m and began the floating phase



Figure 2
The trajectory.

As soon as the balloon entered safety zone B at Esrange, the Iridium command was sent from the ground station to the payload to release the glider. The release system then worked properly releasing the glider, which began its descent in free fall. Unfortunately, the glider started gliding only at 6000 m of altitude, and then landed correctly a few km before the base. The balloon flight duration was of 4 h 45 m, the landing site was in Esrange's zone B 53 km NE of launch point.



Figure 3
A shot from the startosphere.



Figure 4
The glider starts gliding.

GEMTEX, A FREE SOFTWARE FOR EBSD DATA ANALYSIS

Pozzi G.

Electron backscattered diffraction (EBSD) analysis is a powerful tool for quantitative microstructural analysis performed on scanning electron microscopes (SEM). Despite EBSD techniques being widely employed in material and earth sciences, handling of EBSD data is not easy for many non-expert scientists. In fact, commonly used softwares is expensive and users generally rely on licenses purchased by host institutions. A widely used free alternative is a function library designed for Matlab and called MTEX. MTEX, however, requires the user to be familiar with the Matlab programming language and user-made algorithms may result non-accessible to others due to their complicated syntaxes. The aim of this study is to provide a user-friendly interface to MTEX to perform EBSD data handling and analysis in a simple and intuitive fashion, maintaining the free-of-charge access to this resource.

I present GEMTEX (Graphic user interface for Earth sciences to MTEX), a graphic user interface that simplifies the use of MTEX for the handling of EBSD data. GEMTEX is designed to perform the most used analysis procedures of EBSD data in earth sciences. The interface is composed of dedicated panels illustrated in Fig. 1a-d. After loading EBSD data (available for different sources, e.g., Oxford, EDAX, Bruker), the Data panel (Fig. 1a) allows to switch between sets and to control the progress of the analysis in the dedicated log window. The "Refinement" panel (Fig. 1b) contains the fundamental refinement algorithms from MAD correction, grain reconstruction, to denoising functions. The Map panel (Fig. 1c) allows to plot a wide variety of EBSD maps and add-on features (e.g., Fig.1 e). Finally, the tab panel at the bottom (Fig. 1d) contains further plot modes of different EBSD data, for example: grain statistics, pole figures, misorientation plots, and rose diagrams. GEMTEX will be released on GitHub where users will be able to download and immediately use the interface for their EBSD analysis.

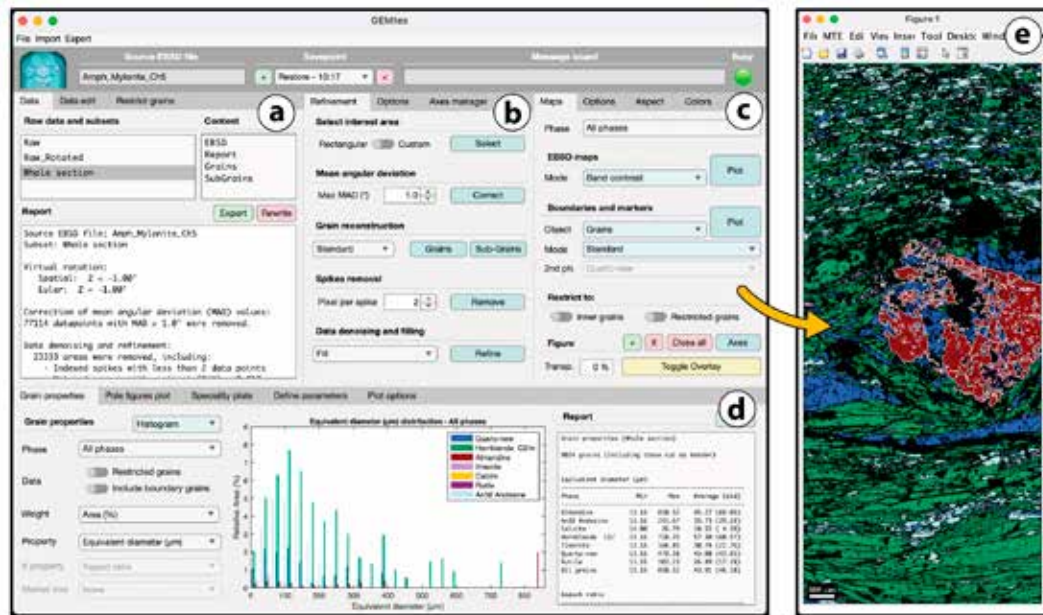


Figure 1

GEMTex appearance: This is a typical view of the interface with EBSD data already loaded and elaborated. Panels a-d provide tools for data handling and plotting (see text for details). Panel e shows an example of a plotted EBSD image (using panel c) where a phase map is overlaid with a grain boundary map.

DEVELOPMENTS AND UPGRADES OF THE ANTI-ALIASING FILTER

Romeo G., Spinelli G., Iarocci A.

An anti-alias filter is an analog filter used, before sampling a signal, in order to narrow the band of the signal itself and approximately satisfy the Nyquist-Shannon sampling theorem.

In collaboration with the Roma Tre University, we designed and assembled, in 2021, an anti-aliasing filter for signals acquisition from an accelerometer.

Its features are:

- Low Pass 7th order Butterworth Bessel
- Gain: 15 Bandpass: -20dB at 40Hz
- Band stop: -70dB at 100Hz

The filter was designed for a 30 Hz cutoff; this cutoff frequency can be doubled (60 Hz cutoff) through the removal of 5 jumpers.

An accelerometer measures the linear acceleration along the three directions of the space at once. Therefore, to investigate accelerations along the x, y, z axes simultaneously, we upgraded the former circuit to a Eurocard. The Eurocard contains 3 channels and each channel hosts a filter. The Eurocard supplies each channel with the power and the input signal, i.e. the acceleration along the axis; moreover it takes outside the signal produced by the filter, i.e. the acceleration along that axis after it has been filtered. In addition the control settings for gain and offset are accessible for each individual channel through the blue trimmer on the right of the filter. To improve the quality of their studies the University researchers required us to have 5 accelerometer workings simultaneously. For this reason we used a rack to hold six Eurocard, one for the power supply and five for the accelerometers.

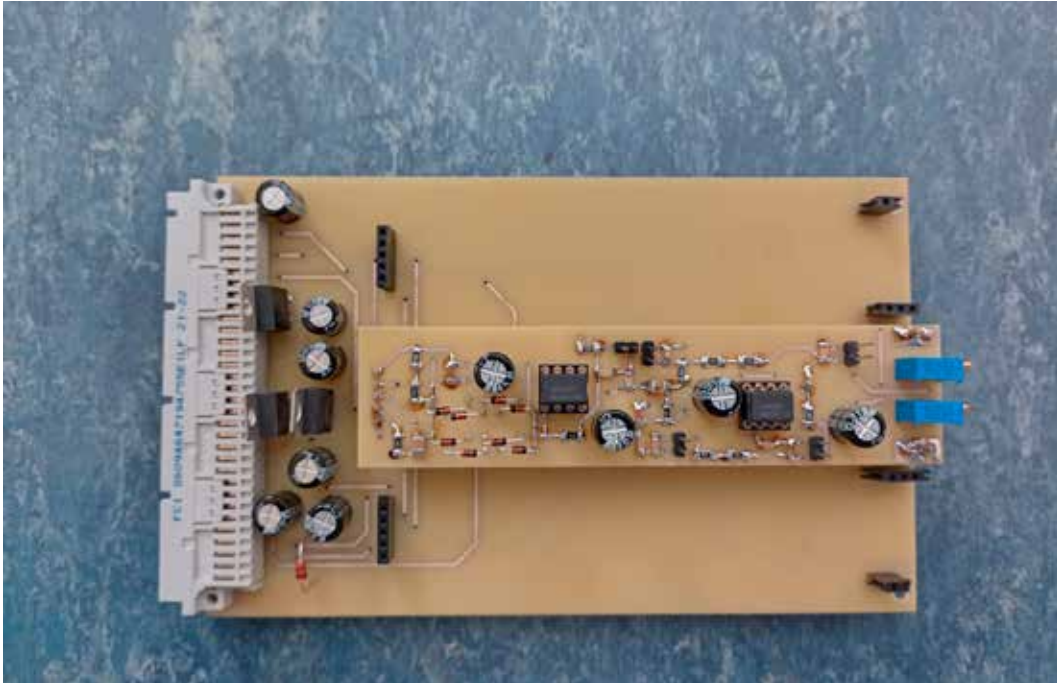


Figure 1
The motherboard with one filter on and the placement for two more filters.



Figure 2
A picture of the rack taken from the top; the power supply is on the left, then the five accelerometers in sequence. We can connect the accelerometer to the Eurocard through a eight pin connector on the related panel. For each component accelerometer there are two pins: the first for the input signal and the second for the output filtered signal; the two remaining pins of the connector are used to supply power to the accelerometer.



Figure 3

A picture of the rack taken from the front; the power supply is on the left, then the five accelerometers in sequence. We can also see one of the five accelerometers. In addition on the panel there are six holes to access (through the blue trimmer we have already spoken) the control settings for gain and offset for each individual channel.

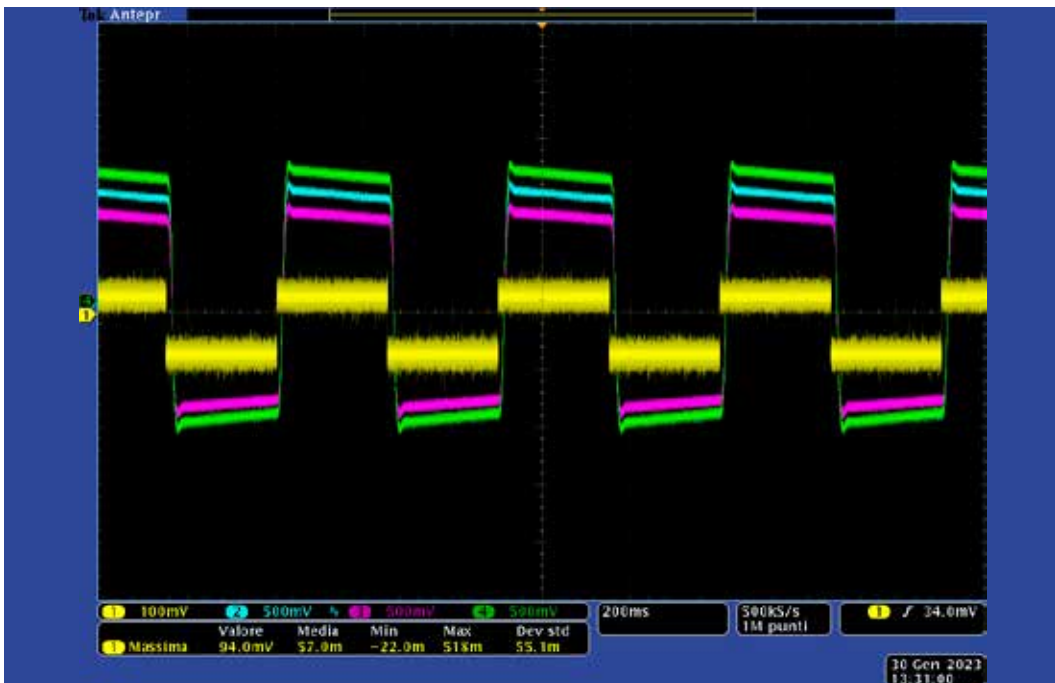


Figure 4

The figure shows the answer (blue, purple and green) produced by the Eurocard to a 2Hz and 50mV square wave (yellow). Pay attention to the different scale of the signals, the filter not only produces a cutoff frequency but also amplifies the input signal.

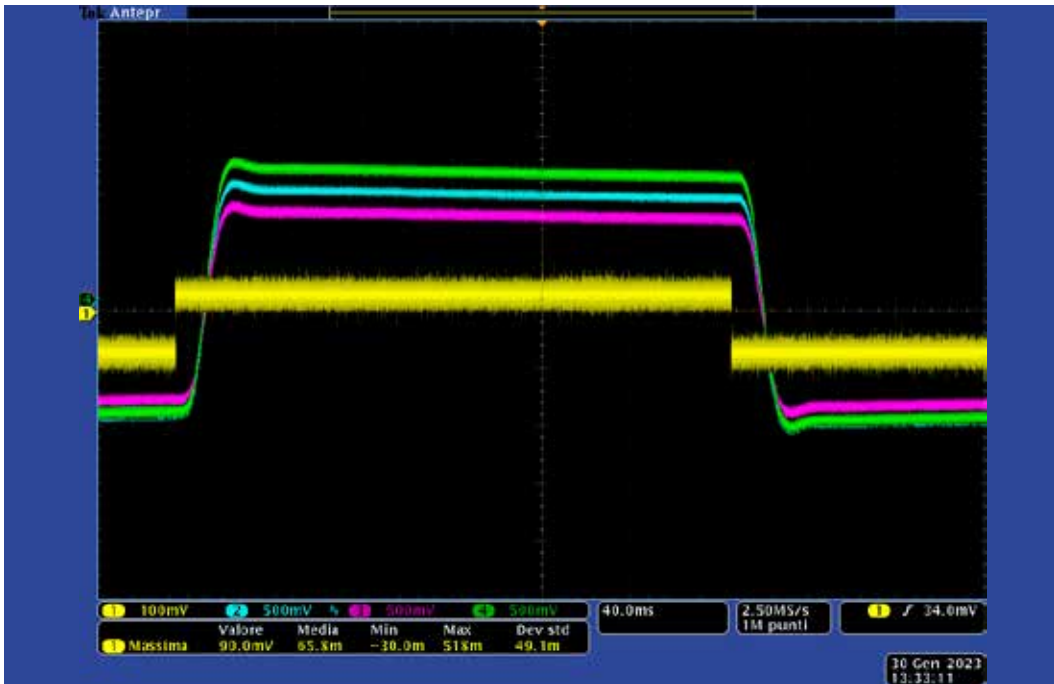


Figure 5
 The figure 5 is the same as figure 4 except that the period is 40ms instead of 200ms. This period is useful to look at the cutoff frequency that occurs when we increase the frequency of the square wave from 2Hz to 62Hz. In fact we have removed the 5 jumpers to have a 60 Hz cutoff frequency.

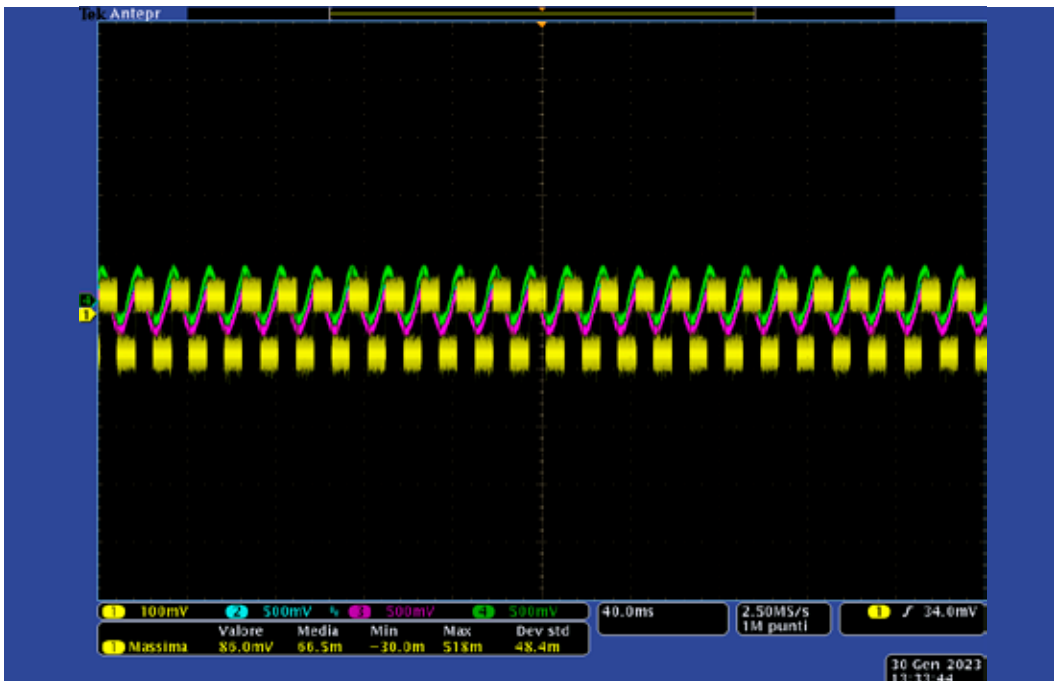


Figure 6
 The last figure shows the acceleration along the three directions, produced by an Eurocard after a pulse on the ground. The blue signal is the acceleration along the x axis, the purple along the y axis, the green along the z axis.

DATALOGGER FOR MEASUREMENT OF CARBON DIOXIDE (CO₂) GAS IN AIR

Pongetti F., Di Stefano G.

The measurement of CO₂ gas has become quite common in many scientific disciplines, thanks to the current availability of reliable, miniaturized and low-cost sensors. It is possible to create a personalized and optimized recorder for each different type of experiment whose characteristics can also be easily modified as it is produced in the laboratory. The proposed datalogger can be integrated into multiparametric environmental measurement stations or as a payload for a drone. A test prototype capable of accommodating up to three gas sensors (i.e. for multiple points measurement) was designed. The gas sensors provide the measurements in digital format, and an Arduino board collects and stores data on local memory (SD card) and it also transmits to the internet via wi-fi interface. A data service platform for the Internet of Things (IoT), a website server, helps to store the measurements in the cloud and allows the formatting, visualization and downloading of data in file format. This is a working-prototype test, which needs to be finalized to the application.

The CO₂ sensor is an NDIR technique type (non-dispersive infra-red), capable of digitizing the measures at an output rate of 2 samples per second, in the range 0-20% of CO₂. The data-collecting and communication board is an ARDUINO Wi-Fi MKR1010 whose microcontroller's internal peripheral availability has been reconfigured in order to expand the number of hardware serial-data-ports to accommodate 3 Serial sensors, and other board-shields (memory SD-shield) or interfaces. The board sends data, via wi-fi, to the internet server of 'ThingSpeak', which is an IoT platform service from 'The MathWorks' that allows to aggregate, visualize, and analyze live data streams, in the cloud.



Figure 1
Sensor's outdoor housings and mounting fixtures are a custom design and are 3-D printed in the laboratory. Various mounting orientations are possible that provide sensor shielding from wind and rain also.

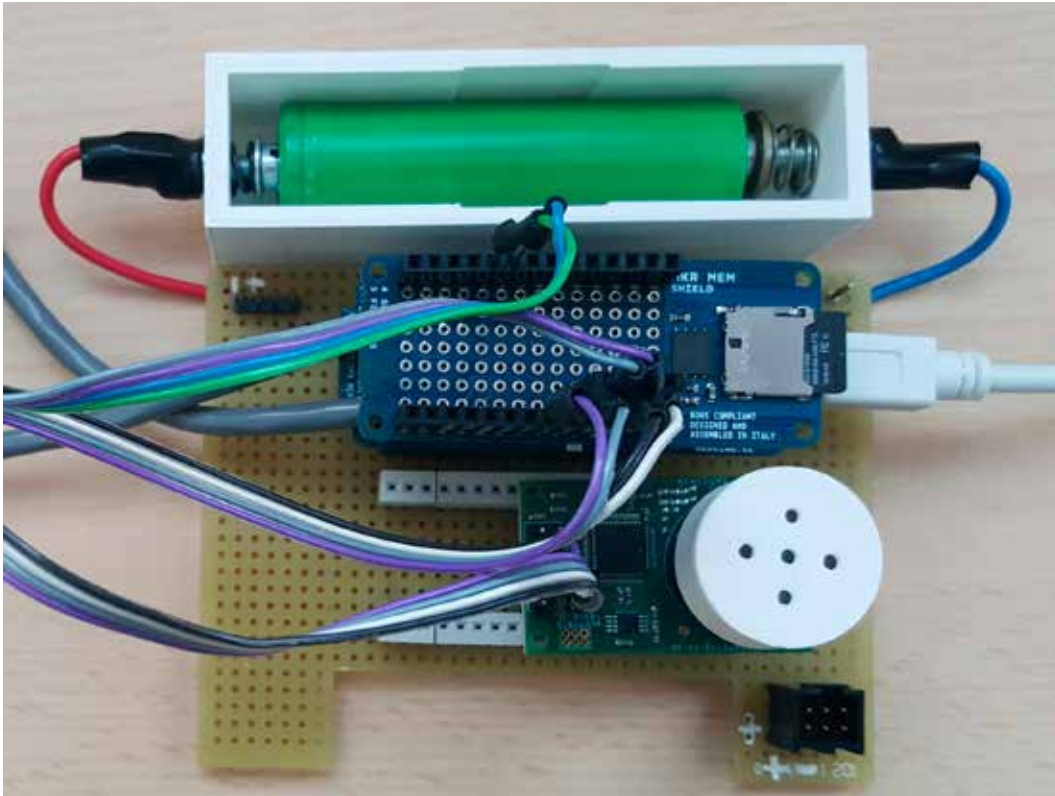


Figure 2
Datalogger data-collecting and internet-connection board.

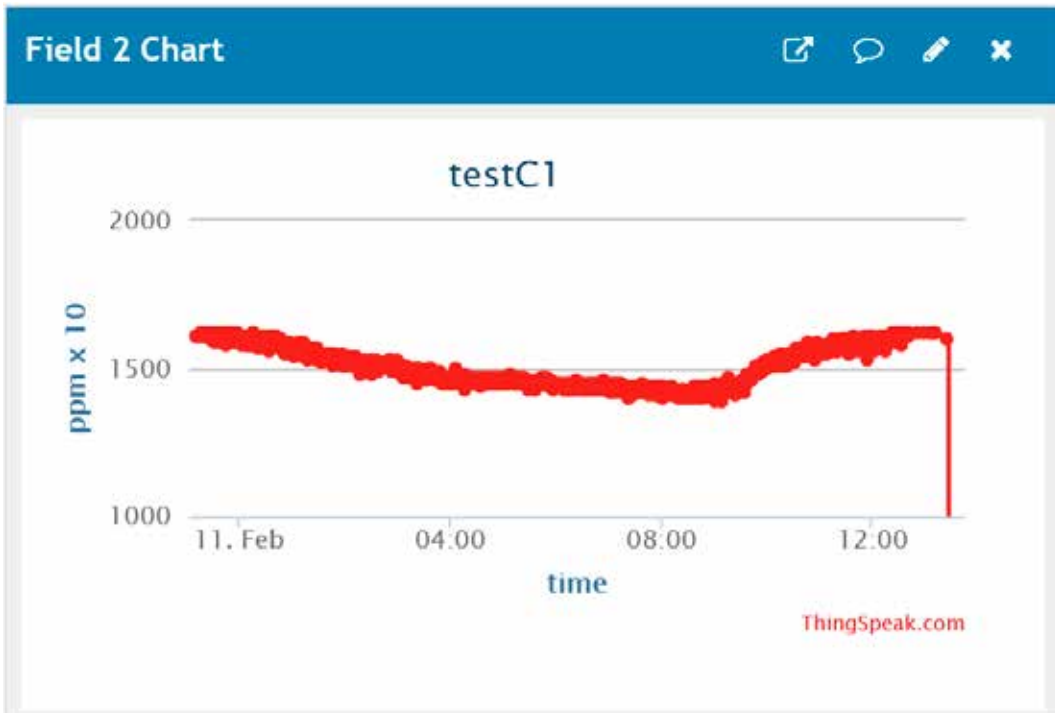


Figure 3
Measured data from CO₂ sensors are sent, stored, visualized and retrieved from the cloud, using an internet of things (IoT) data service.



C H A P T E R N I N E

SEMINARS
and TEACHING

SEMINARS

Andronico D., Del Bello E. | [Le eruzioni parossistiche del 2019 a Stromboli e l'individuazione di possibili segnali precursori attraverso lo studio dell'attività ordinaria](#) | Seminari di divulgazione organizzati dal coordinamento INGV, online, Feb 23rd, 2022.

Di Toro G. | [A glimpse at earthquake physics: field, experimental and numerical studies.](#) | Bern, Switzerland, 24 October

Di Toro G. | [ERC projects: hints for a successful proposal.](#) Marie Curie Alumni Association Università degli Studi di Padova, Padua, Italy, 23 May

Di Toro G. | [Previsione, pericolosità e rischio dei terremoti](#) | Liceo Scientifico Messedaglia, Verona, April 13

Di Toro G. | [I terremoti: fisica, previsione e pericolosità](#) | Università Ca' Foscari, Venezia, April 8

Spagnuolo E. | [Strong or Weak? Achievements, limitations and perspectives on the study of frictional strength of sediments in experimental fault gouges.](#) | ERC TECTONIC-FEAR, on line zoom meetings March 14th, 2022

Spina, L. | [Il vulcano in laboratorio: introduzione alla vulcanologia sperimentale e casi studio](#) Catania (collegamento online), December 6

TRAINING

Catanese S. | [Stage | Analisi della sedimentazione di piroclasti \(ceneri e lapilli fini\) da immagini ad alta velocità](#) | Supervisors : Taddeucci J., INGV, Palladino D.M., Sapienza Università di Roma

THESIS

1. **Amodio A.** | [Master Thesis | Caratterizzazione delle proprietà dell'attrito delle serpentiniti ricche in Antigorite](#) | Supervisors : Collettini C., Sapienza Università di Roma, Pozzi G., INGV

2. **Chiesurin A.** | [Master Thesis | Mineralogical, geochemical and microstructural characterization of fault rocks from the Koyna deep drilling project \(India\).](#)
Supervisors: Di Toro G., Padua University; Spagnuolo E. INGV

3. **Lombardi F.** | [Analisi micro-tessiturale delle fontane dell'Etna: Implicazioni per la stima delle velocità di risalita del magma nel condotto vulcanico](#) | Supervisors: Mollo S. and Moschini P. Sapienza Università di Roma
4. **Moltoni R.** | [Tesi Triennale | Caratterizzazione di rocce di faglia sperimentali](#)
Supervisors: Collettini C. – Sapienza Università di Roma | Ruggieri R. – Sapienza Università di Roma.
5. **Montagnese M.** | [Bachelor Thesis | Caratterizzazione tessiturale e geochimica dei prodotti eruttivi dello Stromboli](#) | Supervisors: Mollo S. and Schiavon B. - Sapienza Università di Roma
6. **Sartini F.** | [Bachelor Thesis | Modeling of the magma ascent rate through the crystal size distribution method](#)
Supervisors: Mollo S. and Moschini P. - Sapienza Università di Roma

PhD

1. **Benà E.** | [Tectonic control on enhanced geogenic radon as a first order factor in radon hazard assessment](#) | Padua University | Supervisors: Ciotoli G., Sassi R., CNR, Spagnuolo E., INGV
2. **Bigaroni N.** | [Riprodurre il ciclo sismico di una faglia complessa in laboratorio e predire l'andamento con il machine learning](#) | Supervisor: Scuderi M. – Sapienza Università di Roma.
3. **Chinello M.** | [Formation of polished surfaces in natural rocks: experimental and field constraints.](#) | Supervisors Di Toro G. - Università di Padova; Spagnuolo E. - INGV; Oliver Plumper - Utrecht University
4. **Feng W.** | [Investigation of seismic slip in experimental faults under hydrothermal conditions. Chinese Government Scholarship.](#) | Supervisor: Di Toro G.
5. **Masoch S.** | [Structure, evolution and deformation mechanisms of large displacement seismogenic faults in the continental crust.](#) | Supervisors: Di Toro G. and Pennacchioni G. - - Università di Padova; Cembrano J. - Universidad Ponteficia de Chile.
6. **Moschini P.** | [Volcanic hazard assessment at Mt. Etna: a time-integrated, polybaric and polythermal perspective.](#) | Supervisors: Gaeta M. - Sapienza Università di Roma | Scarlato P. - INGV.

7. **Schiavon B.** | Petrological monitoring of magma-mush dynamics at Stromboli: Insights on the transition from mild to violent eruptive styles | Supervisors: Mollo S. - Sapienza Università di Roma | Del Bello E. and Pontesilli A. - INGV.

8. **Volpe G.** | Proprietà dell'attrito e permeabilità di faglie in basamento per una migliore caratterizzazione del loro potenziale sismogenico | Supervisor: Collettini C. - Sapienza Università di Roma | Pozzi G. - INGV.

9. **Wu W.H.** | Experimental studies of fluid-rock interaction and seismic cycle in geothermal fields (Acronym EXPRESSO) | European Union's Horizon 2020 research and innovation programme under the Marie Skłodowska-Curie grant agreement no 101034319 and from the European Union – NextGenerationEU. | Tutor Giulio Di Toro

C H A P T E R T E N

VISITING
SCIENTISTS

Within the framework of the European project EXCITE (Electron and X-ray microscopy Community for structural and chemical Imaging Techniques for Earth materials, GA 101005611), a European infrastructure initiative for scientists working on Earth materials, Transnational access to research infrastructures using some of the world's best electron and X-ray imaging facilities is organised and coordinated by INGV-Rome. In 2022, 2 rounds of Trans-National Access (TNA) calls for proposals were organized and performed. This important initiative, financially supported by the EU, enables users from all countries (EU and non-EU) to obtain excellence-driven, free access to the best Research Infrastructure in Europe to perform their research, enhancing scientific collaboration and innovation.

During the first call for access, 6 applications were positively evaluated through peer review conducted by external experts, and were granted funded access at INGV-Rome HPHT lab, EMPA/SEM facilities. All the projects were successfully performed in the first access period (1 May - 31 Oct 2022) at the microanalytical lab of HPHT, and concluded in time. Three more projects were awarded for the second period of access (1 Nov 2022 - 30 April 2023) at INGV-Rome, two of which were just concluded in December. In the following table the list of EXCITE TNA visiting scientists and projects carried out in 2022 is provided.

User Name	Affiliated institute	Project Title	Equipment	Access type	Access period	Access delivered
Philippe Robidoux	Universidad de Chile, Chile	PAIMGSPGAASVZ - Petrological approach for identifying magmatic gas source of post-glacial eruptive activity in the Southern Volcanic Zone (SVZ)	JEOL JXA-8200 (EPMA)	Physical	1st ROUND: 20-24/06/2022	5 days
Chiara Petrone	The Natural History Museum, London, United Kingdom	PLEMH - Using plagioclase crystals to decode magma-mush dynamics during high explosive eruptions at basaltic volcanoes	JEOL JXA-8200 (EPMA) and JEOL JSM-6500F (FE-SEM)	Physical	1st ROUND: 19-27/09/2022	7 days
Alice MacDonald	The University of Queensland, Australia	VOLCREMAG - VOLcanic Crystals as REcorders of MAGmatic histories	JEOL JXA-8200 (EPMA)	Physical	1st ROUND: 06-14/06/2022	7 days
Simge Kaya	Hacettepe University, Department of Geological Engineering, Turkey	YANARDAĞ / YANARDAG - Petrogenetic study of the Dikkartin, Karagullu and Perikartin pyroclastic deposits, Holocene eruption/s of Erciyes volcano, Central Anatolia (Turkey)	JEOL JXA-8200 (EPMA)	Physical	1st ROUND: 17-21/10/2022	5 days
Fátima Rodríguez García	Instituto Volcanológico de Canarias (INVOLCAN), Spain	CUMBREVIEJACHEM - Petrochemical analyses of tephra products from the recent eruption of Cumbre Vieja volcano (La Palma, Canary)	JEOL JXA-8200 (EPMA)	Physical	1st ROUND: 05-13/05/2022	7 days
Alba Martín Lorenzo	Instituto Tecnológico y de Energías Renovables (ITER), Spain	CUMBREVIEJATEXT - Textural analyses of tephra products from the recent eruption of Cumbre Vieja Volcano (La Palma, Canary Island)	JEOL JSM-6500F (FE-SEM)	Physical	1st ROUND: 27/06-06/07/2022	7 days
Charles Beard	Department of Earth Sciences, University of Cambridge, United Kingdom	DREAMS-a - Disequilibrium in Rare Earth-bearing Alkaline-silicate Magmatic Systems	JEOL JSM-6500F (FE-SEM)	Physical	2nd ROUND: 12-16/12/2022	5 days
Caroline Soderman	Department of Earth Sciences, University of Cambridge, United Kingdom	DREAMS-b - Reading the mineral record of REE enrichment in alkaline-silicate magmatic systems	JEOL JXA-8200 (EMPA)	Physical	2nd ROUND: 12-16/12/2022	5 days
Yerko Gonzalez	Universidad Catolica del Norte, Antofagasta, Chile.	Frictional properties of Quaternary fault cores from the Atacama Fault System, northern Chilean forearc: Active faults or weakness zone of the upper plate?	SHIVA, BRAVA	Physical	Oct-Dec 2022	90 days
Chien Cheng Hung	Utrecht University, Utrecht, the Netherlands	Frictional behavior of sandstone-derived fault gouges during short seismic slip-pulse and its implications for induced seismicity in Groningen Gas Field	SHIVA	Physical	4-14/4/ 2022	10 days

C H A P T E R E L E V E N

MEETINGS,
WORKSHOP
and SYMPOSIA

MEETINGS AND SESSIONS ORGANIZATION

Del Bello E., Andronico D., Di Traglia F., D'Auria L., Scarlato P.

Plenary / Special session: *Impact of volcanic activity crises in places of tourist interest: Stromboli, Vulcano, White Island, Cumbre Vieja and other case studies.* Cities on Volcanoes Conference, Crete, Greece, June 2022

Andrews B.J., Houghton B.F., Befus K.S., Taddeucci J. Tisdale C.M.

Explosive Eruption Processes and Their Deposits AGU 2022 Fall Meeting

MEETINGS AND SESSIONS ATTENDANCE

EXCITE Meeting Utrecht, January

Chinello M., Di Toro G., Spagnuolo E., Plümper O., Ohl M.

Formation of polished surface in natural rocks: experimental and field constraints.

EGU, European Geosciences Union General Assembly, Vienna 23-27 May

Aretusini S., Nuñez Cascajero A., Cornelio C., Barrero Echevarria X., Spagnuolo E., Tapetado A., Vazquez C., Cocco M., Di Toro G.

Dynamic weakening in carbonate-built seismic faults: insights from laboratory experiments with fast and ultra-localized temperature measurements

<https://doi.org/10.5194/egusphere-egu22-4583>, 2022.

Chinello M., Bersan E., Fondriest M., Tesei T., Corrado S., Di Toro G.

Field, microstructural and phase characterization of mirror-like fault surfaces in bituminous dolostones (central Apennines, Italy)

EGU22-2415

Cornelio C., Spagnuolo E., Nielsen S., Aretusini S., Passelègue F., Violay M., Cocco M., Di Toro G.

Determination of parameters characteristic of dynamic weakening mechanisms during coseismic slip

EGU22-9866

Costa S., Colle F., Masotta M., Mollo S., Landi P., Pontesilli A., Peres S., Griffiths T., Mancini, L.

Kinetic crystallization of a high-K basalt melt undercooled in laboratory: Implications for modeling open conduit dynamics at Stromboli volcano.

Feng W., Yao L., Ma S., Di Toro G.

Friction behavior of gabbro under hydrothermal conditions

EGU22-981

Harbord C., Brantut N., Spagnuolo E., Di Toro G.

Fault friction during simulated seismic slip pulses,

EGU22-8340

Masoch S., Fondriest M., Gomila R., Jensen E., Magnarini G., Espinosa J., Hofer K., Mitchell T.,
Cembrano J., Pennacchioni G., Di Toro G.

Geological imaging of a crustal-scale seismogenic source in the continental crust (Bolfin Fault
Zone, Atacama Fault System, Chile)

EGU2022-1926

Moschini P., Mollo S., Pontesilli A., Gaeta M., Nazzari M., Scarlato P.

Modeling clinopyroxene and plagioclase growth kinetics at Mt. Etna and Stromboli.

Romero J., Burton M., Cáceres F., Llewellyn E., Polacci M., Asensio-Ramos M., D'Auria L., Ricci T.,
Civico R., Taddeucci J., Andronico D., Scarlato P., Rodríguez F., Pankhurst M., Martín-Lorenzo A.,
Pérez N.

Syn-eruptive edifice collapses during the Cumbre Vieja (Canary Islands) 2021 eruption

EGU22-8873

Scarlato P., Taddeucci J., Andronico D., Ricci T., Civico R., Del Bello E., Spina L., D'Auria L.,
Asensio-Ramos M., Calvo D., & others

Styles of explosive activity during the 2021 Cumbra Vieja eruption, as illuminated by high-
frequency imaging and acoustic sensing

EGU22-9297

Taddeucci J., Cimarelli, C., Alatorre-Ibarguengoitia, M. A., Delgado-Granados, H., Andronico,
D., Del Bello, E., Scarlato, P., & Di Stefano, F.

Features of broken crystals reveal the fracturing and healing of basaltic magmas during explosive
volcanic eruptions

EGU22-9204

Cities on Volcanoes, Crete, Greece, 12-17 June

Andronico D., Del Bello E., Ciancitto F. A., Cristaldi A., D'Oriano C., Landi P., Pennacchia F., Ricci T., Scarlato P., Taddeucci J.

The two powerful explosions during the summer of 2019 at Stromboli

Bagnato E., Andronico D., Cinti D., Del Bello E., Nazzari M., Ricci T., Scarlato P., Taddeucci J.,

Preliminary ash-leachates from some recent eruptions of Stromboli volcano. Presenter

Civico R., Ricci T., Scarlato P., Taddeucci J., Andronico D., Del Bello E., D'Auria L., Hernández P. A., Pérez N., & others

The impact of the 2021 eruption of Cumbre Vieja volcano (La Palma, Canary Islands) on the landscape: morphological changes and observation of volcanic activity from UASs surveys

Corradini S., L. Guerrieri, F. Prata, L. Merucci, D. Stelitano, G. Salerno, T. Ricci, G. Tamburello

Novel TIR ground based systems for volcanic cloud monitoring. Tests on Etna and Stromboli volcanoes and products validation.

Del Bello E., Taddeucci J., Scarlato P., Falcone E., Andronico D., Palladino D., Ricci T.,

Spatiotemporal variations of eruptive parameters and styles at Stromboli volcano (Italy) from high frequency thermal imaging. Presenter

Petrone C. M., Mollo S., Gertisser, R., Buret, Y., Scarlato, P., Del Bello, E., Andronico, D., Ellis, B., Pontesilli, A., De Astis, G., Giacomoni, P.P. Coltorti, M.

Magma-mush dynamics controls paroxysmal eruptions at basaltic volcanoes: the summer 2019 eruptions at Stromboli volcano (Italy)

Pontesilli A., Del Bello E., Andronico D., Taddeucci J., Mollo S., Scarlato P.

Combining quantitative imaging of volcanic eruptions with pyroclasts microtextures to understand short-term variations in eruptive parameters: the May 2019 explosive activity of Stromboli Volcano (Italy)

Solana C., R. Civico, T. Ricci

Clastogenic spatter piles and flows during the early stages of the 2021 La Palma eruption and the change in lava flow hazard assessment

Spina L., Morgavi D., Cannata A., Taddeucci J., Del Bello E., Perugini D., Scarlato P.

A laboratory approach to unravel the link between seismo-acoustic signals and eruptive parameters

Spina L., Del Bello E., Ricci T., Taddeucci J., Scarlato P.

An integrated acoustic and thermal characterization of explosive activity at Batu Tara volcano (East Sunda Arc Indonesia)

Strehlow K., De Beni E., Andronico D., Cantarero M., Civico Del Bello E., Di Traglia, F., Eggersgluess M., & others

The benefit of unmanned aerial vehicles for volcano monitoring and emergency management - a case study for the 2019 paroxysms at Stromboli volcano, Italy

Todesco M., E. Bagnato, B. Behncke, A. Bonforte, G. De Astis, M. De Lucia, S. De Vita, M. Di Vito, F. Grassa, C. Montagna, R. Nave, C. Piccione, T. Ricci, D. Rouwet, L. Sandri, P. Scarlato

INGVvulcani: an (attempted) paroxysm of information

Goldschmidt 2022 Conference, Hawaii, 10-15 July

Petrone C.M., Mollo S., Gertisser R., Buret Y., Scarlato P., Del Bello E., Andronico D., Ellis B.S., Pontesilli A., De Astis G., Giacomoni P.P., Coltorti M., 2022

Magma-mush dynamics control paroxysmal eruptions at basaltic volcanoes: the summer 2019 eruptions at Stromboli volcano (Italy)

Pizzino L., A. Sciarra, G. Galli, L. Ruggiero, S. Graziani, T. Ricci, R. Nave, S. Beaubien, G. Ciotoli, S. Bigi

Indoor Radon measurements in public schools and dwellings in the Ciampino municipality (Greater Rome Metropolitan Area, central Italy) and risk perception assessment

GRC Rock Deformation, Lewiston (ME), Usa, August 7-12,

Aretusini S. et al.

Temperature anomalies during earthquakes: from laboratory to underground experiments

Chinello M. et al.

Mirror-like surfaces and the seismic cycle: insights from field, microstructural and thermal maturity analyses on faults cutting bituminous dolostones (Central Apennines, Italy)

Cornelio C. et al.

Frictional Properties and Dynamic Weakening: An Overview From Laboratory Experiments

Cornelio C., Aretusini S., Spagnuolo E., Di Toro G., Cocco M.

Multiple slip velocity pulses on gouge layer: mechanical response evolution

Feng W., Yao L., Ma S., Di Toro G.

Frictional properties of gabbro under hydrothermal conditions

Feng W., Gomila R., Yao L., Ma S., Di Toro G.

Healing of gabbro and basalt-built experimental faults under hydrothermal conditions

Gomila R., Feng W., Di Toro G.

Healing of granodiorite and its fault-related products under hydrothermal conditions

Hung C.C. et al.

Frictional Behavior of Sandstone-Derived Fault Gouges During Short Seismic Slip-Pulse Experiments and Its Implications for Induced Seismicity in Groningen Gas Field.

Lazari F., Castagna A., Nielsen S., Griffith A., Pennacchioni G., Gomila R., Resor P., Di Toro G.

Frictional power dissipation in a seismic ancient fault.

Masoch S., Fondriest M., Gomila R., Jensen E., Magnarini G., Mitchell T., Cembrano J., Pennacchioni G., Di Toro G.

Architecture of an exhumed crustal-scale seismogenic source in the continental crust (Bolfín Fault Zone, Atacama Fault System, Chile).

Masoch S., Fondriest M., Gomila R., Cembrano J., Pennacchioni G., Di Toro G.

Epidote-rich fault vein networks and seismic cycle in hydrothermal systems (Bolfín Fault Zone, Atacama Desert, Chile)

Spagnuolo E.

Friction and frictional instabilities across scales

SGI-SIMP Geoscienze per un futuro sostenibile, Turin, Italy, 19-21 September

Del Rio L., Moro M., Fondriest M., Saroli M., Masoch S., Doumaz F., Gori S., Falcucci E., Cavallo A., Lutterotti L., Artioli G., Borovin E., Di Toro G.

Slip surfaces associated with seismic faults and gravitational slope deformations in carbonate rocks

Di Toro G., Aretusini S., Chinello M., Cornelio C., Del Rio L., Feng W., Gomila R., Masoch S., Nielsen S., Pennacchioni G., Spagnuolo E., Tesei T.

Mineral reactions during earthquakes

Feng W., Yao L., Gomila R., Ma S., Di Toro G.

Healing of gabbro and basalt experimental faults under hydrothermal conditions

Gomila R., Feng W., Di Toro G.

Hydrothermal fault healing evolution of tonalite, granodiorite and their fault-related products

Misiti V., Riposati D., Di Laura F., Battelli P. & Crescimbene M.

VULCANOPOLY: playing towards a better future

Mitterpergher S., Di Toro G., Bistacchi A., Zanchetta S., Aretusini S., Villa I.

Relative and absolute ages of deformative processes at the base of the seismogenic crust from geochronological, microstructural and geochemical studies of the Gole Larghe Fault (Adamello, Italy)

5° Conferenza A. Rittmann, Catania, Italy, September 29 – October 1

Colle F., Costa S., Masotta M., Mollo S., Landi P., Pontesilli A., Peres S., Griffiths T., Mancini, L.
Kinetic crystallization of a high-K basalt melt undercooled in laboratory: Implications for the modeling of open-conduit dynamics at Stromboli (Aeolian Islands, Italy)

Di Fiore F., Vona A., Costa A., Mollo S., Romano C.

Quantifying the Influence of Cooling Rate and Shear Rate on the Disequilibrium Rheology of a Basaltic Melt from Mt. Etna (Italy)

Petrone C.M., Mollo S., Gertisser R., Buret Y., Scarlato P., Del Bello E., Andronico D., Ellis B.S., Pontesilli A., De Astis G., 2022, Petrone C.M., Mollo S., Gertisser R., Buret Y., Scarlato P., Del Bello E., Andronico D., Ellis B.S., Pontesilli A., De Astis G., Giacomoni P.P., Coltorti M.

Magma-mush dynamics control paroxysmal eruptions at basaltic volcanoes: the summer 2019 eruptions at Stromboli volcano (Italy)

Proietti C., M. Cantarero, E. De Beni, G. Ganci, T. Ricci

Timely mapping and quantification of the 2020-2021 Etna lava flows through the exploitation of multi-sensors remote-sensing data

International Geomechanics Symposium. Abu Dhabi, November 7-10

Di Toro G., Feng W., Gomila R., Tesei T., Aretusini S., Cocco M., Cornelio C., Spagnuolo E., Nielsen S., Yao L., Ma S., 2022. (Invited, webinar)

Rock friction during earthquakes: disputes and future trends

NSF workshop 'PDC dynamics and hazards – Benchmarking of concentrated PDC models and other avenues', Saint-Pierre (Martinique Island, French Caribbean, France) 26 November 26 - 4 December, 2022

Kueppers U., T. Ricci, R. Civico

Small-scale PDCs at Stromboli volcano, Italy, 12 October 2022. Flow behaviour and deposit characteristics

AGU Fall Meeting, San Francisco (USA), December

Scarlato, P., Taddeucci, J., Andronico, D., Ricci, T., Civico, R., Del Bello, E., Spina, L., D'Auria, L., Asensio-Ramos, M., Calvo, D., Padron E., and Perez, N.

Physical Parameters Define Styles and Transitions of Explosive Activity During the 2021 Cumbre Vieja Eruption

C H A P T E R T W E L V E

PUBLICATIONS

Antunes V., Planes T., Obermann A., Panzera F., D'Amico S., Mazzini A., Sciarra A., Ricci T., Lupi M.
Insights into the dynamics of the Nirano Mud Volcano through seismic characterization of drumbeat signals and V/H analysis

Journal of Volcanology and Geothermal Research, 431, 107619,
<https://doi.org/10.1016/j.jvolgeores.2022.107619>

Baize S., Amoroso S., Belić N., Benedetti L., Boncio P., Budić M., ..., Ricci T.

Environmental effects and seismogenic source characterization of the December 2020 earthquake sequence near Petrinja, Croatia

Geophysical Journal International, 230, 2, <https://doi.org/10.1093/gji/ggac123>

Bini G., Chiodini G., Caliro S., Tassi F., Vaselli O., Rizzo A.L., Mollo S., Vougioukalakis G.E., Bachmann O.

Nitrogen, helium, and argon reveal the magmatic signature of fumarole gases and episodes of outgassing from upper-crustal magma reservoirs: The case of the Nisyros caldera (Aegean Arc, Greece)

Geochimica et Cosmochimica Acta, 335, 68-84. <https://doi.org/10.1016/j.gca.2022.08.028>

Carapezza M. L., Tarchini L., Ancona C., Forastiere F., Ranaldi M., Ricci T., ..., Barberi F.

Health Impact of Natural Gas Emission at Cava dei Selci Residential Zone (Metropolitan City of Rome, Italy)

Environmental Geochemistry and Health, 45, <https://doi.org/10.1007/s10653-022-01244-6>

Cívico R., Ricci T., Scarlato P., Taddeucci J., Andronico D., Del Bello E., D'Auria, L., Hernández P. A., & Pérez N. M.

High-resolution digital surface model of the 2021 eruption deposit of Cumbre Vieja volcano, La Palma, Spain

Scientific Data, 9(1), 1–7, <https://doi.org/10.1038/s41597-022-01551-8>

Cocco M., Aretusini S., Cornelio C., Nielsen S. B., Spagnuolo E., Tinti E., & Di Toro G.

Fracture Energy and Breakdown Work During Earthquakes

Annual Review of Earth and Planetary Sciences, 51.

<https://doi.org/10.1146/annurev-earth-071822-100304>

Cornelio C., Spagnuolo E., Aretusini, S., Nielsen S., Passelègue F., Violay M., Cocco M., & Di Toro G.

Determination of parameters characteristic of dynamic weakening mechanisms during seismic faulting in cohesive rocks

Journal of Geophysical Research: Solid Earth, 127(7), e2022JB024356.

<https://doi.org/10.1029/2022JB024356>

Das P.P., Plana-Ruiz S., Galanis A.S., Stewart A., Karavasili F., Nicolopoulos S., Putz H., Margiolaki I., Calamiotou M., Iezzi G.

Structure Determination Feasibility of Three-Dimensional Electron Diffraction in Case of Limited Data

Symmetry 2022, 14, 2355. <https://doi.org/10.3390/sym14112355>

Del Carlo P. , Di Roberto A., Di Vincenzo G., Re G., Albert P.G., Nazzari M., Cannata A.

Tephrostratigraphy of proximal pyroclastic sequences at Mount Melbourne (northern Victoria Land, Antarctica): insights into the volcanic activity since the last glacial period

Journal of Volcanology and Geothermal Research 422, 2022. IF (2021) 2.986

<https://doi.org/10.1016/j.jvolgeores.2021.107457>

Di Fiore F., Vona A., Costa A., Mollo S., Romano C.

Quantifying the influence of cooling and shear rate on the disequilibrium rheology of a trachybasaltic melt from Mt. Etna.

Earth and Planetary Science Letters, 594, 117725. <https://doi.org/10.1016/j.epsl.2022.117725>.

Di Toro G.

Along strike architectural variability of an exhumed crustal-scale seismogenic fault in the continental crust (Bolfn Fault Zone, Atacama Fault System, Chile)

Journal of Structural Geology 165, pp. 1-30 <https://doi.org/10.1016/j.jsg.2022.104745>.

Galderisi A., Iezzi G., Bianchini G., Paris E., de Brito J.

Petrography of Construction and Demolition Waste (CDW) from Abruzzo Region (Central Italy)

Waste Management 137(10): 61-71.

Gennaro E., Iezzi G., Cocchi L., Ventura G.

Anatomy of a back-arc ridge system: the Marsili seamount. *Goldschmidt 2022*

<https://doi.org/10.46427/gold2022.12145>, (Honolulu, Hawaii, USA).

Giudicepietro F., Calvari S., D'Auria L., Di Traglia F., Layer L., Macedonio G., & Spina L. & Esposito A. M.

Changes in the eruptive style of Stromboli volcano before the 2019 paroxysmal phase discovered through SOM clustering of seismo-acoustic features compared with camera images and GBInSAR data

Remote Sensing, 14(5), 1287.

Giuliani L., Vetere F., Iezzi G., Nazzari M., Mollo S., Behrens H., Scarlato P., Ventura G.

Crystal-chemical variations of spinel, clinopyroxene, and plagioclase in MORB basaltic melt induced by continuous cooling

Chemical Geology, 594, 120765. <https://doi.org/10.1016/j.chemgeo.2022.120765>

Kuo L. W., Hung C. C., Li H., Aretusini S., Chen J., Di Toro G., Spagnuolo, E., Di Felice F., Wang H., Si J., & Sheu H. S.

Frictional Properties of the Longmenshan Fault Belt Gouges From WFSD-3 and Implications for Earthquake Rupture

Propagation. Journal of Geophysical Research: Solid Earth, 127(5), e2022JB024081.

<https://doi.org/10.1029/2022JB024081>

Landi P., D'Oriano C., Petrelli M., Nazzari M., Andronico D.

Inferences on the magmatic plumbing system at Stromboli volcano (Italy) from trace element geochemistry of matrix glasses and minerals in different types of explosive eruptions

Contributions to Mineralogy and Petrology 177 (96), 2022. IF 4.107

<https://doi.org/10.1007/s00410-022-01962-1>

Lang S., Mollo S., Lyderic F., Misiti V., Nazzari M.

Partitioning of Ti, Al, P, and Cr between olivine and a tholeiitic basaltic melt: Insights on olivine zoning patterns and cation substitution reactions under variable cooling rate conditions

Chemical Geology, 601, 120870. <https://doi.org/10.1016/j.chemgeo.2022.120870>.

Lanzafame G., Giacomoni P.P., Casetta G., Mancini L., Iezzi G., Coltorti M., Ferlito C.

Degassing, crystallization and rheology of hawaiitic lava flows: the case of the 1669 A.D. eruption of Mount Etna (Italy)

Journal of Petrology, 63, 115, <https://doi.org/10.1093/petrology/egac115>

MacDonald A., Ubide T., Mollo S., Masotta M., Pontesilli A.

Trace element partitioning in zoned clinopyroxene as a proxy for undercooling: Experimental constraints from trachybasaltic magmas

Geochimica et Cosmochimica Acta, 336, 249-268. <https://doi.org/10.1016/j.gca.2022.09.007>

Masoch S., Fondriest M., Gomila R., Jensen E., Mitchell T.M., Cembrano J., Pennacchioni G., Misiti V., Di Laura F., Riposati D., Battelli P.

Catch the plate!

Proceedings of ICERI2022 congress - ISBN 978-84-09-45476-1

Mollo S., Pontesilli A., Moschini P., Palumbo F., Taddeucci J., Andronico D., Del Bello E., Scarlato P.

Modeling the crystallization conditions of clinopyroxene crystals erupted during 2021 February–April lava fountains at Mt. Etna: Implications for the dynamic transfer of magmas

Lithos, 420–421, 106710. <https://doi.org/10.1016/j.lithos.2022.106710>.

Petrone C.M., Mollo S., Gertisser R., Buret Y., Scarlato P., Del Bello E., Andronico D., Ellis B., Pontesilli A., De Astis G., Giacomoni P., Coltorti M., Reagan M.

Magma recharge and mush rejuvenation drive paroxysmal activity at Stromboli volcano

Nat Commun 13, 7717 (2022). <https://doi.org/10.1038/s41467-022-35405-z>

Pontesilli A., Brenna M., Mollo S., Masotta M., Nazzari M., Le Roux P., Scarlato P.

Trachyte-phonolite transition at Dunedin Volcano: Fingerprints of magma plumbing system maturity and mush evolution

Lithos, 408–409, 106545. <https://doi.org/10.1016/j.lithos.2021.106545>.

Potere D., Scisciani V., Piochi M., Pierantoni P.P., Mormone A., Nazzari M., Scarlato P., Iezzi G.

The Volcanic-Rich Layer of the “Camporotondo (Marche, Italy)”: petrography and sedimentation of an unknown distal Messinian eruption

Minerals, 12: 893, <https://doi.org/10.3390/min12070893>

Pozzi G., Scuderi M., Tinti E., Nazzari M., Collettini C.

The role of fault rock fabric in the dynamics of laboratory faults

Journal of Geophysical Research - Solid Earth 127 (6), 2022. IF 4.397

<https://doi.org/10.1029/2021JB023779>

Romero J. E., Burton M., Cáceres F., Taddeucci J., Civico R., Ricci T., Perez N. M.

The initial phase of the 2021 Cumbre Vieja ridge eruption (Canary Islands): Products and dynamics controlling edifice growth and collapse

JOURNAL OF VOLCANOLOGY AND GEOTHERMAL RESEARCH, 107642.

<https://doi.org/10.1016/j.jvolgeores.2022.107642>

Sonder I., Graettinger A., Neilsen T. B., Matoza R. S., Taddeucci J., Oppenheimer J., et al.

Experimental multiblast craters and ejecta seismo acoustics, jet characteristics, craters, and ejecta deposits and implications for volcanic explosions

JOURNAL OF GEOPHYSICAL RESEARCH: SOLID EARTH, 127, e2022JB023952.

<https://doi.org/10.1029/2022JB023952>

Spina, L., Cannata, A., Morgavi, D., Privitera, E., & Perugini, D.

Seismo-acoustic gliding: An experimental study

Earth and Planetary Science Letters, 579, 117344.

Vetere F., Iezzi G., Perugini D., Holtz F.

Rheological Changes in Melts and Magmas Induced by crystallization and strain rate

Journal of CR-Geosciences, <https://doi.org/10.5802/crgeos.125>

Volpe G., Pozzi G., Carminati E., Barchi M. R., Scuderi M. M., Tinti E., Aldega L., Marone C., Collettini C.

Frictional controls on the seismogenic zone: Insights from the Apenninic basement, Central Italy

Earth and Planetary Science Letters, <https://doi.org/10.1016/j.epsl.2022.117444>

Volpe G., Pozzi G., Collettini C.

YBPR or SCC'? Suggestion for the nomenclature of experimental brittle fault fabric in phyllosilicate-granular mixtures

Journal of Structural Geology, <https://doi.org/10.1016/j.jsg.2022.104743>

Vossen C. E., Cimarelli C., Bennett A. J., Schmid M., Kueppers U., Ricci T., Taddeucci J.

The electrical signature of mafic explosive eruptions at Stromboli volcano, Italy

SCIENTIFIC REPORTS, 12(1), 1-13. [10.1038/s41598-022-12906-x](https://doi.org/10.1038/s41598-022-12906-x)

Wang H., Li H., Di Toro G., Kuo L. W., Spagnuolo E., Aretusini S., Si J. L., & Song S. R. (NA).

Fault gouge melting at shallow depth during the 2008 Mw 7.9 Wenchuan earthquake

Accepted in Geology on November 2022.

Wessels, R., ter Maat, G., Del Bello, E., Cacciola, L., Corbi, F., Festa, G., Funicello, F., Kaviris, G., Lange, O., Lauterjung, J., Pijnenburg, R., Puglisi, G., Reitano, D., Ronnevik, C., Scarlato, P., Spampinato, L.

Transnational Access to Research Facilities: an EPOS service to promote multi-domain Solid Earth Sciences in Europe

Annals of Geophysics, 65(2), DM214–DM214, <https://doi.org/10.4401/ag-8768>

SUBMITTED

Galderisi A., Bravo M., Iezzi G., Cruciani G., Paris E. & de Brito J.

Mortars with recycled aggregates from CDW rubbles of the 2016/2017 earthquakes in central Italy: Petrography and mechanical performance

SIMP-SGI meeting “Geosciences for a sustainable future” (Torino).

Gennaro E., Iezzi G., Cocchi L., Ventura G.

Large silicic magma chambers at the Moho depth characterize the multi-level plumbing system of back-arc spreading ridges

Communications Earth & Environment, under review.

Gennaro E., Iezzi G., Cocchi L. & Ventura G.

The inner structure of the Marsili seamount revealed by coupling petrological and geophysical data.

SIMP-SGI meeting “Geosciences for a sustainable future” (Torino).

Potere D., Iezzi G., Scisciani V., Tangari A.C., Nazzari M.

Provenance and deposition of a lithified volcanic-rich layer (VRL-5.5) at 5.5 Ma from Central Apennines (Italy)

Scientific Reports, under review.

Radica F., Iezzi G., Trotta O., Bonifazi G. & Serranti S.

Discriminating the petrography of CDW via rapid spectroscopic tool

SIMP-SGI meeting “Geosciences for a sustainable future” (Torino).

Design by Laboratorio Grafica e Immagini INGV

Editing by Valeria Misiti

Rome, April 2023

DISCLAIMER CLAUSE

This report contains data and information property of Istituto Nazionale di Geofisica e Vulcanologia in Rome (Italy). The information contained in this report don't imply the responsibility of the Istituto Nazionale di Geofisica e Vulcanologia.

Our purpose is to supply reliable scientific information to the members of the national and international scientific community and to whoever could be interested in them. Istituto Nazionale di Geofisica e Vulcanologia does not engage any responsibility for the content. This material is constituted by information of general character, result of specific researches, or data coming from the laboratory activity. Copy and the dissemination of this report are authorized only under licence of HP-HT Laboratory people.